ABSTRACT

VANOUNI, MAZIAR. Operation and Management of Thermostatically Controlled Loads for Provision of Regulation Services to Power Grids. (Under the direction of Dr. Ning Lu).

The notion of demand-side participation in power systems operation and control is on the verge of realization because of the advancement in the required technologies an tools like communications, smart meters, sensor networks, large data management techniques, large scale optimization method, etc. Therefore, demand-response (DR) programs can be one of the prosperous solutions to accommodate part of the increasing demand for load balancing services which is brought about by the high penetration of intermittent renewable energies in power systems. This dissertation studies different aspects of the DR programs that utilized the thermostatically controlled loads (TCLs) to provide load balancing services. The importance of TCLs among the other loads lie on their flexibility in power consumption pattern while the customer/end-user comfort is not (or minimally) impacted.

Chapter 2 discussed a previously presented direct load control (DLC) to control the power consumption of aggregated TCLs. The DLC method performs a power tracking control and based on central approach where a central controller broadcasts the control command to the dispersed TCLs to toggle them on/off. The central controller receives measurement feedback from the TCLs once per couple of minutes to run a successful forecast process. The performance evaluation criteria to evaluate the load balancing service provided by the TCLs are presented. The results are discussed under different scenarios and situation. The numerical results show the proper performance of the DLC method. This DLC method is used as the control method in all the studies in this dissertation.

Chapter 3 presents performance improvements for the original method in Chapter 2 by communicating two more pieces of information called forecast parameters (FPs). Communicating improves the forecast process in the DLC and hence, both performance accuracy and the amount of tear-and-wear imposed on the TCLs.

Chapter 4 formulates a stochastic optimization model for a load aggregator (LA) to participate in the performance-based regulation markets (PBRM). PBRMs are the recently developed and practiced regulation market structure recommended by Federal Energy Regulatory Commission (FERC) in 2011. In PBRMs, regulation resources are paid based on both regulation capacity bids and the regulation performance including the provided mileage and the performance accuracy. In order to develop the income from the PBRM, the convention of California Independent System Operator (CAISO) is used. In the presented optimization model, the amount of tear-and-wear imposed on the TCLs are confined to prevent abrupt switching of TCLs.

In Chapter 5, a two-stage reward allocation mechanism is developed for a LA recruiting TCLs for regulation service provision. The mechanism helps the LA to distribute the total reward (earned from regulation service provision) among the TCLs according to their contribution in the whole provided service. In the first stage, TCLs are prioritized based on their service provision capability. In order to do so, an index called $SPCI$ is presented to quantify TCLs capability/flexibility and therefore, prioritize them. After prioritization TCLs a priority list is constructed in the first stage. In the second stage, a reward curve is constructed representing the functionality of the possible total reward with respect to the number top TCLs in the priority list. Then, the allocated reward to individual TCLs is calculated by applying the incremental method on the constructed reward curve. This presented reward allocation

mechanism is based on the definition of maximum service capacity (MSC) for a control group including TCLs. MSC is defined and its calculation method is presented before discussing the two stages of the reward allocation mechanism. The numerical results proves the suitability of the proposed prioritization method as it is observed the TCLs with higher rankings can contribute more to the total reward in comparison to the TCLs with lower rankings in the priority list.

Operation and Management of Thermostatically Controlled Loads for Providing Regulation Services to Power Grids

by
Maziar Vanouni

A dissertation submitted to the Graduate Faculty of
North Carolina State University
in partial fulfillment of the
requirements for the Degree of
Doctor of Philosophy

Electrical Engineering

Raleigh, North Carolina

2017

APPROVED BY:

_____	_____
Ning Lu Committee Chair	Mesut Baran
_____	_____
Srdjan Lukic	Joseph DeCarolis

DEDICATION

To My Family members, Mostafa, Gity, and Geranaz

BIOGRAPHY

Maziar Vanouni was born in Isfahan, Iran. He received the B.Sc. degree from the Isfahan University of Technology in 2005, and the M.Sc. degree in electrical power engineering from the Sharif University of Technology in 2007. He is currently pursuing his Ph.D. degree from North Carolina State University. In 2012, he joined the NSF-funded Future Renewable Electric Energy Delivery and Management Systems Center at North Carolina State University. He interned in the Research and Technology Development department at New York Power Authority in summer 2015. His main research interests include power systems operation, stability, and economics with special interest in micro-grids and renewable energy integration. He is currently doing research on control, operation, and payment mechanisms of demand response programs for provision of energy and ancillary services in smart grids.

TABLE OF CONTENTS

LIST OF TABLES

LIST OF FIGURES

Chapter 1

Introduction

The increase of electricity demand, economic and environmental constraints to expand and upgrade the power assets, have made the power systems in the verge of significant transformation to smart grids. This transition have been facilitated by the advancement in smart metering, sensor networks, communication, and control technologies, large-data analysis, and large-scale optimization techniques. One of the distinguishing features of smart grids in comparison to the traditional power systems is the promising active role of demand response in provision of different services used to be provided only by the dispatchable generators.

The US Department of Energy (DOE) has defined demand response (DR) as follows, [1],

"*Changes in electric usage by end-use customers from their normal consumption patterns in response to changes in the price of electricity over time, or to incentive payments designed to include lower electricity use to times of high wholesale market prices or when system reliability is jeopardized*".

1.1. Types of DR Programs

According to the classification of the DOE, DR programs are classified to two main

programs depending on how change in electricity demand is brought about. The two main programs themselves are furthered classified to different sub-programs summarized as follows.

1.1.1. Price-based DR Programs

In this class of DR programs, the driving factor to bring about the change in electricity consumption is the electricity price. In other words, the end-users respond to electricity prices and try to reduce consumption in the time periods with high electricity price and instead shift their power consumption to the hours with low price. The response to electricity price is not mandatory and completely depend on the end-users decision. The price-based DR programs are further classified to three different sub-programs depending on the tariff model, [1].

1) Time-of-Use (ToU): In this tariff, the electricity price has mainly two or three levels during a day and are called off-peak, partial-peak, and peak prices. This tariff is mainly used for large industrial and commercial end-users. The prices are generally fixed and might only change on a seasonal or yearly basis. The prices are determined in such a way that they reflect (on average) the cost of electricity generation and delivery.
2) Real-Time-Price (RTP): In this tariff the electricity price changes on hourly basis to more accurately reflect the cost of electricity generation and delivery. The prices are provided to the end-users on a day-ahead or an hour-ahead basis. The end-users participating in RTP (or in ToU) programs need to have some level of automated scheduling software and hardware infrastructure to get advantage from the fluctuating electricity price over time and minimize their electricity bill, [2]-[9].
3) Critical-Peak Price (CPP): The main characteristic of a CPP is assigning a very high

price for a specific period of the time, known as critical peak. In critical peak period, the price of electricity provision is very high because of either high market price (due to market power) or reliability problems (due to contingencies). This tariff can be superimpose on either ToU or RTP. Unlike the other two tariffs, CPP is applied/triggered a limited number of hours in a year and the end-users are noticed ahead of the critical time period. The participants in CPP are generally granted discount on electricity consumption in the non-critical periods.

1.1.2. Incentive-Based DR Programs

In this class of DR programs the customers let the utilities of system operators to directly or indirectly reduce their power consumption in cases that the power system faces reliability issues or very high electricity price. Unlike the price-based DR programs, the end-users might get penalized if they fail to reduce their power consumption at the required time. The end-users are provided with a separate incentives that is separate from their retail electricity rate. Generally speaking, while using these types of DR programs, the methods to estimate the normal baseline power consumption of end-users should be established so that the amount of load change can be measured and verified. Different types of incentive-based DR programs are summarized as follows, [1].

1) Direct Load Control (DLC): in this type of program, the load aggregator (load serving entity) to the system operator directly shut down or changes the operating cycles of the loads (like on/off status of the thermostatically controlled loads) to adjust aggregated power consumption. This type of programs are generally offered to the residential and small

commercial loads. The payment to the participants are generally in the from of bill credit or discount in the electricity rate.

2) Interruptible/Curtailable Programs: Similar to DLC, the participants in this program are required to reduce or shut down loads when a reliability issue is declared by the system operator. Unlike, DLC, this program and DLC targets the large commercial and industrial loads.

3) Demand Bidding/Payback Programs: In this type of incentive-based program, the loads are allowed to bid in the electricity market for selling power (like generators). In order to be eligible to participate in this kind of programs, the offer should have a minimum value (say for instance 1 MW).

4) Emergency DR Programs: this refers to programs wherein the customers are called upon the declaration of a reliability-triggered events. The customers are paid only if they provide any load reduction. In other words, they do not receive any up-front money as they are not required to set-aside a specific amount of capacity for load reduction. The customers might or might not be penalized in case of failure to responds to the utility request.

5) Capacity Market Programs: this refers to the programs through which the customers are allowed to bid in the capacity market like a conventional generators. They are paid by the market clearing prices. They receive the capacity payment up-front as they have strict commitment to set-aside the amount of declared capacity bids. The customers may also be paid according to the amount of the load reduction and the energy price at the time event.

6) Ancillary Service Market Program: this program is similar to capacity market program and the customers are allowed to bid in ancillary services markets and provide operating reserves. If their bid is accepted, they are paid up-front and expected to commit the stand-by capacity and provide load adjusting upon the call from the system operator.

As it will be seen in the upcoming chapters, two types of incentive-based DR programs are considered in this dissertation; the ancillary service market program and the DLC program. As the higher level of control/scheduling, a load aggregator participates/bids in regulation market on behalf of individual loads to maximize the profit from regulation market. In the lower control level, the load aggregator directly controls (toggles on/off) the individual loads in order to deliver the amount of regulation service committed in scheduling stage.

1.2. The Benefits of DR Programs

DR programs reward both technical and environmental benefits that encourage policy makers and utilities to consider DR as effective tool in power systems operation, control, and planning and hence, facilitate expansion and participation of DR programs. These benefits are summarized as follows, [10].

One of the main incentives to use DR programs is to reduce power consumption during the peak periods. Peak periods last for a very limited amount of time (say couple of hours a week), however, it is needed to be met which in turn results in inefficient utilization of the available generation, transmission, and distribution capacity. With the load increase, the peak

power is potentially increase as well. Therefore, in order to meet the peak power, it is required to install new generation, transmission, and distribution capacities which are partially utilized. Therefore, the traditional trend is going to be both economically and environmentally expensive. DR can be a good replacement for the required capacities.

The second benefit of the DR programs lies in the vein of ancillary service provision capability. Ancillary services are mainly provided by traditional generating units making them operate in sub-optimal manner with lower efficiency. If DR programs can provide part or ideally the whole ancillary service requirements of a power system, the trapped capacity of the generators can be release and set-aside for energy provision purposes making them to operate more close to the optimal point. Also, some of the costly generators used for peak load hours or quick start reserve (mainly fueled by diesel or oil) can be replaced by DR resources which in turn contribute in decreasing the production cost/price and gas emission.

Finally, the third advantage of DR programs are considered as loss reduction, [10]. In some operational situations that power lines are congested, the system operator can relieve the congestion by adjusting the load level at different parts of a power system which in turn reduce the power losses and more optimal operation of the whole system.

1.3. Thematically Controlled Loads as an Important DR Resources

Thermostatically controlled loads, like water heaters, freezers, refrigerators, heating, ventilation, air conditioning (HVAC) systems, are one the promising load resources to be used

in DR programs. Some demonstrative studies and projects in the U.S. and the U.K. has shown the successful usage of TCLs for provision of primary and secondary frequency regulations, [11]-[13]. One of the main characteristics of TCLs is the capability to change their power consumption pattern such that the comfort level of the end-users is either unchanged or minimally impacted, depending on the design and application of the DR program. This capability comes from the fact that they can store heat in the environment they are heating/cooling. Therefore, they can shift their power consumption to some extent making them suitable resources specifically for provision intra-hour ancillary services, like regulation service. A vast amount of different TCLs are already present in residential and commercial buildings and always a portion of them are connected to power grids. For instance, according to the report of the US Energy Information Administration, almost 20% of the electricity consumption belongs to the TCLs, [14]. Therefore, the aggregated flexibility of TCLs can be considerable as long as they properly controlled and the corresponding communication, sensor, and control infrastructure are provided. In this dissertation, the TCLs are considered to be the type of load resources used for the considered DR programs.

1.4. Dissertation Outlines

In Chapter 2, a previously proposed centralized DLC method is reviewed. In Chapter 3, a performance enhancement for the DLC method in Chapter 2 is presented. Chapter 4 presents a stochastic optimization model to find the optimal bidding strategy for a price taker load aggregator to participate in performance-based regulation market. Finally, a reward

allocation mechanism is presented in Chapter 5 to address the issue of sharing the total reward among different TCLs and according to their contribution in the whole provided regulation service.

Chapter 2: Controlling Thermostatically Controlled Loads for Providing Intra-Hour Load Balancing Services

In this chapter a previously proposed centralized DLC method is reviewed in detail. The DLC method is used to perform the power tracking control in the whole dissertation. First, the dynamic thermal models and basic operation of TCLs are briefly reviewed and then the control method is presented in detail. Then, the performance criteria to evaluate the demand response provided by TCLs are presented. Different simulation scenarios are investigated and discussed to better understand the functionality of the DLC method.

Chapter 3: Design Considerations for Performance Enhancement of the DLC

Chapter 3 proposes performance enhancement for the DLC method presented in Chapter 2. The performance enhancement is brought about by communicating two more pieces of information from individual TCLs to the central controller. The additional information is slope of temperature increase/decrease. Although the amount of measurement data to be communicated to the central controller gets twice, the rate communication can be reduced up to 2-3 time whereas still a better performance is achieved in comparison to the original DLC method.

Chapter 4: Optimal Bidding in Real-time Performance-Based Regulation Markets for the Aggregators of Thermostatically Controlled Loads

In Chapter 4, a stochastic optimization model is presented to obtain the optimal bidding strategy for the TCLs aggregator of TCLs to participate in performance-based regulation markets. The performance-based regulation market is a recent regulation market mechanism recommended by Federal Energy Regulatory Commission (FERC) Order 755 in 2011. In traditional regulation markets regulation resources were paid only based on the provided regulation capacity bid. However, in performance-based markets, the resources are paid based on both provided regulation capacity and regulation performance. The TCLs aggregator is considered to be price taker and the convention of California Independent System Operator (CAISO) is considered for market settlement and hence, developing the optimization model. Also, it is proposed to model the tear-and-wear imposed on the TCLs as a constraint. It is shown that this constraint has noticeable impact on the optimal bidding decision and neglecting this constraint can result in abruptly frequent switching of TCLs and therefore, tear-and-wear of them.

Chapter 5: A reward Allocation Mechanism for Thermostatically Controlled Loads Participating in Regulation Services

One important aspects of investigating demand response programs is how to pay the individual loads participating in the service. This aspect is so vital for successful realization and exploitation of potential benefits in load resources because if the loads are not satisfied with the received incentive, they eventually lose interest participate in the programs.

As previously mentioned, the policy makers in energy sectors have been facilitating the participation of loads in different power markets (energy, capacity, and ancillary service markets) and the ultimate goal is to treat them similar to other centralized resources such as synchronous generators and battery bank, etc. Therefore, the payment mechanism to the load aggregations is simply based on the market rules or the certain contracts with the utilities. But another level of the payment problem still remain and that is how to distribute the total reward among the individual loads.

Generally speaking, as long as energy and reserves services are concerned, the contribution and hence, the payment to the individual loads can be determined as the amount of (estimated) change in average power consumption within the period of service delivery. However, this rule cannot be simply applied while TCLs are participating in regulation services because the payment criteria in regulation service totally different and is not based on the value of average power consumption. The on/off status of TCLs cannot be used as a criteria for payment because it is determined by central controller to adjust the aggregated power of the whole control group. There are TCLs that are off within a time interval and they could be on (and vice versa), however, the controller make decision about their operating status. In other hand, if the TLCs override the commend of the controller, there will be discrepancy between the reference power profile and the power profile of load aggregation which in turn results in performance accuracy degradation and hence, reducing the income from performance-based regulation markets. Therefore, at any time moment all TCLs can potentially have contribution in the whole service.

Chapter 5 is investigating this issue and proposes a three-stage reward allocation mechanism that pays the TCLs based on their contribution in the whole provided regulation service. In order to do so, the concept of maximum service capacity (MSC) is introduced and two mathematical methods are presented to numerically calculate it. Based on the MSC concept, TCLs are prioritized (according to their flexibility for regulation service provision) in the first stage and therefore, a priority list is constructed. Then, using the prioritization results, the MSC curve and reward curve are constructed in the second stage. The MSC and reward curve represents the functionality of MSC and total reward with respect to the in-service TCLs. Finally, as the third stage, the reward to individual TCLs are determined by applying the incremental method on the constructed reward curve.

Finally, Chapter 6 presents the summary of this dissertation and provides some propositions for relevant future research works.

Chapter 2

Controlling Thermostatically Controlled Loads for Providing Intra-Hour Load Balancing Services

Abstract—This chapter investigates in detail a previously proposed centralized direct load control (DLC) method for controlling thermostatically controlled loads (TCLs) to provide load balancing services (LBSs) in power systems. This DLC method is considered as the control methodology for TCLs in the whole dissertation. The DLC method controls the aggregated power consumption of a group of TCLs so that it tracks a reference power profile. The control methodology includes two main stages: a forecasting stage and a unit prioritization/selection stage. The performance of the DLC method is evaluated under different conditions and scenarios. The performance evaluation is done regarding two main criteria: service quality and device life time. The numerical results show that the DLC method provides satisfactory LBSs in most scenarios.

2.1. Introduction

Thermostatically controlled loads (TCLs) are one of the main resources in demand side management (DSM) as the TCLs exist in most of all residential and commercial buildings. According to [14], about 20% of electricity in the U.S. is consumed by the TCLs. Therefore, there is a significant potential for providing different ancillary and energy services by

controlling and managing even part of this vast amount of resources. The key concept in controlling the aggregated power of TCLs (specifically for intra-hour balancing services) is that the power profile of a TCL can be modified while the temperature trajectory is still within the desired range of the end-user. This is shown conceptually in Fig. 2.1 where the temperature and power profile of a TCL are shown and compared in uncontrolled manner (when it is controlled only by the thermostat logic) and controlled manner (when it is controlled by an external controller).

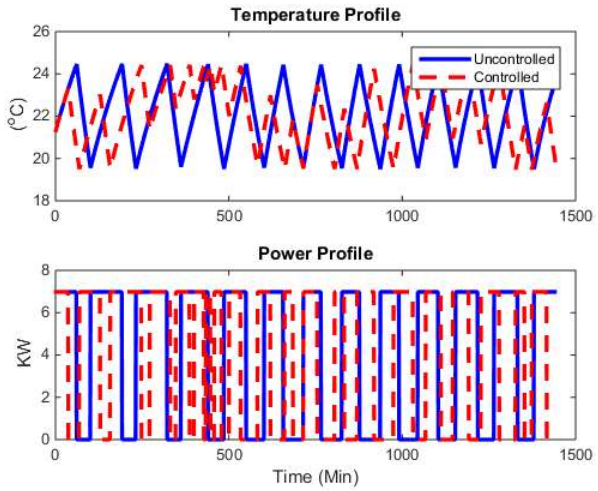

Fig. 2.1. Comparison of the temperature and power profiles of a TCL in uncontrolled and controlled modes.

Generally speaking, there are three main control approaches to control the aggregate response of TCLs; centralized methods, [15]-[23], decentralized methods, [24]-[27], and distributed methods, [28]-[29]. Centralized methods are highly efficient to satisfy the global objectives and constraint, however, they might suffer scalability and reliability issues because of the dependency on real-time communication. For very fast response and reliable services like primary frequency regulations, decentralized approaches are proper methods as they don't

count on the real time communication infrastructure and act independently based on the local measurement data (like frequency). Distributed methods is another alternative that require some TCLs interact and communicate with each other actively. Distributed methods have good scalability and robustness. In this chapter, we present in detail a previously proposed centralized control method, [21]-[22] and consider it as the control method used in the whole dissertation. In [21] and [22] a DLC method is presented where TCLs are controlled individually by receiving on/off commands from a central controller. In this method the TCL states (e.g. temperature and on/off status) of an individual TCL are forecasted at a central controller using feedback measurement data from the TCLs states every few minutes. According to the forecasted states the power imbalance is forecasted and the proper control decision is broadcasted to the TCLs. This chapter describes the DLC method in detail because it is the adopted control method throughout this dissertation.

This chapter is organized as follows. Section 2.2 presents some modeling requirements and some basic concepts to provide a better insight of the DLC method. In Section 2.3, the DLC method is presented in detail. In Section 2.4, performance indices are presented for evaluation and quantification of the DLC performance. Section 2.5 presents and discussed the numerical results where the performance of DLC is investigated under different scenarios. Finally, some conclusion remarks are provided in Section 2.6.

2.2. General Concepts and Modeling Requirements

In this section, some modeling requirements and concepts are presented in advance to provide a better understanding and insight of the DLC method. Generally speaking, in order to

operate TCLs under any demand response (DR) programs, three main objectives are to be considered at the same time, service quality (utility aspect), occupant comfort (end-user aspect), and resources tear-and-wear (end-user aspect). Service quality concerns the quality of procured load balancing service (LBS) by a group of TCLs and occupant comfort concerns the violation of the desired indoor temperature range (the residents' room temperature) and finally, tear-and-wear concerns degrading the TCLs life time because of tear-and-wear imposed by operating under an external controller. Full satisfaction of all the objectives coincidently may not be always possible as they are not independent. For instance, consider the case where the utility wants some HVAC units to be turned off for long time, say one hour. Then, the indoor temperature drops (considering heating mode operation) and pass the desired indoor temperature range and results in customer discomfort. It should be noted that customer comfort is very important in DR programs in the sense that they should have enough comfort and incentive to participate in those programs. In order to have the insight of how to operate TCLs regarding all the objectives, a mathematical model is needed to relate the TCL power consumption (or equivalently its on/off status), the indoor, and the outdoor temperature. This mathematical model, called equivalent thermal parameter (ETP) model, basically represents the heat transfer process among a TCL, indoor, and outdoor space. This section presents two different ETP models together with some of the simplifications applied on them. Then, the concept of baseline power profile for a group of TCLs, load balancing signals, and reference power profile are presented and discussed.

2.2.1. *Dynamic Thermal Model of TCLs*

The principle operation of most TCLs is similar. For instance, the principle operation

of a typical HVAC unit operating in heating mode is conceptually shown in Fig. 2.2.

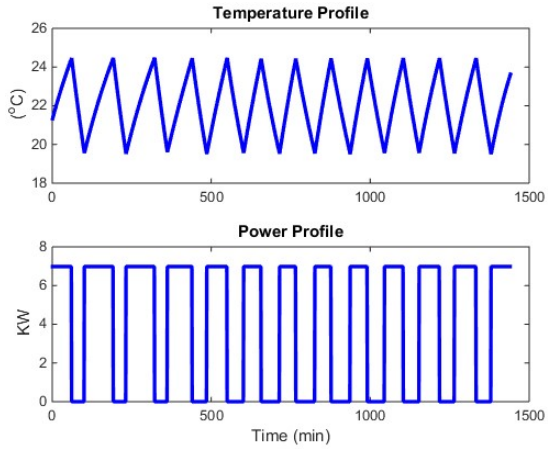

Fig. 2.2. The graphical demonstration of an HVAC unit principal operation.

As it is observed in Fig. 2.2, the heat content of the indoor space is wasted to the outdoor environment (through windows, walls, ceiling, and floor) making the temperature decreasing and finally hitting the lower limit. Then, the unit turns on and remains in on status until the temperature reach to the upper limit. Then, the unit turns off and remains in off status till the temperature hit the lower limit and this cycle is continued. Therefore, in this way, the temperature always falls within the deadband assuring the occupant comfort.

The dynamic thermal modelling of this principle operation (heat transfer process) with interest in the indoor temperature variations is fairly well described by a set of hybrid-differential equations, called ETP model. These equations can be related to an electrical circuit, called ETP equivalent electrical circuit, where capacitors' charge and discharge process can imitate the increase and decrease of temperature. These models are needed to relate the power consumption of an HVAC unit to its indoor and outdoor temperature. Figure 2.3 represents the

electrical circuit of two common ETP models for some residential or small commercial buildings is shown in Fig. 2.3.

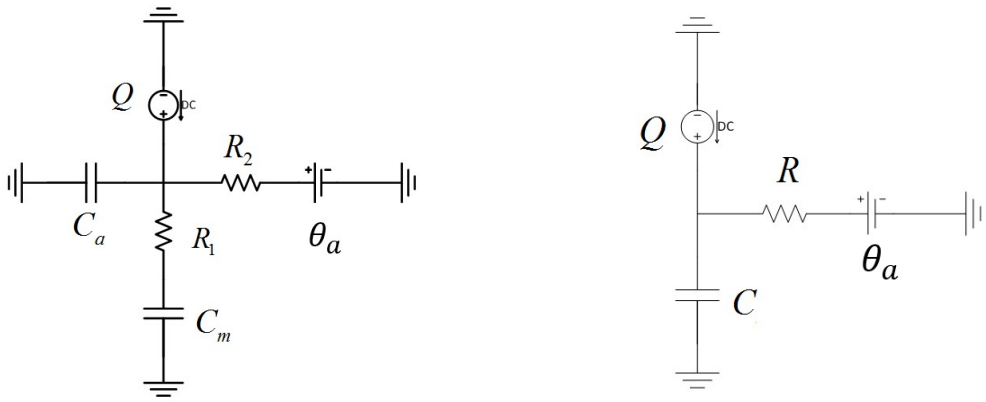

(a) (b)

Fig. 2.3. The equivalent electrical circuits, (a) for 2nd order ETP (b) and 1st order ETP model.

Figure 2.3(a) represents the circuit for the 2nd order ETP model where the variables and parameters are summarized as follows.

C_a	Thermal capacity of indoor air ($KWh/$℃)
C_m	Thermal capacity of equivalent interior mass (including furniture and etc.) ($KWh/$℃)
R_1	Thermal resistance between the equivalent interior mass and indoor air (℃$/KW$)
R_2	Thermal resistance between indoor air and outdoor (℃$/KW$)
θ_a	Outdoor temperature (℃)
θ	Indoor air temperature (℃)
θ_m	Equivalent interior mass temperature (℃)
Q	Injected heat rate by the HVAC (KW)

P_{Rated}	Rated power of the HVAC (KW)
COP	Coefficient of performance

The state space representation of the 2nd order ETP model shown in Fig. 2.3(a) is presented as follows.

$$\dot{x} = Ax + B\widehat{U} \tag{2-1}$$

where

$$x = \begin{bmatrix} \theta \\ \theta_m \end{bmatrix} \qquad \widehat{U} = \begin{bmatrix} \theta_a \\ q \end{bmatrix}$$

$$A = \begin{bmatrix} -\left(\frac{1}{R_2C_a} + \frac{1}{R_1C_a}\right) & \frac{1}{R_1C_a} \\ \frac{1}{R_1C_m} & \frac{-1}{R_1C_m} \end{bmatrix} \qquad B = \begin{bmatrix} \frac{1}{R_2C_a} & \frac{1}{C_a} \\ 0 & 0 \end{bmatrix}$$

$$q = QU = \begin{cases} Q & ON \\ 0 & OFF \end{cases} \qquad Q = P_{Rated}\, COP$$

Another common model to capture the dynamic thermal behavior of TCLs is the 1st order ETP model with the electrical circuit shown in Fig. 2.3(b). The model parameters are summarized as follows

C	Thermal capacity of indoor air ($KWh/$℃)
R	Thermal resistance between the equivalent interior mass and indoor air (℃$/KW$)
θ_a	Outdoor temperature (℃)
θ	Indoor air temperature (℃)
Q	Injected heat rate by the HVAC (KW)
P_{Rated}	Rated power of the HVAC (KW)
COP	Coefficient of performance

The state space representation of the 1st order ETP model is derived as follows

$$\dot{x} = Ax + B\widehat{U} \tag{2-2}$$

where

$$x = \theta \qquad \widehat{U} = \begin{bmatrix} \theta_a \\ q \end{bmatrix}$$

$$A = \frac{-1}{RC} \qquad B = \begin{bmatrix} \frac{1}{RC} & \frac{1}{C} \end{bmatrix}$$

$$q = \begin{cases} Q & ON \\ 0 & OFF \end{cases} \qquad Q = P_{Rated}\, COP$$

The thermal parameters of ETP models (like R, C, Q in the 1st order model) can be derived using building information (like the type of wall, ceiling, floor thickness and materials, floor areas, and etc.) or they can be derived using measurement based methods where the parameters are calculated by some identification techniques, [30] and [31].

It is noted that there are different types of ETP models with different orders in the literature, [24], to model the dynamic thermal model of TCLs. However, in this dissertation, we use the 1st ETP model shown in Fig. 2.3(b). Also, the TCLs are considered to have two level of power consumption, P_{Rated} when it is on status and 0 when it is the off status. Based on the space representation of (2-1) and according to the fact that $Q \neq 0$ ($Q = 0$) during on (off) period, the discretized solution for indoor temperature is derived from the following equations.

$$\theta(k+1) = U(k+1)\theta^{on}(k+1) + (1 - U(k+1)\theta^{off}(k+1)) \tag{2-3-a}$$

$$\theta^{off}(k+1) = \theta_a(k) - (\theta_a(k) - \theta(k))e^{-(T_s/RC)} \tag{2-3-b}$$

$$\theta^{on}(k+1) = \theta_a(k) + QR - (QR + \theta_a(k) - \theta(k))e^{-(T_s/RC)} \tag{2-3-c}$$

$$U(k+1) = \begin{cases} 1 & \theta^h \le \theta(k+1) \\ U(k) & \theta^l \le \theta(k+1) \le \theta^h \\ 0 & \theta(k+1) \le \theta^l \end{cases} \quad \text{(2-3-d)}$$

$$Q = P_{Rated}\, COP \quad \text{(2-3-e)}$$

where $\theta(k)$ ($\theta_o(k)$) stands for the indoor (outdoor) temperature at the time instant $k\Delta t$ and Δt stands for sampling period to discretize the HVAC thermal dynamic model and it is considered to be 4-second in this report. Also, θ^h/θ^l, $Db = \theta^h - \theta^l$, and θ_{set} represent the upper/lower temperetaure limit, the operating deadband of the thermostat, and setpoint temperature. It is noted that Q is a positive and negative quantity for the heating and cooling operation mode, respectively. The above equations determine the relation between an HVAC unit power consumption (switch status), its indoor temperature, and outdoor temperature.

It should be noted that if the considered TCL is a water heater or freezer/refrigerator, the term Q is modified to $Q + Q_L(k)$. The term Q_L represents the amount of heat rate taken out of a water tank when hot water is consumed (a negative quantity) while for a freezer/refrigerator it is heat rate entered to the indoor environment by opening the door or entering food (positive value).

According to the fact that the operating deadband of an HVAC unit is usually falls within a small range (around 1℃ to 4℃), a simplification can be made and the trajectory of indoor temperature during both on and off period can be fairly well considered to be linear. Therefore, considering the heating operation mode of a HVAC, (2-3-a) and (2-3-b) can be simplified as

$$\theta^{on}(k+1) = K_u \Delta t + \theta(k) \quad \text{(2-4-a)}$$

$$\theta^{off}(k+1) = -K_d \Delta t + \theta(k) \qquad \text{(2-4-b)}$$

where K_u and K_d are absolute value for the slope of temperature trajectory when the unit is on and off, respectively. K_u and K_d are actually dependent on the building thermal parameters and settings, as well as outdoor temperature. Therefore, they are not constant during a day as the outdoor temperature changes. However, in [21] and [22] these parameters are considered to be the same for all units and are assumed to be derived from a common set of HVAC model parameters based on some practical estimates. Figure 2.4. compares the indoor temperature trajectory derived from the first order ETP model and the linear model during one cycles. The thermal parameters of the house are considered to be $R = 6.06\ ℃/KW$, $C = 1.13\ KWh/℃$, $Q = 10.3\ KW$, $COP = 2.1$ and an outdoor temperature profile with the average temperature of $0℃$ was used (see Fig. 2.5).

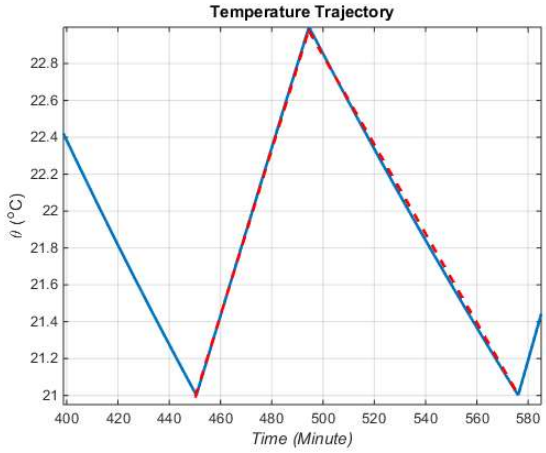

Fig. 2.4. Comparison of actual and linear temperature trajectory.

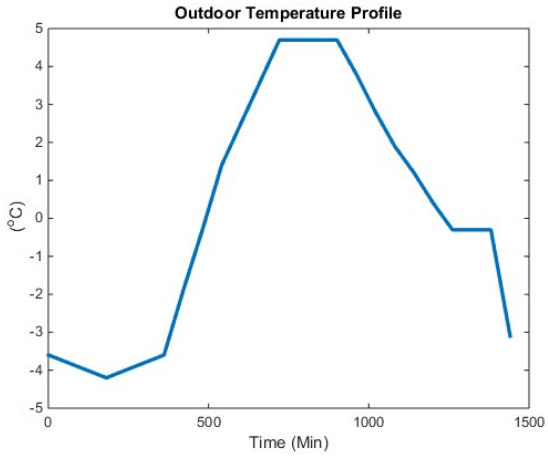

Fig. 2.5. The outdoor temperature profile.

It is observed from Fig. 2.4 that the indoor temperature trajectories, derived from the first ETP model (equations (2-3-a) and (2-3-b)), can be well approximated by the straight lines

(equations (2-4-a) and (2-4-b)) with $K_u = 0.0541$ and $K_d = 0.1230$.

Till this point, three methods of modeling heat transfer process in a building have been presented. Initially, a second order and first ETP model, which is more close to the actual/physical model, was introduced in (2-1)-(2-3) and then, according to the fact that the operating deadband of TCLs usually falls within a small range, further simplification was made and the temperature trajectory is assumed to be linear and the model of (2-4) was derived. The first order ETP model is used to simulate the actual heat transfer process for HVACs and the linear model is used for the purpose temperature forecast in the presented DLC, as it will be shown and described later. In the rest of this chapter, it is assumed that HVACs operates as heater without loose of generality.

2.2.2. *Baseline Power Profile of HVAC Units*

If HVAC units are not externally controlled (by an operator or central controller) and their operation is only based on the decision of the local controller (thermostat) to keep the temperature within the deadband, each HVAC unit has a discrete power profile similar to what shown in Fig. 2.2. According to the fact that the temperature and switch status of different HVAC units are different at each time instant, the aggregated power consumption of a group of HVACs construct an almost continuous load power profile, called uncontrolled power profile, $P_{unc}(\cdot)$. Hourly averaging the uncontrolled power profile yields the baseline power profile, $P_b(\cdot)$. In general, $P_b(\cdot)$ can be forecasted either through the common forecast techniques and using the historically recorded data or by simulating the HVACs over the desired forecasting time horizon. In this chapter, we assume that the $P_b(\cdot)$ is derived using the second approach. In other words, the $P_{unc}(\cdot)$ is constructed using the 1st order ETP model of

HVACs and then it is averaged on hourly basis to construct $P_b(\cdot)$. It is evident that the on/off periods and hence power profile of an HVAC unit, depends on the outdoor temperature profile and therefore, $P_{unc}(\cdot)$ and $P_b(\cdot)$ are dependent on $\theta_a(\cdot)$ as well. Figure 2.8 represents the 24-hour profile of $P_{unc}(\cdot)$ and $P_b(\cdot)$ for a group of 1000 heterogeneous HVACs for six different outdoor temperature shown in Fig. 2.7. The histogram of HVACs thermal parameters are shown in Fig. 2.6. Also, the HVACs' θ_{set} and Db are considered to be random integers in $[19℃, 23℃]$ and $[2℃, 5℃]$. It should be noted the way parameters and settings are randomized are explained in Appendix in detail. Also, the initial switch status and indoor temperature of all units are randomized using discrete and continuous uniform probability distribution function (PDF), respectively. As observed from the Fig. 2.8, when the weather gets colder and T_o is decreased, then power consumption is increased.

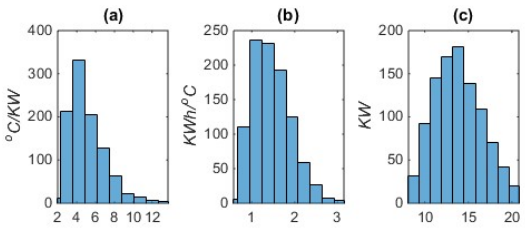

Fig. 2.6. The PDF of thermal parameters for 1000 HVACs.

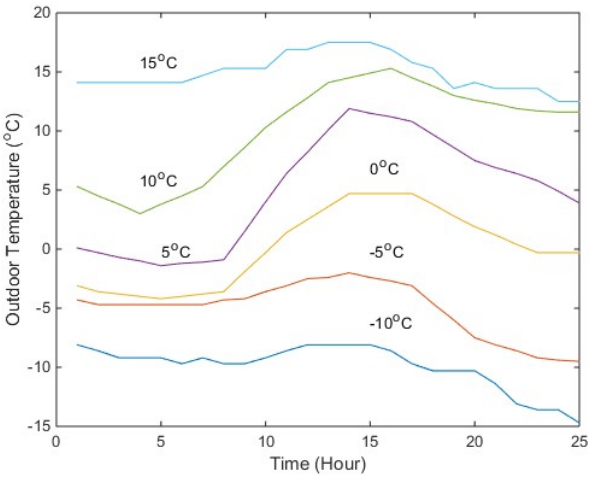

Fig. 2.7. The profile of different typical outdoor temperature.

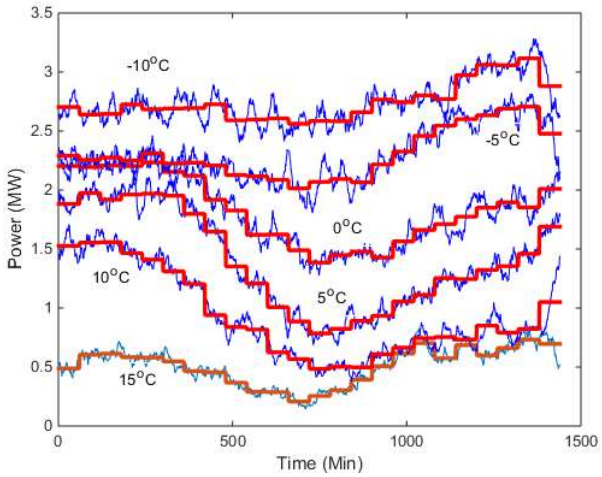

Fig. 2.8. The profile of P_{unc} and P_b for different outdoor temperatures.

2.2.3. Load Balancing Signal (LBS) and Reference Power Profile

In real power systems, there is always difference between the actual and forecasted load and hence, the actual generation need and the scheduled generation. Load forecasting and the corresponding generation commitment/scheduling are performed in different time scales, like week-ahead, day-ahead, hour-ahead, and real-time. Based on the requirements of California Independent System Operator (CAISO), the hour-ahead load forecaster provides the hourly forecasted load two hours ahead of the beginning of the operating hour based on which hour-ahead schedule is determined [1]. On the other hand, real-time load forecaster (very short-term load forecaster), which provides more accurate load forecast rather than the hour-ahead, forecasts the load for intervals of 5 minutes and provide it 7.5 minutes before the beginning of the actual operational time interval based on which the generation of some units are changed to compensate for the discrepancy between the hour-ahead and real-time load forecast [1]. The discrepancy between the forecasted generation schedule in the hour-ahead schedule and real-

time schedule is defined as the load following signal [1], which is compensated by change in the schedule of the generation units participating in load following services. Those generators are provided with the new schedule some minutes before the real operation (2.5 minute for CAISO). The discrepancy between the actual generation requirement and the real-time generation dispatch is referred to regulation signal [1], which is compensated by change in the schedule of the generation units participating in regulation services. In this chapter, it is intended to include HVAC units in load balancing (load following/regulation) services as well. In order to do that, it is assumed that the share of the load balancing signal (load following/regulation signal) to be compensated by the group of HVAC units is determined by sort of technical problems (like economic dispatch) which is out of the concern of this chapter. Assuming that the load balancing signal to be provided by the HVAC group is either sent by the dispatching center or through the automatic generation control (AGC) system and is represented by $P_{lbs}(\cdot)$. Define a reference power profile, $P_{rf}(\cdot)$, as follows.

$$P_{rf}(\cdot) = P_b(\cdot) + P_{lbs}(\cdot) \tag{2-5}$$

Assuming that the aggregated power profile of HVAC units tracks the $P_{rf}(\cdot)$, one can consider that the control group is actually providing LBS. Equation (2-5) states that the group is changing their normal power consumption ($P_b(\cdot)$) by $P_{lbs}(\cdot)$ to provide LBS to the grid. According to (2-5), if $P_{lbs}(\cdot) = 0$, then the HVACs are supposed to follow $P_b(\cdot)$ meaning that they have to smooth out their uncontrolled power profile, $P_{unc}(\cdot)$. It should be noted that $P_b(\cdot)$ is to be provided to the grid operator in advance (e.x. the day before) so that the grid operator can compare the actual aggregated power consumption of HVACs and $P_{rf}(\cdot)$ in order to verify

the quality of the provided LBS. Typical load balancing signals are normalized to $\mp 1\ MW$ and shown in Fig. 2.9.

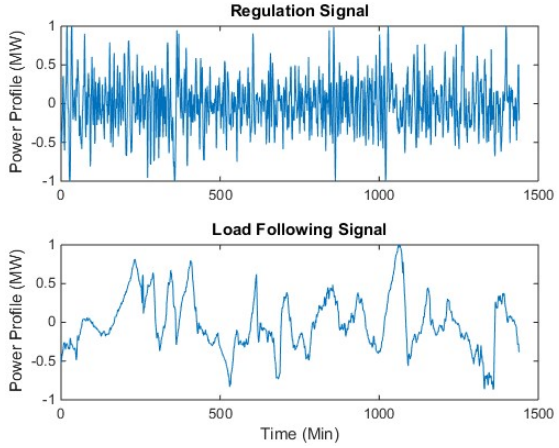

Fig. 2.9. Two type of load balancing signals.

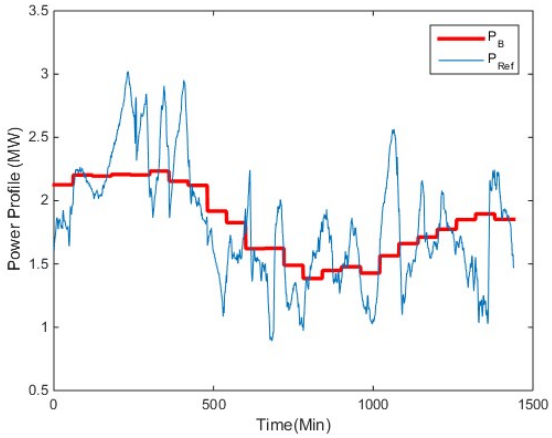

Fig. 2.10. The $P_b(\cdot)$ and $P_{rf}(\cdot)$.

Figure 2.10 also shows the profile of $P_b(\cdot)$ and the constructed $P_{rf}(\cdot)$ using the presented regulation signal. The goal is to design a DLC method so that the aggregated power consumption of an HVAC group tracks the P_{rf} while considering the occupant comfort and HVACs wear-and-tear (life time). The DLC method is explained in detail through next section.

2.3. DLC Method

The objective of the presented DLC method is to control or actually toggle on/off the HVACs in such a way that their aggregated power consumption profile of HVAC, $P_a(\cdot)$, track the control signal, $P_{rf}(\cdot)$ and at the same time to consider some constraints regarding consumer comfort and HVACs number of switching which in turn affect its life time. The DLC method is based on the central control approach where a central controller toggles on/off the geographically dispersed HVACs which are equipped with local intelligence (retrofit circuit).

This circuit is capable of measuring the room temperature and the unit on/off status, and send them back to the central controller with a predetermined rate, called feedback rate or sampling rate (SR) in this report. The SR is considered to be one sample per some minutes (say 5-15 minutes). Also, the availability of two-way-communication infrastructure is presumed. Using this communication system, the central controller send the control command (on/off) to the dispersed HVACs and reversely, the HVACs send back their state variables (temperature and on/off status) to the central controller. It should be noted rate of sending commands from the central controller to the individual HVACs depends on the load balancing signal granularity. For instance, if the load balancing signal is a regulation signal with the granularity of the 4-seconds, then the communication system is supposed to handle the rate of transmitting the control command on 4-second basis. However, if the load balancing signal is 1-minute-based signal, the communication system need to handle lower communication rate to transmit the control command.

The presented DLC includes two main steps, forecasting step and resource selection step. In the first step the state variables of each HVAC are forecasted in the central controller. In the second step, the HVACs are prioritized and then the proper units are selected to be toggled.

2.3.1. Forecast Step

Consider the control time horizon to be represented by T_h (for instance 24-hrs) and the granularity of $P_{lbs}(\cdot)$ and therefore $P_{rf}(\cdot)$ are 4-second. The goal is to forecast the states of each HVAC in the next interval without applying any external control. In another words, the goal is to know that the temperature of the unit at the end of k_{th} time interval and the on/off status of the unit during the k_{th} interval if it is not controlled by the central controller. Noted

that the forecast stage is performed in the central controller. In order to perform the forecast stage, the approximate linear model presented in Section 2.2.1 is used. The forecast stage is formulated, as follows. Knowing the temperature and switch status at the end and within the k^{th} time interval (regardless it was forecasted before or updated by measurements) and assuming that the switch status is not changed, the temperature at the end of the next time interval ($(k+1)^{th}$ time interval) is forecasted by

$$\theta^f(k+1) = \begin{cases} K_u \Delta t + \theta^f(k) & U^f(k+1) = U^f(k) = 1 \\ -K_d \Delta t + \theta^f(k) & U^f(k+1) = U^f(k) = 0 \end{cases} \tag{2-6}$$

where $\theta^f(\cdot)$ and $U^f(\cdot)$ represents the forecasted temperature and forecasted switch status, respectively. Note that the superscript f in the following equations stands for the forecasted value. Then, the switch status at the beginning of the next operational time interval is forecasted using the following logic.

$$U^f(k+1) = \begin{cases} 0 & \theta^h \le \theta^f(k+1) \\ U^f(k) & \theta^- \le \theta^f(k+1) \le \theta^+ \\ 1 & \theta^f(k+1) \le \theta^- \end{cases} \tag{2-7}$$

The above equation verifies that if the assumption $U^f(k) = U^f(k+1)$ is valid or not. In other words, if $\theta^f(k+1)$ falls within the Db, the assumption is valid, otherwise the assumption is not valid and $\theta^f(k+1)$ should be recalculated using the correct value of $U^f(k+1)$, as follows.

$$\theta^f(k+1) = \begin{cases} K_u \Delta t + \theta^f(k) & U^f(k+1) = 1 \\ -K_d \Delta t + \theta^f(k) & U^f(k+1) = 0 \end{cases} \tag{2-8}$$

As mentioned before, the slopes (K_u and K_d) in the linear model vary during the day as the outdoor temperature change, however, they are considered to be constant in the DLC method

which is the main source of forecast error. Therefore, the forecast error is accumulated after a while if the units' states are not communicated back to the central controller once a while. This is the main reason for telemetering the units' states back to the central controller through two-way communication infrastructure. The measurements tune the temperature and switch status every some minutes (say 5-15 minutes) and limits the forecast error. Ideally, it is desired to receive the measurements fast enough, say every 1 minute. But it requires installing high rate communication infrastructure, which may be cost prohibitive. Therefore it is assumed that measurement data is communicated every some minute. After forecasting the $U^f(k+1)$ for all of the units, one can easily calculate the forecasted aggregated power consumption of the group if no control command is applied. This power is calculated as follows.

$$P_a^f(k+1) = \sum_{i=1}^{N} U^f(k+1)\, P_{Rated,i} \tag{2-9}$$

As a result, the discrepancy between $P_a^f(k+1)$ and $P_{rf}(k+1)$ can be easily calculated as follows.

$$P_e(k+1) = P_{rf}(k+1) - P_a^f(k+1) \tag{2-10}$$

If $P_e(k+1)$ is negative, then upward balancing is required and therefore, some units have to be toggled on. Similarly, if it the mismatch is positive, then downward balancing is required and some units are to be turned on. The next step would be selecting the proper units among the available ones to be toggle and therefore, compensate for the $P_e(k+1)$. This problem is addressed in the next step.

2.3.2. Unit Prioritization and Selection

Generally, in order to compensate for the $P_e(k+1)$, the central controller can choose different combinations of HVACs (among the available units) to toggle. However, this section present a prioritization methodology so that a central controller can uniquely select the proper units from the top of the list to the bottom. The objective of this prioritization is to reduce the HVACs number of switching over the control time horizon which in turn reduces the wear-and-tear imposed on the units. In order to do so, a temperature priority list method is presented as follows.

First, the available units are to be determined at the $(k+1)^{th}$ time interval considering the following conditions.

1) A unit is to be unlocked. Each HVAC is assumed to have a minimum on/off time meaning that if a unit is toggled on/off, it has to remain in on/off status for a required amount of time. This consideration is related to protection of the HVACs compressor system. Therefore, a unit which has not satisfied this constraint is considered to be unavailable.

2) A unit is to be able to keep its status in the next time interval if the unit is toggled. Assume a unit is in the on status. This unit is considered to be available for toggling off if it can keep its status in the off position at least for the next time interval ($(k+1)_{th}$ time interval). Some units might not be able because they might hit the temperature limit. The reasons a unit might not be able to keep its status can be violation of the desired temperature range.

After determining the available units, they are divided to two groups based to their on/off status, on-group and off-group. Considering the heating (cooling) operating mode, the on-group is prioritized based on their normalized indoor temperature in descending (ascending) order and the off-group is prioritized based on their normalized indoor temperature in ascending (descending) order to make on-priority-list and off-priority-list, respectively. The normalized indoor temperature for the i_{th} unit is calculated as follows.

$$\theta_i^{f,n}(k+1) = \frac{\left(\theta_i^f(k+1) - \theta_{set,i}\right)}{Db_i} \tag{2-11}$$

Therefore, if $B\ MW$ of upward balancing is needed, proper number of units are selected form the top to the bottom of the off-priority list so that the difference between the summation of their rated power and the power mismatch, $P_e(k+1)$, is minimized. Similarly, if $B\ MW$ of downward balancing is required, proper number of units are selected form the top to the bottom of the on-priority list so that the difference between the summation of their rated power and the power mismatch, $P_e(k+1)$, is minimized.

Therefore, by toggling the required number of units the $P_e(k+1)$ is minimized and makes the $P_a^f(k+1)$ to track the $P_{rf}(k+1)$. It should be noted the main purpose and justification behind temperature based prioritization is to choose the units which are about to hit their temperature sooner than the others. Therefore, the units are less diverged from their normal switching (under no external control) pattern that results in the reduction of the extra number of switching imposed on the units on average.

The steps of the DLC method are summarized as follows.

1) At the beginning of each time interval, check for new measurements and update the

units' states if any.

2) Forecast the units' states for the next time interval if no external control command is applied, using (2-6)-(2-8).

3) Based on the forecasted $U^f(k+1)$, determine the $P_a^f(k+1)$ and hence the amount of power mismatch, $P_e(k+1)$.

4) Determine the available units.

5) Construct on-priority-list and off-priority list based on $U^f(k+1)$ and $T^{f,n}(k+1)$.

6) Based on the amount of mismatch and the priority lists, determine the required units to be toggled.

7) Based on the most updated $U^f(k+1)$, broadcast the command signals (on/off status of each unit) to all HVAC units.

It should be noted that although HVAC units are operated by the central controller/operator that takes care of temperature violation, (2-6)-(2-8) in the forecast stage, the HVAC units are still considered to be equipped with thermostats as another layer of protection against temperature violation which may happen due to the forecast error or probable malfunctioning of the central controller. Another point to be considered in the presented DLC method is that due to forecast error, specifically near the temperature limits, θ^+ and θ^-, some units are forecasted to be on (off) while they are actually off (on) which may affect the quality of LBS provision. One practical solution to moderate this problem is to consider a slightly wider deadband for the local thermostat (Db_t) in comparison to the deadband considered in the

forecast stage of the central controller (Db_c) which is compatible to the occupant comfort. The cost of this solution is to violate the desired temperature range for some minutes during the day, [21]-[22]. However, in this dissertation, it is assumed $Db_t = Db_c$ and thus, if the desired range of the end-user is violated, the local retrofit circuit turn on/off the unit. Therefore, the end-user comfort is strictly respected.

2.4. DLC Performance Evaluation Criteria

In this section, the performance criteria used to evaluate the performance of the DLC method are presented. Two main criteria called, service quality, and device (HVAC unit) life time are considered in order to evaluate the performance of the DLC. Service quality implies the quality of the provided LBS by the HVAC group, or in other words, how closely the $P_a(\cdot)$ tracks $P_{rf}(\cdot)$. The other performance criteria concerns the tear-and-wear imposed on HVACs by the increased number of switching (in effect of participating in the LBS) in comparison to the manner that they are only controlled by their local thermostat. In order to compare the DLC performance (regarding each criterion) in different scenarios, each criterion is quantified by an index (indices) presented as follows.

For qualitative evaluation of the service quality, the following performance accuracy index is used.

$$PA^{U/D}(t) = Max\left\{0, \frac{\sum_k \left(\left|P_{lbs,in}^{U/D}(k)\right| - \left|P_{lbs,in}^{U/D}(k) - P_{lbs,a}^{U/D}(k)\right|\right)}{\left|\sum_k P_{lbs,in}^{U/D}(k)\right|}\right\} \quad (2\text{-}12)$$

where $P_{lbs,in}^{U/D}(\cdot)$ is the instructed upward/downward load balancing signal that is sent by the

system operator and can be considered as AGC setpoint, while, $P_{lbs,a}^{U/D}(\cdot)$ is the actual upward/downward load balancing signal that the control group (HVAC aggregation) has already provided. Recall that the provided load balancing signal by the control group is the deviation of the aggregated power from the baseline power and therefore,

$$P_{lbs,a}^{U/D}(\cdot) = P_a(\cdot) - P_b(\cdot) \tag{2-13}$$

where $P_a(\cdot)$ and $P_b(\cdot)$ stand for the HVAC group aggregated power profile and the baseline power profile, respectively. t and k represent the index for $PA^{U/D}$ evaluation time interval (market settlement time interval) and the index for control time interval (granularity of the load balancing signal). The presented $PA^{U/D}$ index is currently used by CAISO, [32], and the regional transmission operator of Pennsylvania, New Jersey, and Maryland (PJM), [33]. However, CAISO calculates PA over intervals of 15-minutes while PJM calculates it over intervals of 5-minutes. In this dissertation, we consider the convention of the CAISO and therefore, t is the index for 15 minutes time intervals and k is the index for the granularity of the load balancing signal which is 4-seconds. Therefore, the above equation can be rewritten as follows,

$$PA^{U/D}(t) = Max\left\{0, \frac{\sum_{k=225(t-1)+1}^{225t}\left(\left|P_{lbs,in}^{U/D}(k)\right| - \left|P_{lbs,a}^{U/D}(k) - P_{lbs,a}^{U/D}(k)\right|\right)}{\sum_{k=225(t-1)+1}^{225}\left|P_{lbs,in}^{U/D}(k)\right|}\right\} \tag{2-14}$$

Note that $PA^{U/D}$ index is derived based on the mean value of the absolute error signal (second term in the nominator) and the mean value of the absolute instructed balancing signal (the denominator). Thus, the above equation is rewritten as follows,

$$PA^{U/D}(t) = \frac{\overline{P_{lbs,in}^{U/D}}(t) - \overline{E^{U/D}}(t)}{\overline{P_{lbs,in}^{U/D}}(t)} \tag{2-15}$$

It is evident that the power profile of an individual HP is discrete (either P_{rated} or 0). Thus, $P_{lbs,a}^{U/D}(\cdot)$ is discrete as well and even if the power tracking is performed as accurate as possible, there is always a power mismatch between $P_{lbs,in}^{U/D}(\cdot)$ and $P_{lbs,a}^{U/D}(\cdot)$. In the best manner, the mismatch will be less than the rated power of an HP (usually less than 10-kW because the rated power of an HP is usually less than 10-kW). This implies that the mean value of error cannot be equal to zero and therefore, a deadband for error calculation is to be considered. Therefore the modified mean value of absolute error and the $PA^{U/D}$ are defined as follows,

$$\overline{E_m^{U/D}}(t) = \begin{cases} 0 & \overline{E^{U/D}}(t) \le P_c \\ \left(\overline{E^{U/D}}(t) - P_c\right) & \overline{E^{U/D}}(t) > P_c \end{cases} \tag{2-16-a}$$

$$PA^{U/D}(t) = \frac{\overline{P_{lbs,in}^{U/D}}(t) - \overline{E_m^{U/D}}(t)}{\overline{P_{lbs,in}^{U/D}}(t)} \tag{2-16-b}$$

Considering the time interval l, if the average of the absolute mean value, $\overline{E^{U/D}}(l)$, is less than a break-point power, P_c, then the performance accuracy is considered to be perfect at that time interval ($PA^{U/D}(l)$). However, if $\overline{E^{U/D}}(l) > P_c$, then the $PA^{U/D}(l)$ starts decreasing from one. The value of P_c is determined according to the practical considerations of an LA regarding the required accuracy for LBS provision. In this study, P_c is considered to be 1% of the summation of whole control group rated power ($0.01\sum_{i=1}^{N} P_{Rated,i}$). Therefore, (2-16) is used to evaluate the performance accuracy of the LBS provided by the load aggregation.

Finally, the following index is presented to quantify the device life time criterion, [34]

$$RSW = \frac{N_{cnt}^{sw}}{N_{unc}^{sw}} = \frac{\frac{1}{N}\sum_{i=1}^{N} N_{i,cnt}^{sw}}{\frac{1}{N}\sum_{i=1}^{N} N_{i,unc}^{sw}} \quad (2\text{-}17)$$

where $N_{i,cnt}^{sw}$ stands for the total number of the switching of i^{th} unit during the control time horizon while they are controlled under the DLC method and $N_{i,cnt}^{sw}$ stand for the same quantity while it operates only subject to its thermostat and without external control.

In the next section, the above three mentioned indices are calculated for a variety of scenarios in order to better evaluate and compare the performance of DLC method under different scenarios.

2.5. Numerical results

In this section, the presented DLC method is used to control a group of heterogeneous HVACs for provision of intra-hour LBSs. The numerical results are presented and the performance of the DLC is evaluated. In order to derive the numerical results, the same group of 1000 heterogeneous HVACs with the thermal parameters and settings presented in Section 2.2.2 are used. Different sensitivity analysis are performed to observe the effect of different factors on the DLC performance. Note that while studying the sensitivity analysis, it is assumed that $SP = 1$ to minimize the effect of forecast stage error and to better observe the sensitivity results. Then, the effect of SP on the performance of the DLC is studied separately. Also, the magnitude of the balancing signal is considered to be 1 MW unless otherwise it is mentioned.

2.5.1. Providing ± 1 MW of Regulation Service

First, we implement the DLC method for the control group to provide a $\pm 1MW$ LBS

over 24-hours and the SP is considered to be 10-minutes. The profile of the load balancing signal, $P_{lbs}(\cdot)$, and outdoor temperature profile, $\theta_a(\cdot)$, are shown in Fig. 2.11 and Fig. 2.12 and the constructed $P_b(\cdot)$ and $P_{rf}(\cdot)$ are shown in Fig. 2.13 . Figure 2.14 compares the aggregated power of the control group, $P_a(\cdot)$, with the $P_{rf}(\cdot)$ where it is observed $P_a(\cdot)$ closely tracks $P_{rf}(\cdot)$. The numerical values of $PA^{U/D}$ index has been calculated at every 15-minutes time interval and the results are shown in Fig 2.16 where it is seen that $PA^{U/D}$ indices are fairly well close to one (except in couple of intervals) which is compatible with the results of Fig. 2.15. Figure 2.16 and Fig. 2.17 also shows the normalized temperature profile of the control group before and after control, respectively. As it is expected the external control affects the temperature trajectories, however, the temperature is still within the desired range of the end-users as the DLC method strictly respects the end-users comfort.

Finally, the value of RSW is derived as 1.88 meaning that on average, the HVACs are switched 1.88 times more in comparison to the uncontrolled mode which is brought about because of providing load balancing services.

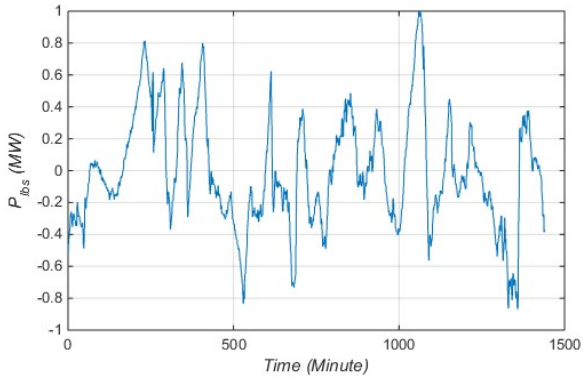

Fig. 2.11. The profile of the $P_{lbs}(\cdot)$.

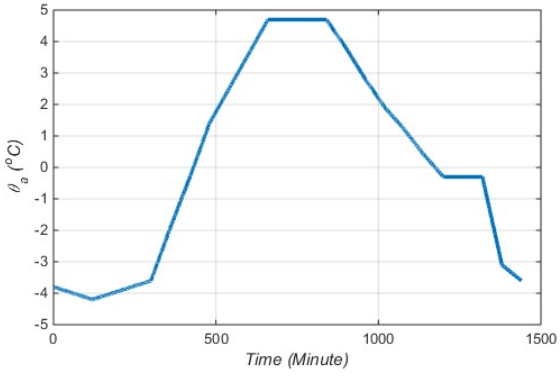

Fig. 2.12. The profile of the $\theta_a(\cdot)$.

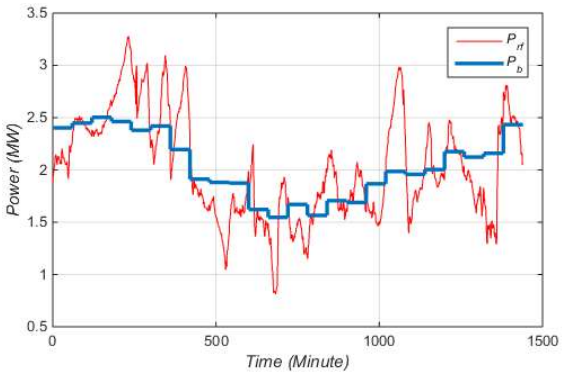

Fig. 2.13. The profile of the constructed $P_{rf}(\cdot)$ and $P_b(\cdot)$.

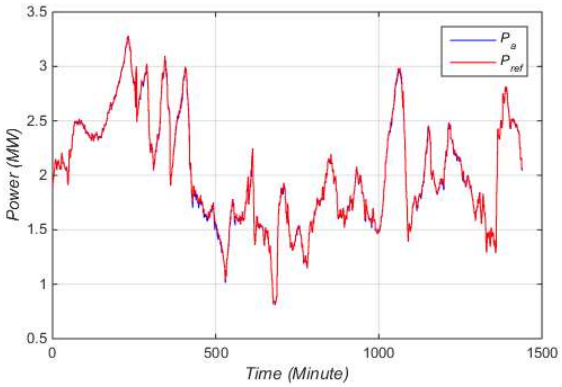

Fig. 2.14. The profile of the constructed $P_{rf}(\cdot)$ and $P_a(\cdot)$.

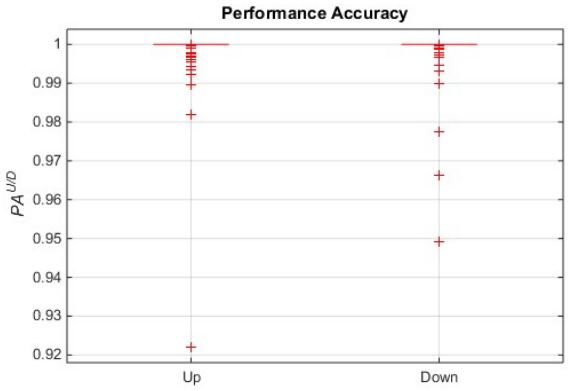

Fig. 2.15. The calculated $PA^{U/D}$.

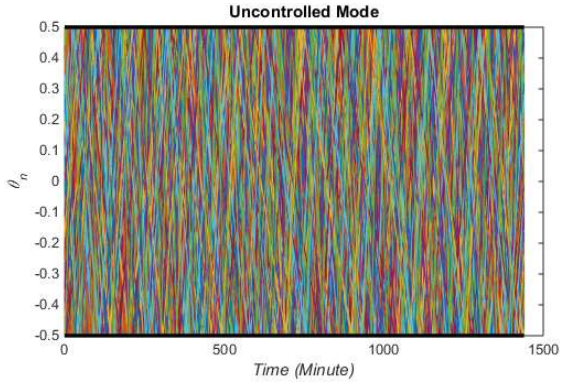

Fig. 2.16. The normalized temperature profile of the control group before applying control.

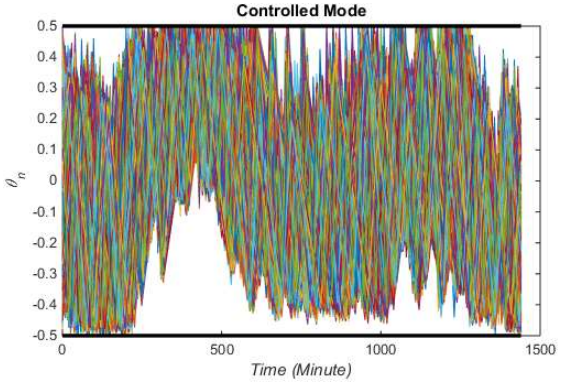

Fig. 2.17. The normalized temperature profile of the control group after applying control.

2.5.2. The Effect of Load Balancing Signal Magnitude

In this part, the effect of load balancing signals magnitude on the DLC performance is studied and the results are presented as follows. Figure 2.14 represents the $PA^{U/D}$ for different magnitudes of the $P_{lbs}(\cdot)$ shown in Fig. 2.11. As it is evident, the service quality is degraded as the magnitude of the balancing signal gets larger than 2 MW. This implies a very evident fact that the HVAC group, like other type of centralized balancing resources, has a limited capacity for service provision.

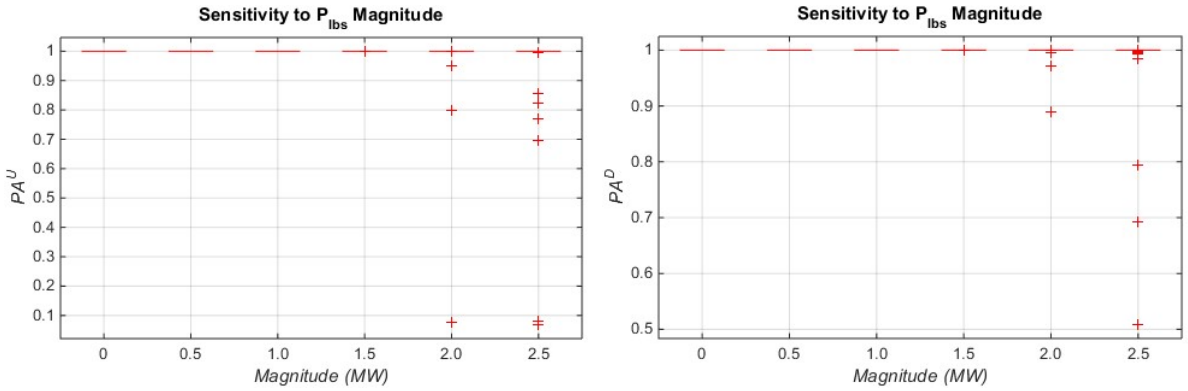

Fig. 2.18. Sensitivity of service quality w.r.t. P_{lbs} magnitude.

Figure 2.19 compares $P_a(\cdot)$ and $P_{rf}(\cdot)$ when the maximum magnitude of $P_{lbs}(\cdot)$ is 0 MW and 2.5 MW and Fig. 2.20 compares the normalized temperature of the group for the two scenario. It is noticeable that when $P_{lbs}(\cdot) \equiv 0$ MW, the HVAC tracks their $P_b(\cdot)$ or basically they smooth out their $P_{unc}(\cdot)$. Table 2.1 presents the numerical value RSW where it is seen that RSW is increased as the magnitude of load balancing service is increased.

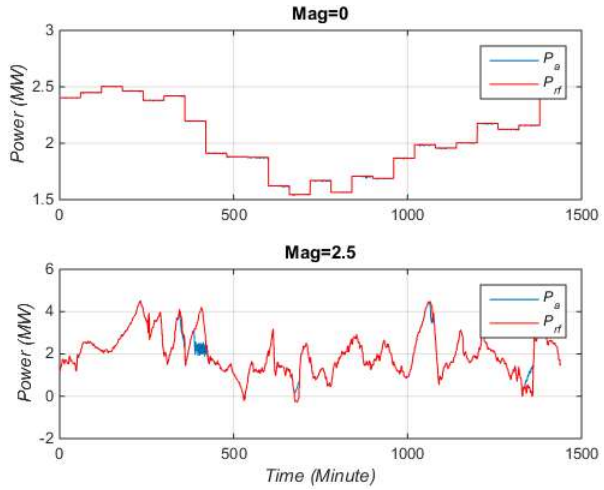

Fig. 2.19. Comparison of P_a and P_{rf} when the maximum magnitude of P_{lbs} is 0 MW and 2.5 MW.

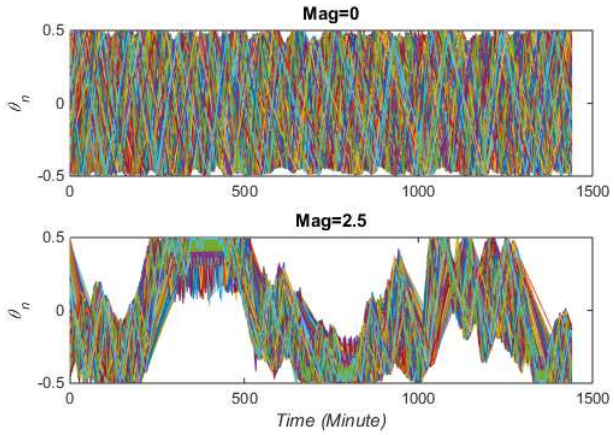

Fig. 2.20. Comparison of normalized temperature profile when the maximum magnitude of P_{lbs} is 0 MW and 2.5 MW.

Table 2.1. The variation of RSW w.r.t. the variation of P_{lbs} magnitude.

$P_{lbs}(\cdot)$ (MW)	0	0.5	1	1.5	2.0	2.5
RSW	1.03	1.18	1.40	1.80	2.82	4.23

2.5.3. The Effect of $\theta_a(\cdot)$

It is evident that $\theta_a(\cdot)$ and θ_{set} directly influence the power consumption of HVACs,

$P_b(\cdot)$, and hence the balancing service capability. Figure 2.21 represents $P_a(\cdot)$ and $P_{rf}(\cdot)$ for two different $\theta_a(\cdot)$ profile with the average of 0℃ and 15℃ as shown in Fig. 2.22.

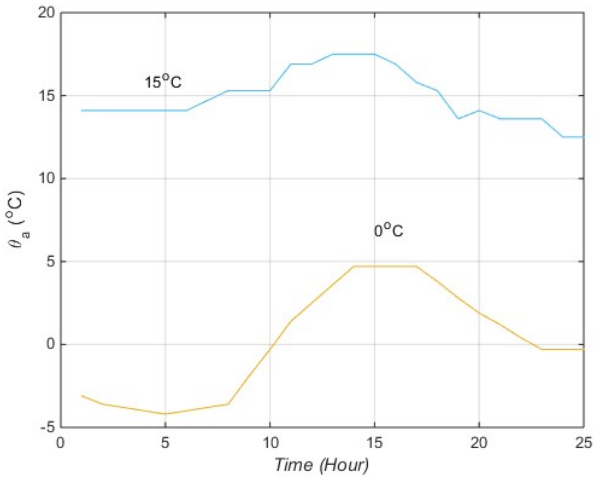

Fig. 2.21. The $\theta_a(\cdot)$ profiles with the average of 0℃ and 15℃.

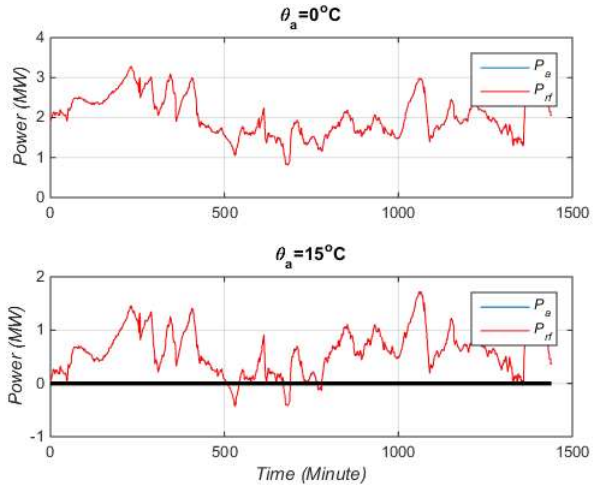

Fig. 2.22. Comparison of $P_a(\cdot)$ and $P_{rf}(\cdot)$ for two $\theta_a(\cdot)$ profile with the average of 0℃ and 15℃.

It is seen that the group of HVAC can afford the LBS while the ambient temperature is $\theta_a(\cdot)$ with the average of 0℃. However, the same group cannot afford the LBS when the outdoor temperature is $\theta_a(\cdot)$ with the average of 15℃. This is because of the fact that P_b is smaller for the higher outdoor temperature and therefore, the large values of P_{lbs} at some intervals can

make the P_{rf} negative, as shown in Fig. 2.22. Therefore, the downward balancing capability of HVAC group is degraded because they cannot generate power. It is noteworthy to mention that θ_{set} has similar effect on the balancing service capability.

2.5.4. The Effect of SP

In this part the effect of different SPs on the performance of DLC is studied. The results are presented in Fig. 2.19 to Fig. 2.21 and Table 2.2 where the following observations are made.

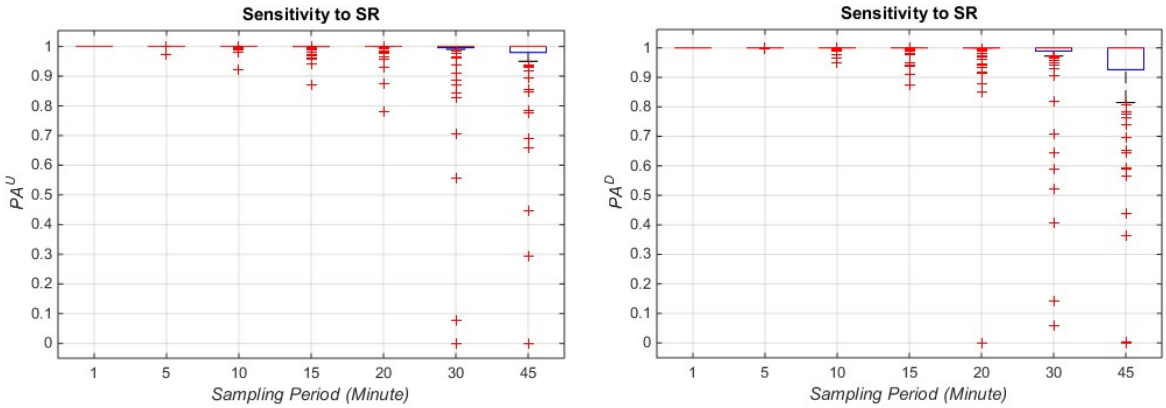

(a) (b)

Fig. 2.23. Sensitivity of service quality w.r.t. SP.

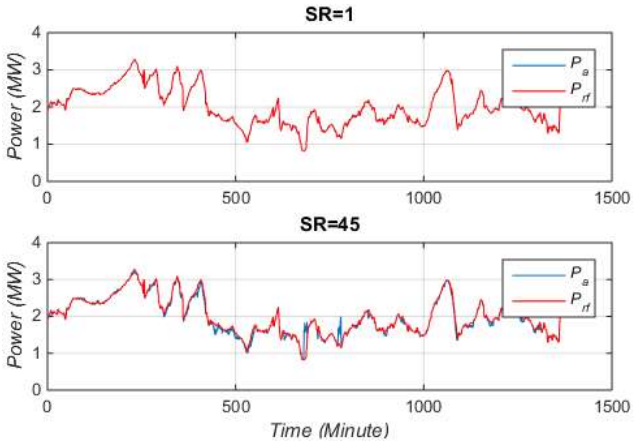

Fig. 2.24. Comparison of P_a and P_{rf} for $SP = 1$ and $SP = 20$.

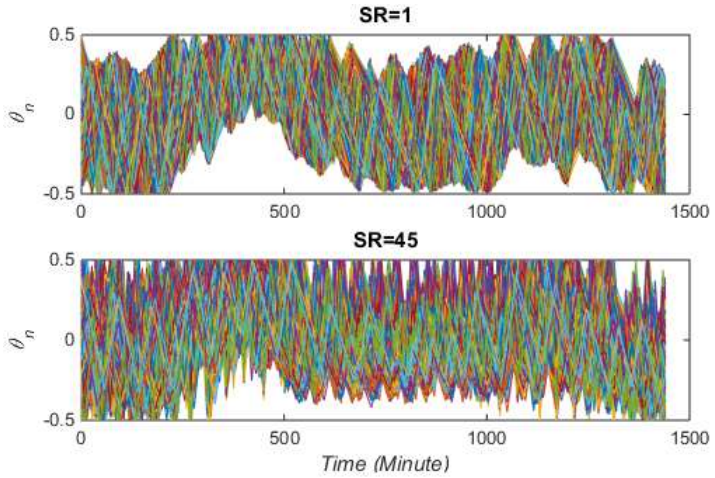

Fig. 2.25. Comparison of normalized temperature profile for $SP = 1$ and $SR = 20$.

Table 2.2. The variations of RSW w.r.t. SP.

SR	1	5	10	15	20	30	45
RSW	1.40	1.57	1.75	1.88	2.55	3.62	5.15

According to Fig. 2.23, as the SP is decreased, the service quality is degraded as well. This is because the accumulated forecast error is increased as the correction (by sending back the measurements) is done on a lower rate. When the forecast accuracy decreases, some units are forecasted to be on (off) while they are actually off (on) which in turn results in degrading service quality. The visualized comparison of service quality for $SP = 1$ and $SP = 20$ is provided in Fig. 2.24 as well. According to Table 2.2, increasing the SR also increase the RSW index value. This is because of the fact that the temperature of some units changes steeper than what the central controller considers (K_u/K_d). Therefore, when the updates are received with lower rate, based on the central controller forecasts they hit the temperature limit sooner and those unit are switched more frequently which in turn increase the RSW.

2.6. Summary

This chapter presents a DLC method to centrally control (toggle on/off) geographically dispersed HVAC units through two-way communication infrastructure for the purpose of intra-hour LBSs. The DLC includes two main steps, forecasting, and unit prioritization. In the first step HVACs' states in the uncontrolled manner are forecasted and then in the second step, the required amount of units are selected in order to form a temperature based priority list. The performance of the DLC has been evaluated regarding two main criteria, called service quality, and device life time. Two indices were presented to quantify the DLC performance corresponding to each criterion. The numerical results are presented and discussed where performance of the DLC method is evaluated. Also, the sensitivity of the DLC performance under different scenarios are studied. It is also shown that the HVACs have limited capability for provision of LBSs meaning that if the magnitude of the load balancing signal is larger than a certain value, the performance accuracy will degrade (the index become smaller than one). It is also shown that outdoor temperature (and similarly indoor temperature setpoint) is a detrimental factor in the service provision capability of HVACs as it affects the baseline power profile and hence, the amount of potential power reduction/increase by the control group. The sensitivity of the DLC performance with respect to the SP are presented where it is observed that longer sampling period degrade the service quality and brings about higher amount of tear-and-wear imposed on the TCLs.

Chapter 3

Design Considerations for Performance Improvement

Abstract-This chapter presents performance enhancements for the direct load control (DLC) method presented in the previous chapter where a central controller controls (toggles on/off) dispersed thermostatically controlled loads (TCLs) through two-way-communication infrastructure for providing intra-hour load balancing services (LBSs). It is highlighted that the forecast stage error in the DLC method is highly dependent on the forecast parameters (FPs) and therefore, it is proposed to communicate two more pieces of information, in addition to device operating temperature and on/off status (TCL states), to the central controller. These pieces of information, called the TCL FPs, decrease the forecast process error and therefore results in improvements in service quality. It is observed that the same or even better performance can be achieved at almost two-times longer sampling periods (SPs).

3.1. Improvement of forecast error

In chapter 2, we discussed a direct load control (DLC) method to control aggregation of thermostatically controlled loads (TCLs) for provision of intra-hour load balancing services (LBSs). It was observed that one of the key parts of the DLC scheme is forecasting the TCLs states that directly affect the quality of LBS provision. Considering a heat pump (HP), the

states of the i^{th} HP in k^{th} time interval, $[kT_s, (k+1)T_s]$, are forecasted, using the following equations,

$$\theta_i^f(k+1) = U_i^f(k)\left(K_u + \theta_i^f(k)\right) + \left(1 - U_i^f(k)\right)\left(-K_d + \theta_i^f(k)\right) \quad \text{(3-1-a)}$$

$$U_i^f(k+1) = \begin{cases} 0 & \theta_i^+ \le \theta_i^f(k+1) \\ U_i^f(k) & \theta_i^- \le \theta_i^f(k+1) \le \theta_i^+ \\ 1 & \theta_i^f(k+1) \le \theta_i^+ \end{cases} \quad \text{(3-1-b)}$$

$$\theta_i^f(k+1) = U_i^f(k+1)\left(K_u + \theta_i^f(k)\right) + \left(1 - U_i^f(k+1)\right)\left(-K_d + \theta_i^f(k)\right) \quad \text{(3-1-c)}$$

where $\theta_i^+, \theta_i^-, \theta_i^f(k)$, and $U_i^f(k)$ represent desired upper and lower temperature limits, the forecasted indoor temperature at the time instant kT_s, and the forecasted on/off status of in the time interval $[kT_s, (k+1)T_s]$, respectively. Also, it is evident that the temperature trajectory during on/off periods are approximated by lines with the slope of K_u/K_d, which is referred to forecast parameters (FPs). According to (3.1-a), first, temperature at the time instant $(k+1)T_s$ is forecasted ($\theta_i^f(k+1)$) assuming that the on/off status will not change within the next time interval. Then, the assumption about on/off status is verified and corrected (if needed) using (3-1-b). Finally, the updated temperature forecast is derived from (3-1-c). After forecasting HPs on/off status, their no-control aggregated power consumption, is forecasted within the time interval. Then, discrepancy between the aggregated power profile and the reference power profile are calculated so that a certain amount of units determined by the temperature-priority-list (TPL) algorithm are toggled on/off to compensate for the discrepancy (refer to either Chapter 2 or [21] and [22] for more detail).

Note that the forecasted temperature, calculated by the simplified linear temperature trajectory

model in (3-1) may not match exactly the actual temperature value. In fact, even if more sophisticated exponential models are used, forecast errors may still be significant because the exact heat transfer model parameters are not exactly known for each individual HP.

The forecast errors may result in a mismatch between the forecasted and actual HP on/off status. A unit that is forecasted to be "on" (or "off") within the next interval may actually be turned "off" (or "on") by its local thermostat as the actual temperature reaches the thermostats temperature limits (θ_i^+, θ_i^-). This yields discrepancy between the actual and reference power profiles and hence, degrading the service quality. The above discussion and observation of (3-1) shows that the accuracy of K_u and K_d determines how large the forecasted errors are. Assuming the linear temperature trajectory within the operating deadband, if K_u and K_d are close estimate of the actual slopes of temperature profiles, the forecast errors will be minimized. However, in [21] and [22], for simplicity, K_u and K_d are the same for all HP units and are derived from a common set of HP model parameters based on some practical estimates. This assumption results in greater forecast error for some HP units because of two main reasons: 1) K_u and K_d are not the same for all HPs because of the thermal parameters diversity for different HPs and 2) even for one HP, K_u and K_d are dependent on the outdoor temperature. For instance for a heating unit, the lower the outdoor temperature is, the longer/shorter the on/off period is and thus, the K_u and K_d is decreased/increased.

In the following, it is proposed to improve the DLC performance by communicating two more pieces of information, called forecasting parameters (FPs), which are calculated

locally at the retrofit circuit of each HP and send back to the central controller (together with the HP states) at the communication time instant.

3.1.1. Updating and communicating the linear temperature trajectory model parameters

We still stick to the assumption of linear model structure for temperature trajectory but let K_u and K_d be calculated and updated locally using the switching point measurements (time and temperature) and then sent back to the central controller to improve forecast accuracy. In this method the FPs are K_u and K_d. Consider the i^{th} unit which is turned off at the n^{th} switching event (SE). Therefore, the unit was turned on in the $(n-1)^{th}$ SE and it was on between the two SEs. Assuming the retrofit circuit measures time and temperature at switching points and heating mode operation of the unit, the K_{ui} can be calculated locally, as follows.

$$K_{ui} = \left|\left(\theta_i^{s,n} - \theta_i^{s,n-1}\right)/\left(t_i^{s,n} - t_i^{s,n-1}\right)\right| \tag{3-2}$$

where $\left(t_i^{s,n}, \theta_i^{s,n}\right)$ represents the measurement pair at the n^{th} SE. Similarly, when the unit turns on at the n^{th} switching event (SE), K_{di} can be calculated locally, as follows.

$$K_{di} = \left|\left(T_i^{s,i} - T_i^{s,i-1}\right)/\left(t_i^{s,n} - t_i^{s,n-1}\right)\right| \tag{3-3}$$

It should be noted that only one of K_{ui}/K_{di} is updated right after each SE depending the unit is turned on or turned off. The last updated values of K_{ui} and K_{di} are sent back to the central controller at each communication time instant.

3.1.2. Discussion

It should be noted that it is possible for some units not be switched within a sampling

period (SP) (or actually between two consecutive instant of communicating the data). It can happen when the cycling period of a unit is large (due to the outdoor temperature, building thermal parameters, or thermal setting of the unit) and at the same time it has not been commanded by the central controller to be toggled on/off within the SP. Thus, none of the FPs for those units are updated at least once within a SP if only the switching point measurements are used to update the parameters. This situation has been shown graphically in Fig. 3.1 and Fig. 3.2. However, it is desired to have at least one of the parameters updated within a SP to reduce the forecast error accumulation effect and hence, better forecast process. In order to deal with this situation, it is recommended that the retrofit circuit measures the time and room temperature right before the communication instant and consider it as one of the measurements required to update the FPs.

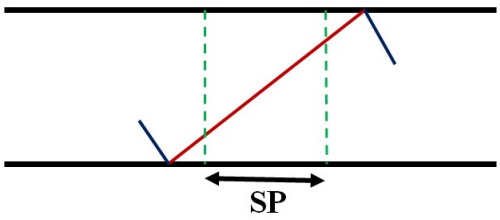

Fig. 3.1. The visualization of the situation where the unit stays in on status between two sampling time instant.

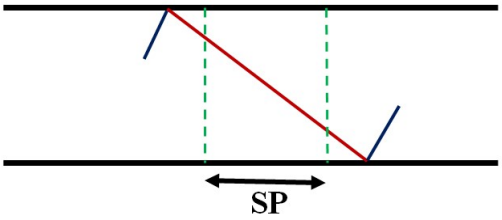

Fig. 3.2. The visualization of the situation where the unit stays in off status between two sampling time instant.

It is noted that the other measurement corresponds to the last SE and has already been recorded. In this manner, the FPs for both methods are updated as follows

$$K_{ui} = \left|\left(\theta_i^b - \theta_i^{s,n-1}\right)/\left(t_i^b - t_i^{s,n-1}\right)\right| \qquad (3\text{-}9\text{-a})$$

$$K_{di} = \left|\left(\theta_i^b - \theta_i^{s,n-1}\right)/\left(t_i^b - t_i^{s,n-1}\right)\right| \qquad \text{(3-9-b)}$$

where $\left(t_i^b, \theta_i^b\right)$ stand for the measurement pair right before the communication instant and the other measurement pair, $\left(t_i^{s,n-1}, \theta_i^{s,n-1}\right)$, belong to the last SE.

It is noted that at each SE only one of the parameters is updated. However, within a SP a unit might be switched couple of times and therefore, both parameters are updated at least one time within a SP. Also, the parameters needs to be initialized for each HP before the start of control time horizon which is considered to be 24-hrs in this report. In order to do that, we simulate the HP in the uncontrolled mode for a while so that most of HPs go through at least one cycle (two SEs). In the simulations, we consider this period to be two hours. However, after controlling a HP for a control time horizon, the central controller have access to the sequence of FPs which were updated and sent back to it. Therefore, it can use the mean value of the parameters as the initial value for future uses of that HP.

Generally, it is possible to model the temperature trajectory with higher order polynomials (instead of linear model), however, these higher order modellings need more measurement pairs apart from the ones for the SEs. On top of that, even more sophisticated algorithms like least square and hence, local retrofit circuits are required to identify FPs.

3.2. Simulation results

In this section, the idea of communication slopes, presented in 3-1-1, is applied on the DLC scheme of Chapter 2 and the performance improvements are demonstrated and discussed

through the numerical results. In order to set up the simulations, a control group of 1000 heterogeneous HP units with the same parameters and settings given in Chapter 2 are used and it is assumed that they are operating in heating mode. The considered $\theta_a(\cdot)$ profile, the baseline power consumption profile of the control group ($P_b(\cdot)$), the considered load balancing signal ($P_{lbs}(\cdot)$), and reference power profile ($P_{rf}(\cdot)$) are shown in Fig. 3.3.

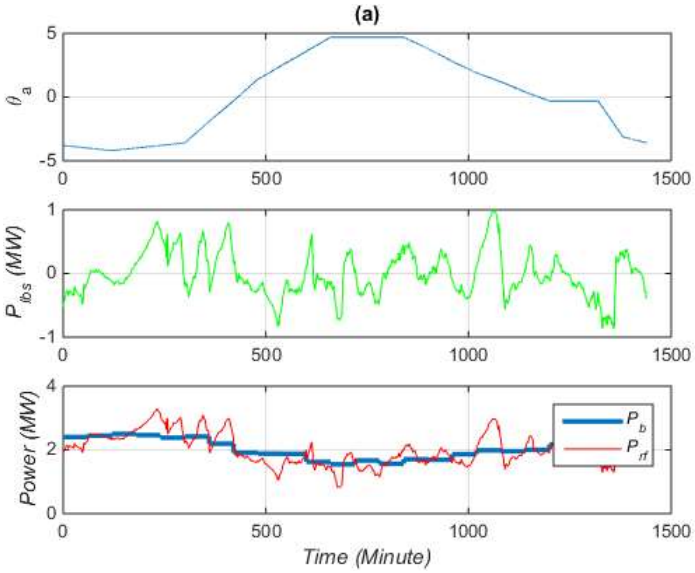

Fig. 3.3. The profile of (a) θ_a, (b) P_{lbs}, (c) P_b and P_{rf}.

Two different cases are considered where the DLC scheme employs two different forecast methods. In Case 1, the forecast process is performed by linear temperature trajectory model where the line slopes (FPs) are considered to be constant and the same for all units (as performed in [21] and [22]), and equal to

$$K_u = \frac{1}{N}\sum_{i=1}^{N}\frac{Db_i}{T_i^{on}} \qquad \text{(3-11-a)}$$

$$K_d = \frac{1}{N}\sum_{i=1}^{N}\frac{Db_i}{T_i^{off}} \quad (3\text{-}11\text{-b})$$

where T_i^{on}, T_i^{off}, Db_k, and N stand for on-time duration off-time duration, the deadband of the i_{th} HP, and the control group population, respectively. The variables T_i^{on} and T_i^{off} are derived using the HP parameters/setting and assuming the average of $\theta_a(\cdot)$ over the control time horizon (24-hrs). While in the Case 2, the forecast process is performed considering linear model with updating/communicating the FPs. It is noted that in both cases, the TPL method is used to select the proper units to be switched on/off. Figure 3.4 to Fig. 3.5 compare the service quality of LBS provision in each case using the $PA^{U/D}$ index (presented in Chapter 2) for different values of sampling periods (SP). As it is observed from the figure, for any given value of SP, the better and worse service quality belongs to Case 2 and Case 1, respectively, because of updating the FPs over time in the central controller. Another interesting observation one can make from Fig. 3.4 to Fig. 3.5 is that by improving the forecast process (updating and communication the FPs) one can get the same or even better service quality while increasing the SP. Therefore, although the amount of communicated information is increased, the sampling period can be decreased to alleviate the required communication upgrades in comparison to Case 1 wherein lees amount of data is transmitted from the dispersed HPs to the central controller.

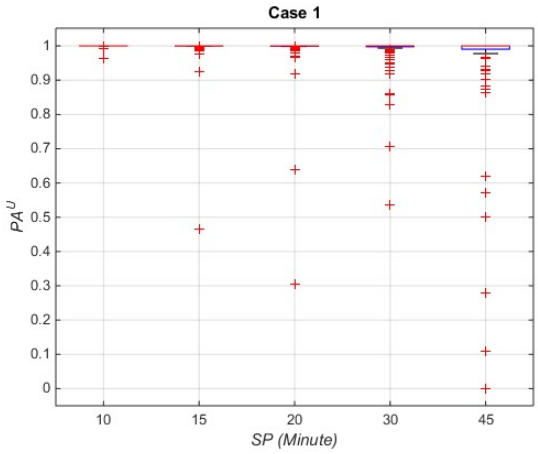

Fig. 3.4a. PA^U in Case 1.

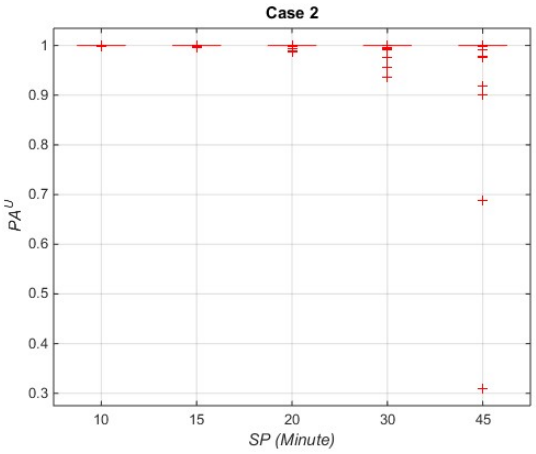

Fig. 3.4b. PA^U in Case 2.

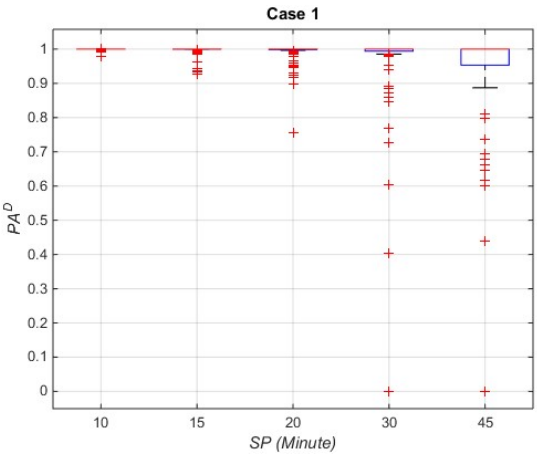

Fig. 3.5a. PA^D in Case 1.

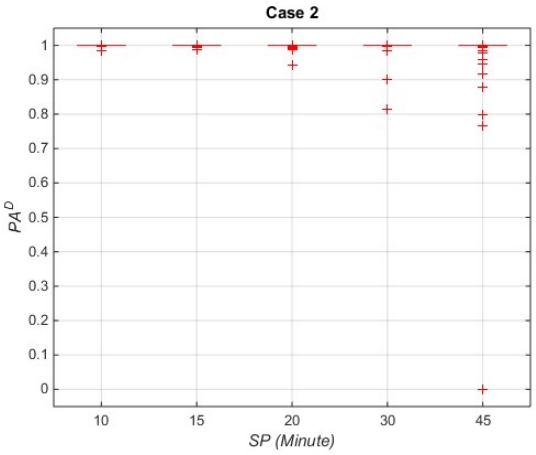

Fig. 3.5b. PA^D in Case 2.

The variation of the communicated FPs for a unit in Case 2 during the control time horizon is shown in Fig. 3.6 where it is observed that the FPs (K_u/K_d) change considerably during the day and as $\theta_a(\cdot)$ changes which in turn proves the importance of updating the FPs.

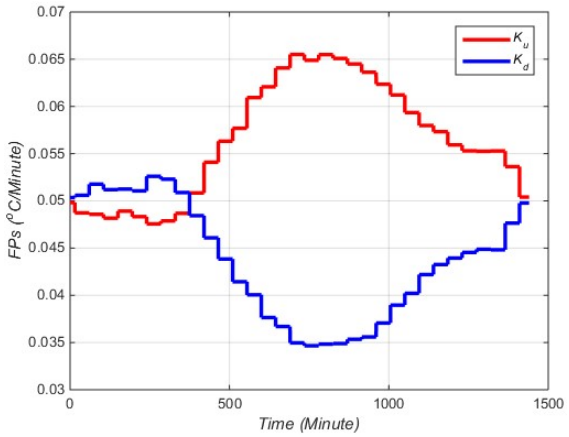

Fig. 3.6. The variations of FPs for a unit over the control time horizon, linear model.

Table 3.1. The variation of RSW w.r.t. SP in Case 1 and Case 2.

$SP\ (samp/min)$	10	15	20	30	45
RSW (Case1)	2.05	2.56	3.25	5.55	8.2
RSW (Case2)	1.94	1.96	2.03	2.29	2.97

Finally, Table 3.1 shows the numerical values of the average switching ratio, represented by RSW, for the whole group in both cases. As discussed in Chapter 2, the RSW is a criteria to evaluate the performance of the DLC with respect to device (HP) tear-and-wear. As it is observed from the table, when SP is increased in Case 1, the RSW is increased. This is because of the fact that FPs are fixed and constant in Case 1 and as long as FPs are not updated, the forecast error would be highly dependent on the SP. Therefore, by increasing SP, the accumulated forecast error is increased. Some of the units with the FPs set larger (steeper

slopes) than the actual one will be forecasted to hit the temperature limits sooner that the actual time and therefore they are switched more frequently which in turn results in the increase of RSW. However, in Case 2, the forecast process error is decreased because of updating the FPs and therefore it is less dependent on the SP, as shown in Fig. 3.4 to Fig. 3.5. Therefore, by increasing the SP the RSW does not change considerably.

3.3. Summary

A performance enhancement is presented for a previously proposed DLC method where geographically dispersed TCLs are toggle on/off by a central controller to provide LBSs. It is highlighted that the forecast process error is considerably dependent on the numerical values of FPs. Therefore, it is proposed to calculate/update the FPs locally (and by using the switching point measurement data) and then sent back to the central controller together with the HP states. It is shown through numerical results that by updating and communicating the FPs, both the service quality and the imposed tear-and-wear on the HPs are considerably improved. Updating and communicating the FPs, the SPs can be prolonged from every 10-15 minutes to every 20-30 minutes while observing the same or even better performance from the DLC. Prolonging the SPs can compensate for the increased amount of communicated data and hence, alleviate the need for upgrading the communication infrastructure used for the original DLC method.

Chapter 4

Optimal Bidding in Real-Time Performance-Based Regulation Markets for the Aggregators of Thermostatically Controlled Loads

Abstract—When properly controlled, thermostatically controlled loads (TCLs) can shift their power consumption by storing heat in the thermal mass, making them one of the prosperous resources for providing intra-hour ancillary services, such as load following and regulation services. As a result, there is potential benefit for aggregating TCLs to participate in the regulation markets through a load aggregator (LA). This chapter presents a stochastic optimization model to obtain the optimal bidding strategy for a price taker LA that participates in the real-time performance-based regulation market (PBRM). While determining the optimal bidding strategy to maximize the income from PBRM, the end-users comfort level and TCLs operational limits (minimum on/off time) are respected. Also, the amount of extra switching imposed on the TCLs is confined to prevent intense tear-and-wear of TCLs. The presented model is formulated considering California independent system operator (CAISO) conventions. The numerical results are presented and discussed for a LA controlling 1000 heat pumps (HPs). It is shown that without considering a bound for the TCLs switching cycles, the optimal bidding problem can lead to abrupt increase of switching cycles imposing radical tear-and-wear on TCLs.

4.1. Nomenclature

Indices, Subscribes and Superscripts

t	Index of real-time market settlement time intervals
k	Index of the 4-second time interval
i	Subscript of a TCL ($1 \leq i \leq N$)
s	Subscript of scenario ($1 \leq s \leq N_s$))
U/D	Superscript for regulation up/down
n	Superscript for normalized profiles

Parameters and Variables

T	Total number of real-time market intervals
N	Total number of TCLs
N_s	Total number of scenarios
R_i	Equivalent thermal resistance ($℃/KW$) for the i^{th} TCL
C_i	Equivalent thermal capacity ($KWh/℃$) for the i^{th} TCL

Q_i	Heat rate of the i^{th} TCL unit (KW)
COP_i	Coefficient of performance for the i^{th} TCL
$P_{Rated,i}$	Rated power of the i^{th} TCL (KW)
$U_i(\cdot)$	On/off status of the i^{th} TCL ($\{0,1\}$)
$U_{c,i}(\cdot)$	On/off control command for the i^{th} TCL ($\{0,1\}$)
$\theta_a(\cdot)$	Ambient temperature profile (℃)
$\theta_i(\cdot)$	Indoor temperature profile of the i^{th} TCL (℃)
$[\theta_i^-, \theta_i^+]$	Desired indoor temperature range of the i^{th} TCL
$\theta_{set,i}/Db_i$	Temperature setpoint/deadband of the i^{th} TCL (℃)
$P_b(\cdot)$	Baseline power profile of TCLs (MW)
$P_a(\cdot)$	Aggregated power profile of TCLs (MW)
$P_{rg,s}^{U/D,r}(\cdot)$	Power profile of recorded actual regulation up/down signals in scenario s (MW)

$P_{rg,s}^{U/D,n}(\cdot)$	Normalized power profile of recorded regulation up/down signals in scenario s (MW)
$P_{rg,s,in}^{U/D}(\cdot)$	Power profile of instructed regulation up/down signals in scenario s (MW)
$P_{rg,s,a}^{U/D}(\cdot)$	Regulation signal power profile provided by aggregation of TCLs in scenario s (MW)
$P_{rf,s}(\cdot)$	Reference power profile in scenario s (MW)
MP	Maximum power consumption of TCLs (MW)
$N_{Cnt,i}^{sw}/N_{Unc,i}^{sw}$	Number of switching for i^{th} TCL in the controlled/uncontrolled mode
$\overline{N}_{Cnt}^{sw}/\overline{N}_{Unc}^{sw}$	Average number of switching for a group of TCLs in controlled/uncontrolled mode
RSW (RSW_s)	Index of the ratio of switching (for scenario s)
RSW^*	Upper bound for the ratio of switching index

$MCPC_s^{U/D}(t)$	Market clearing price for regulation up/down capacity ($/MW) in scenario s
$MCPM_s^{U/D}(t)$	Market clearing price for regulation up/down mileage ($/MW) in scenario s
$RCI_s(t)/RPI_s(t)$	Income from regulation capacity/mileage ($) in scenario s
$C^{U/D}(t)$	Regulation up/down capacity bid (MW)
$M_s^{U/D}(t)$	Mileage of the normalized regulation up/down signal (MW) in scenario s
$PA_s^{U/D}(t)$	Performance accuracy of the regulation up/down service in scenario s

4.2. Introduction

Secondary regulation service (hereafter is called regulation service for simplicity) is one of the vital ancillary services that is under growing demand because of the increasing penetration of intermittent renewable energy resources such as wind and solar energies. Regulation service is provided through a separate market mechanism that has gone through changes after the United States Federal Energy Regulatory Commission (FERC) issued order No. 755 in Oct. 2011, [35]. Based on the FERC order No. 755, conventional regulation markets have been transformed to performance-based-regulation-markets (PBRM) wherein the

payment to regulation resources consists of two main parts: regulation capacity payment and regulation performance payment. The regulation performance payment is the new component that evaluates the quality of regulation services. Thus, when providing the same amount of service, resources with better service quality (regulation performance) will be paid more. This payment strategy motivates high quality resources (e.g. battery banks) to actively participate in regulation markets which in turn improves the regulation market efficiency and reduce the total payment for regulation service provision. For instance, the total payment for regulation services in MISO has been decreased by 24% in 2013 compared to 2012 while the regulation resources were paid only for provision of regulation capacity, [36]. Currently, majority of independent system operators (ISOs) and regional transmission operators (RTOs) submitted compliance filings to the FERC Order 755, [36].

There are different types of resources for provision of regulation service. For example, fast response generators, flywheels, battery banks, and flexible loads are all suitable resources. The profitability of participating in the PBRM for different qualified resources has been studied in the literature. For instance, [37] presents a co-optimization model for a central battery banks to maximize its profit in energy and ancillary services markets. In [38], a similar problem is investigated by aggregation and coordination of decentralized small size battery energy storage systems in distribution networks. While all those references consider the resources as price takers, [39] presents the same problem for a price maker resource and illustrates the methodology and results considering a generation firm. However, to the best of the authors' knowledge, no one has studied the similar problem for the aggregation of thermostatically

controlled loads (TCLs), which can be one of the promising resources for regulation service provision.

TCLs include water heaters, space heaters/coolers, refrigerators, and freezers and exist in large amount in residential and commercial districts. According to the report of the U.S. Energy Information Association, 20% of electricity in the U.S. is consumed by the TCLs, [14]. Because TCLs can store heat in thermal mass, they are able to shift electricity consumption from tens of minutes to hours. Therefore, the aggregated flexibility of a large TCL population can be considerable if they are controlled properly and the required control and communication infrastructure are provided. The flexibility of TCLs in changing their power consumption pattern makes them one of the promising resources for different energy and ancillary services like renewable energy smoothening [40], intra-hour load balancing [41], primary and secondary regulation [42], [16], [21], [43], and reserve provision [44].

The service provision capability of the aggregated TCLs provides them with the opportunity to participate in different power markets through an aggregator and make income like other centralized resources. There are some references in the literature studies the profit making aspects of aggregated TCLs. For instance, [41] studies the arbitrage opportunity of aggregated TCLs in real-time energy market. In [45], an optimization model is presented to use the TCLs flexibility for minimizing the energy procurement cost in day-ahead energy markets. In [46], the TCL flexibility is utilized to minimize the total imbalance cost for a group of prosumers by participating in an intra-day electricity market. In [47], the authors model the aggregated TCLs with a leaky storage system and study the profit maximization problem

through a co-optimization model when providing both energy and ancillary services. However, this reference does not consider the features of PBRM.

The main contribution of this chapter is the development of a stochastic optimization model to obtain the optimal bidding strategy for a price taker load aggregator (LA) participating in a real-time PBRM where capacity offer, provided mileage, and the performance accuracy can influence the LA's income. The optimization model strictly respects the end-users comfort level and also the operational limits of TCLs, i.e. minimum on/off time. Most importantly, the presented optimization model confines the amount of extra switching imposed on the loads (in effect of service provision) by a predefined level. This constraint prevents TCLs from frequent switching which cause the rapid tear-and-wear of TCLs. We will show that considering this constraint significantly affects the amount of income from PBRM. Thus, if the LA ignores this constraint, it will submit larger capacity bids for higher income. However, TCLs will suffer from a drastically increased number of switching that causes abrupt tear-and-wear. To the best of authors' knowledge, none of the existing research works studying the optimal bidding strategy either in energy or ancillary service markets considers putting a limit on the amount of switching cycles to limit the wear-and-tear of the TCLs.

The structure of this chapter is as follows. Section 4.3 introduces the basic concepts in TCLs dynamic thermal modelling, TCLs' tear-and-wear modelling, and the control method of TCLs where, without loss of generality, the TCLs are considered to be heat pumps (HPs). In Section 4.4, the procedure of PBRM settlement based on the convention of the California Independent System Operator (CAISO) is described in detail. Section 4.5 presents the proposed stochastic optimization model to obtain the optimal bidding strategy. The numerical

results are presented and discussed in Section 4.6 and finally, the conclusion remarks are summarized in Section 4.7.

4.3. Preliminaries

Before presenting the proposed optimization model, the modellings, methods, and concepts used throughout the chapter are briefly explained in this section.

4.3.1 TCLs Modelling

Without loss of generality, the studied TCLs in this chapter are considered to be heat pumps (HPs). There are different mathematical models in the literature to model the thermal dynamics of HPs, [31]. In this chapter, the 1st order (discretized) model presented in [31] and [50] is used.

$$\theta_i(k+1) = U_i(k+1)\,\theta_i^{ON}(k+1) + \big(1 - U_i(k+1)\big)\,\theta_i^{OFF}(k+1) \tag{4-1-a}$$

$$\theta_i^{ON}(k+1) = \theta_a(k) + Q_i R_i - \big(\theta_a(k) + Q_i R_i - \theta_i(k)\big)e^{-T_s/R_i C_i} \tag{4-1-b}$$

$$\theta_i^{OFF}(k+1) = \theta_a(k) - \big(\theta_a(k) - \theta_i(k)\big)e^{-T_s/R_i C_i} \tag{4-1-c}$$

$$U_i(k+1) = \begin{cases} 1 & \theta_i(k+1) < \theta_i^- \ \ or\ U_{c,i}(k) = 1 \\ U_i(k) & \theta_i^- < \theta_i(k+1) < \theta_i^+ \\ 0 & \theta_i^+ < \theta_i(k+1)\ or\ U_{c,i}(k) = 0 \end{cases} \tag{4-1-d}$$

$$Q_i = COP_i\ P_{Rated,i} \tag{4-1-e}$$

$$\theta_i^+ = \theta_{set,i} + Db/2 \qquad \theta_i^- = \theta_{set,i} - Db/2 \tag{4-1-f}$$

A heterogeneous control group including 1000 HPs are constructed to numerically simulate the proposed method. The randomization process presented in the Appendix is used to

randomize the thermal parameters and settings. After implementing the randomization, the PDFs of R_i, C_i, and Q_i $(1 \leq i \leq N)$ are obtained, as shown in Fig. 4.1.

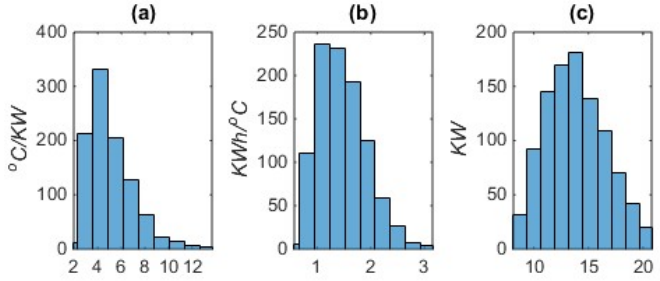

Fig. 4.1. PDFs of R, C, and Q for 1000 HPs.

4.3.2. Power Tracking Control Method

A group of HPs can provide regulation service if they are properly controlled so that their aggregated power profile, $P_a(\cdot)$, track a reference power profile, $P_{rf}(\cdot)$. The $P_{rf}(\cdot)$ is derived from the summation of baseline power profile, $P_b(\cdot)$, and the regulation signal, $P_{rg}(\cdot)$. In other words, the controlled deviation of $P_a(\cdot)$ from $P_b(\cdot)$ is equivalently considered as regulation service provision, [21]. It should be noted that $P_b(\cdot)$ is the averaged power profile of HPs if they operate in the uncontrolled mode where HPs are controlled only based on their thermostat control logic (and not through an external controller). In order to control $P_a(\cdot)$, the centralized direct load control (DLC) method based on temperature-priority-list (presented in Chapter 2) is used where all HPs are observable and controllable. In this study, the thermal parameters and settings of the TCLs are assumed to be known. Therefore, the DLC method is implemented in open-loop manner and without feedback measurements. Figure 4.2(a) represents the $P_b(\cdot)$ for a control group including 1000 heterogeneous HPs. $P_b(\cdot)$ is constructed

using the outdoor temperature profile, $\theta_a(\cdot)$, that is shown in Fig. 4.2(d). Fig. 4.2(b) shows the profile of a 1 MW $P_{rg}(\cdot)$ (adopted from [51]) and then $P_{rf}(\cdot)$ is constructed as shown in Fig. 4.2(c).

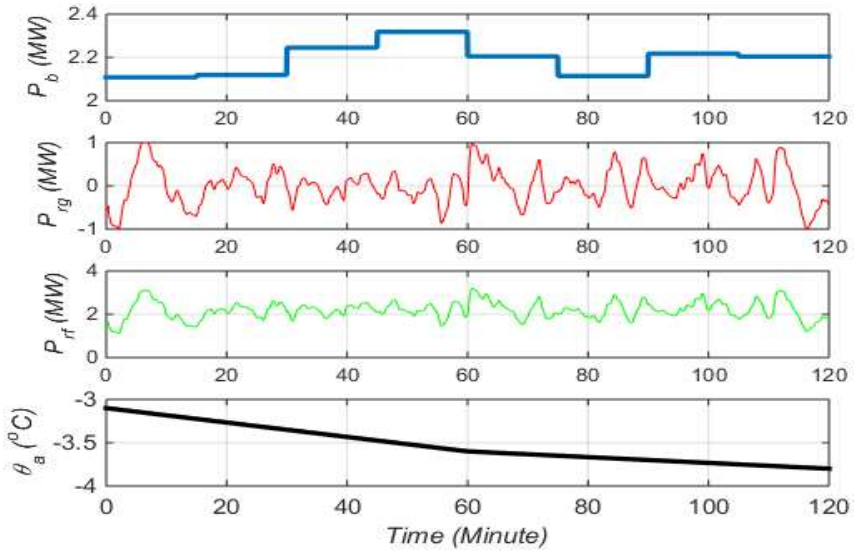

Fig. 4.2. Profile of (a) P_b, (b) a typical P_{rg}, (c) P_{rf}, and (d) θ_a within two hours.

4.3.3. Ratio of Switching Index

Controlling HPs for provision of regulation services impose extra amount of switching cycles on the individual HPs which in turn results in tear-and-wear of HPs, [21] and [34]. In order to model the imposed tear-and-wear quantitatively, the RSW index is used, [34], and presented as follows,

$$RSW = \bar{N}_{Cnt}^{SW} / \bar{N}_{Unc}^{SW} \tag{4-2}$$

where

$$\bar{N}_{Cnt}^{SW} = \frac{1}{N}\sum_{i=1}^{N} N_{Cnt,i}^{SW} \quad (4\text{-}3\text{-a})$$

$$\bar{N}_{Unc}^{SW} = \frac{1}{N}\sum_{i=1}^{N} N_{Unc,i}^{SW}. \quad (4\text{-}3\text{-b})$$

It is important to clarify the difference between the operational constraints of TCLs and the concept of the RSW index. Different types of HPs, freezers and refrigerators perform the space heating/cooling through their compressors which are electromechanical devices with their own physical specifications and constraints. The minimum on/off time constraint requires TCLs not to change their on/off status for a specified amount of time, similar to the minimum on/off time of generation units. Even by respecting the minimum on/off constraints, the switching cycles of a TCL can still change in comparison to the uncontrolled operation mode. The cycling modifications are brought about by the external control in order to deliver regulation service and make the TCL to be switched more frequently. This in turn imposes tear-and wear on the TCL as the compressor is toggled more frequently. The RSW is the index to quantify the amount of tear-and-wear imposed on the TCLs.

4.4. Regulation Market Settlement

According to the FERC Order No.755, the payment to the regulation service resources consist of two parts called capacity payment and performance payment with the following general forms, [35], [50].

$$RCI^{U/D}(t) = C^{U/D}(t)\ MCPC(t)\ PF^{U/D}(t) \quad (4\text{-}4)$$

$$RPI^{U/D}(t) = M^{U/D}(t)\, MCPM(t)\, PF^{U/D}(t) \tag{4-5}$$

However, the implementation of the above payment settlements is slightly different for each ISO/RTO. Without loss of generality, this chapter considers the settlement procedure used by California ISO (CAISO) in order to implement (4-4)-(4-5) and therefore, the detailed formulation is presented as follows.

4.4.1. Mileage Calculation

Mileage is a performance measure representing the amount of up/down power movement in the instructed regulation signal or the actual response of the resource, depending on the ISO/RTO convention, [50]. CAISO uses both instructed regulation signal and the actual response of regulation resource for mileage calculation within every 15 minute time interval, [32]. Considering scenario s with the instructed regulation up/down signal, $P_{rg,s}^{U/D}(\cdot)$, CAISO calculates the mileage over the t^{th} time interval as follows, [32, pp. 16-17] and [50].

$$M_s^{U/D}(t) = \sum_{k=225(t-1)+1}^{225t} \left| m_s^{U/D}(k) - m_s^{U/D}(k-1) \right|, \tag{4-6}$$

where

$$\text{If } \left(P_{rg,s,in}^{U/D}(k) - P_{rg,s,in}^{U/D}(k-1)\right)\left(P_{rg,s,in}^{U/D}(k-1) - P_{rg,s,in}^{U/D}(k-2)\right) > 0 \tag{4-7-a}$$

$$\text{Then } m_s^{U/D}(k) = \left| P_{rg,s}^{U/D}(k) - P_{rg,s}^{U/D}(k-1) \right| \tag{4-7-b}$$

$$\text{If } \left(P_{rg,s,in}^{U/D}(k) - P_{rg,s,in}^{U/D}(k-1)\right)\left(P_{rg,s,in}^{U/D}(k-1) - P_{rg,s,in}^{U/D}(k-2)\right) < 0 \quad \text{and} \quad \left(P_{rg,s,in}^{U/D}(k) \geq P_{rg,s,in}^{U/D}(k-1)\right) \tag{4-7-c}$$

Then $m_s^{U/D}(k) = \left|P_{rg,s,in}^{U/D}(k) - P_{rg,s,in}^{U/D}(k-1)\right| - Min\Big\{Max\{P_{rg,s,a}^{U/D}(k-1) - P_{rg,s,in}^{U/D}(k-1), 0\}, P_{rg,s,in}^{U/D}(k) - P_{rg,s,in}^{U/D}(k-1)\Big\}$ (4-7-d)

If $\left(P_{rg,s,in}^{U/D}(k) - P_{rg,s,in}^{U/D}(k-1)\right)\left(P_{rg,s,in}^{U/D}(k-1) - P_{rg,s,in}^{U/D}(k-2)\right) < 0$ and $\left(P_{rg,s,in}^{U/D}(k) \le P_{rg,s,in}^{U/D}(k-1)\right)$ (4-7-e)

Then $m_s^{U/D}(k) = \left|P_{rg,s,in}^{U/D}(k) - P_{rg,s,in}^{U/D}(k-1)\right| - Min\Big\{Max\{P_{rg,s,in}^{U/D}(k) - P_{rg,s,a}^{U/D}(k), 0\}, P_{rg,s,in}^{U/D}(k) - P_{rg,s,in}^{U/D}(k+1)\Big\}$ (4-7-f)

Note that t represents the index of market settlement time interval (15 minutes time intervals) and 225 represents the number of the 4-second intervals (the granularity of regulation signal) in one 15-minute interval.

According to (7a)-(7b), if $P_{rg,s,in}^{U/D}(\cdot)$ is monotonically increasing/decreasing, the mileage is calculated only based on the instructed regulation signal, $P_{rg,s,in}^{U/D}(\cdot)$. In other words, the mileage is derived by $\left|P_{rg,s,in}^{U/D}(k) - P_{rg,s,in}^{U/D}(k-1)\right|$ which is called "*instructed mileage"*. However, according to (7c)-(7f), if $P_{rg,s,in}^{U/D}(\cdot)$ is not monotonically increasing/decreasing, a slightly different mileage calculation rule is applied to reflect the effect of under-response, [32, pp. 16-17] and [50]. In this manner, mileage calculation is based on both instructed regulation signal and the actual response, $P_{rg,s,in}^{U/D}(\cdot)$ and $P_{rg,s,a}^{U/D}(\cdot)$, respectively, and the mileage term in (7d)-(7f) are called "*adjusted mileage"*. The adjusted mileage is derived by subtracting a "*mileage reduction term"* from the instructed mileage.

Figure 4.3 demonstrates the situations that $P_{rg,s,in}^{U/D}(\cdot)$ is not monotonically increasing/decreasing. The solid lines indicates $P_{rg,s,in}^{U/D}(\cdot)$ and the numbered circles indicate $P_{rg,s,in}^{U/D}(\cdot)$ in three different cases. In Fig. 4.3(a), $P_{rg,s,in}^{U/D}(\cdot)$ first decreases and then increases. In Case1, $P_{rg,s,a}^{U/D}(k-1)$ is smaller than $P_{rg,s,in}^{U/D}(k-1)$ and according to (4-7), the mileage reduction is zero. Therefore, the adjusted mileage is the same as the instructed mileage. In Case2, $P_{rg,s,a}^{U/D}(k-1)$ is larger than $P_{rg,s,in}^{U/D}(k-1)$ and smaller than $P_{rg,s,in}^{U/D}(k)$. Therefore, according to (7d), the mileage reduction term of $\left\{P_{rg,s,a}^{U/D}(k-1)-P_{rg,s,in}^{U/D}(k-1)\right\}$ is subtracted from the instructed mileage to reflect the actual movement of $P_{rg,s,a}^{U/D}(\cdot)$. In this case, the resource changes its power as much as $\left\{P_{rg,s}^{U/D}(k)-P_{rg,s,a}^{U/D}(k-1)\right\}$ and moves toward the third instructed power value. Thus, the amount of movement is smaller than $\left\{P_{rg,s,in}^{U}(k)-P_{rg,s,in}^{U}(k-1)\right\}$ and counting mileage based on the instructed mileage is mileage over-counting. In Case3, $P_{rg,s,a}^{U/D}(k-1)$ is larger than both $P_{rg,s,in}^{U/D}(k)$ and $P_{rg,s,in}^{U/D}(k-1)$. Recall that the actual response is expected to first decrease at the time instant $k-1$ and then increase at the time instant k. However, the actual response at time instant $k-1$ is so larger that it still has to decrease to follow the instructed signal at time instant k and thus, CAISO does not count any mileage in this case. A similar analysis can be applied to Fig. 4.3(b) where $P_{rg,s,in}^{U/D}(\cdot)$ increases first and then decreases.

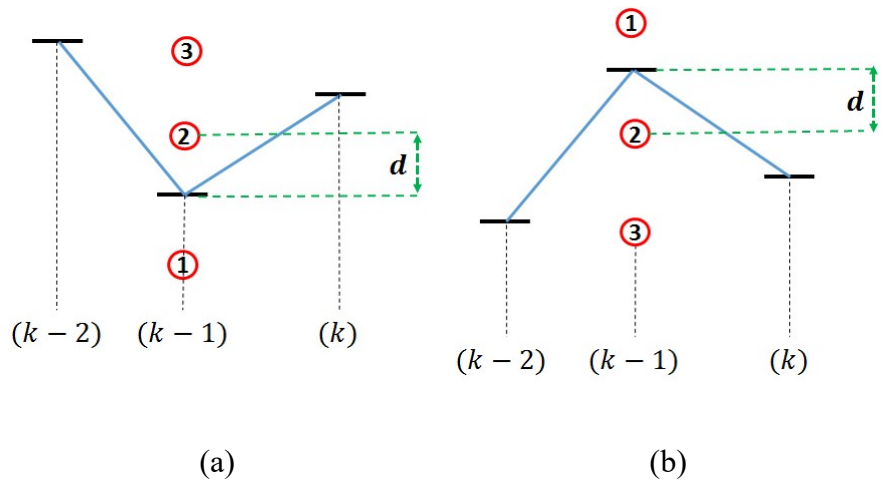

(a) (b)

Fig. 4.3. An illustrative example for mileage calculation of non-monotonically increasing/decreasing regulation signals.

4.4.2. Performance Accuracy

Accuracy is a performance measure representing how closely the actual responses of a regulation resource ($P_{rg,s,a}^{U/D}(\cdot)$) tracks the instructed regulation signal ($P_{rg,s,in}^{U/D}(\cdot)$). Despite the similar concept, different ISOs/RTOs use slightly different methods to define and calculate performance accuracy. Similar to mileage, CAISO calculates the performance accuracy for a resource over 15 minute time intervals, [32, pp. 19]. Given an instructed up/down regulation signal for scenario s, CAISO calculates the performance accuracy using the following formulation

$$PA_s^{U/D}(t) = Max\left\{0, \frac{\sum_{k=225(t-1)+1}^{225t}\left(\left|P_{rg,s,in}^{U/D}(k)\right| - \left|P_{rg,s,in}^{U/D}(k) - P_{rg,s,a}(k)\right|\right)}{\left|\sum_{k=225(t-1)+1}^{225} P_{rg,s,in}^{U/D}(k)\right|}\right\} \quad (4\text{-}8)$$

It is noteworthy to mention that CAISO reflects the effect of accuracy "*only in the mileage payment*" and "*not in the capacity payment*", [32], [50]. Thus, the performance accuracy only

affects the mileage payment.

4.5. Problem Formulation

This section presents the optimization model to derive the optimal bidding for a LA participating in a real-time PBRM assuming that the LA only participates into the PBRM. The objective is to maximize the income from the PBRM while respecting end-users' comfort and the HP operating constraints, and also confining the RSW to a predefined value.

4.5.1. Objective Function

According to the payment structure defined by (4-4)-(4-5), the expected income from PBRM is calculated as

$$f = \frac{1}{N_s}\sum_{s=1}^{N_s}\left[\sum_{t=1}^{T}\left(RCI_s^U(t) + RCI_s^D(t)\right) + \sum_{t=1}^{T}\left(RPI_s^U(t) + RPI_s^D(t)\right)\right], \quad (4\text{-}9)$$

where

$$RCI_s^{U/D}(t) = C^{U/D}(t)\, MCPC_s^{U/D}(t) \quad (4\text{-}10)$$

$$RPI_s^{U/D}(t) = MCPM_s^{U/D}(t)\, M_s^{U/D}(t)\, PA_s^{U/D}(t). \quad (4\text{-}11)$$

The objective function is the expected value of total income from the PBRM and therefore, it is stated in the stochastic form because of the uncertainties in the following variables: 1) capacity prices, 2) mileage prices, and 3) regulation signals that affect mileage. The first summation term in (4-9) is the income from provided regulation capacity and the second summation term is the income from regulation performance. It is noted that each scenario corresponds to a set of data including $P_{rg,n,s}^{U/D}(\cdot)$, $MCPC_s^{U/D}(\cdot)$, and $MCPM_s^{U/D}(\cdot)$ over the

considered time horizon T. The decision variables are $C^{U/D}(t), 1 \leq t \leq T$ that are actually the quantity of regulation capacity bids (in MW).

Generally, a regulation resource submits two types of bids to the PBRM: capacity and mileage. In CAISO, capacity bid has utmost three attributes: a) capacity bid quantity (MW), b) capacity bid price ($/MW), c) and optional opportunity cost ($/MW). The mileage bid has only one attribute, which is the mileage price ($/MW), [32, pp. 25-27]. As mentioned before, this chapter studies the case of a price-taker regulation resource. Therefore, the LA does not consider prices as decision variables in (4-9) and its capacity price bids only covers the cost of service provision (which can be for instance the amount of contract with the end-users to control their TCLs). Also, it is assumed that the LA only participates in the PBRM and the opportunity cost is considered as zero. Therefore, the goal of the optimal biding problem is to determine the "*optimal capacity bid quantities"* over a time horizon T to maximize the income received from the real-time PBRM.

It is also important to point out how to prepare the actual recorded regulation signal profiles so that they are appropriate to be used in the stochastic optimization model defined by (4-9). The actual recorded regulation signal data ($P_{rg,s,ins}^{U/D,r}(\cdot)$) are normalized with respect to the maximum absolute value in every time interval t and the corresponding normalized regulation signal profiles are constructed. Then, using the decision variables, the regulation power profile for scenario s and within time interval t is constructed as follows,

$$P_{rg,s,in}^{U/D}(k) = C^{U/D}(t)\, P_{rg,s,in}^{U/D,n}(k) \tag{4-12}$$

where

$$225(t-1)+1 \le k \le 225\,t$$

$$1 \le t \le T$$

$$P_{rg,s,in}^{U/D,n}(k) = \frac{P_{rg,s,in}^{U/D,r}(k)}{\max\limits_{225(t-1)+1 \le k \le 225t} \left| P_{rg,s,in}^{U/D,r}(k) \right|}. \tag{4-13}$$

After constructing the regulation signal for scenario s, the reference power profile within the time interval t is constructed as follows,

$$P_{rf,s}(k) = P_b(k) + P_{rg,s,in}^{U}(k) + P_{rg,s,in}^{D}(k)$$

$$225(t-1)+1 \le k \le 225t \tag{4-14}$$

$$1 \le t \le T.$$

It is obvious that at every moment, either $P_{rg,s}^{U}(\cdot)$ or $P_{rg,s}^{D}(\cdot)$ is zero because regulation-up and regulation-down services are not needed simultaneously.

4.5.2. Constraints

Three main constraints are considered while modeling the optimal bidding strategy problem for a LA. The first constraint respects the end-users comfort by keeping the temperature within the desired range. The second constraint is the operational limit (minimum on/off time) of HPs and finally, the third constraint confines the amount of tear-and-wear imposed on the loads by keeping the RSW index less than or equal to an upper bound, RSW^*. The first and second constraints are respected through the local retrofit circuit of HPs. That is, if the external control command results in the violation of an end-user comfort level, the local

retrofit circuit overrides the external control command. Similarly, if an HP is commanded to turn on/off while its operational limit has not been satisfied yet, the circuit avoids the control command. The protective action of the local retrofit circuits to consider the two constraints are modelled within the DLC method code package. The third constraint is modeled as follows

$$RSW_s \leq RSW^* \ \ (1 \leq s \leq N_s) \tag{4-15}$$

It is noted that the RSW in (4-16) appears with the subscript s because its numerical value depends on the profile of $P_{rg,s,in}^{U/D}(\cdot)$ corresponding to the scenario s. The constraint in (4-16) states that the ratio of switching index should be smaller than or equal to RSW^* for all scenarios. The calculation procedure of RSW is discussed more in subsection *4.5.4*.

4.5.3. Bounds

The decision variables ($C^{U/D}(t)$, $1 < t < T$) are required to be within a specific bound determined by the physical limits of the HPs. It is evident that $P_{a,s}(\cdot)$ is maximum when all HPs are "on" and it is minimum (zero) when all HPs are "off". Therefore, the decision variables are chosen so that $0 \leq P_{rf,s}(\cdot) \leq MP = \sum_{i=1}^{N} P_{Rated,i}$. Therefore, according to (4-14) and the fact that $\left|P_{rg,s,in}^{U/D,n}(\cdot)\right| \leq 1$, the bounds for decision variables are derived as follows.

$$0 \leq C^U(t) \leq MP - P_b(t) \tag{4-16}$$

$$0 \leq C^D(t) \leq P_b(t) \tag{4-17}$$

The above concept is shown conceptually in Fig. 4.4 for the considered control group in Section 4.3.

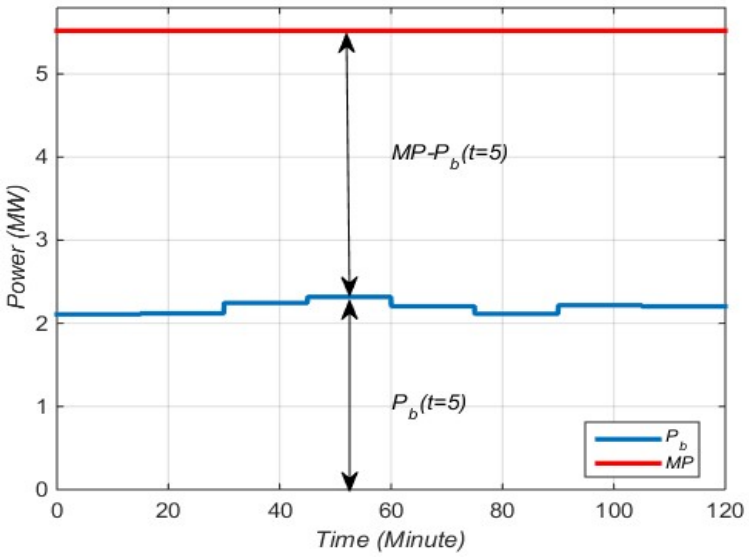

Fig. 4.4. Representation of regulation up/down capacity bounds for a group of 1000 HPs.

4.5.4. Discussion on the Optimization Problem

Unlike other central resources such as generators and battery banks, one of the main characteristic of the optimization problem of TCL resources is the non-explicit functionality of both objective function and the constraint in terms of the decision variables.. The objective function is non-explicit function because the $P_{a,s}(\cdot)$ is non-explicit functions of $C^{U/D}(t)$ so does $M_s^{U/D}(\cdot)$ and $PA_s^{U/D}(\cdot)$. Similarly, according to (4-2)-(4-3), the RSW does not have closed-form relation with respect to the decision variables. Therefore, considering a set of decision variables and after construction of $P_{rf,s}(\cdot)$ using (4-14), the numerical values of f and RSW are determined after performing the DLC over the time horizon T. Fig. 4.5 shows the general framework of solving the optimization problem.

In the literature (e.g. [47] and [48]), compact models for aggregation of TCLs were proposed. However, those modeling approaches have two main problems. First, the minimum

on/off time of the TCLs is not considered when modelling TCLs, so the capability of the TCL group for providing services can be significantly overestimated. Second, because the switching cycles of TCLs are not accounted for, the amount of tear-and-wear of TCLs because of providing the service are not considered in their optimization problem formulation. To overcome those problems, we modeled each TCL as well as the DCL control logic in detail when solving the optimization problems.

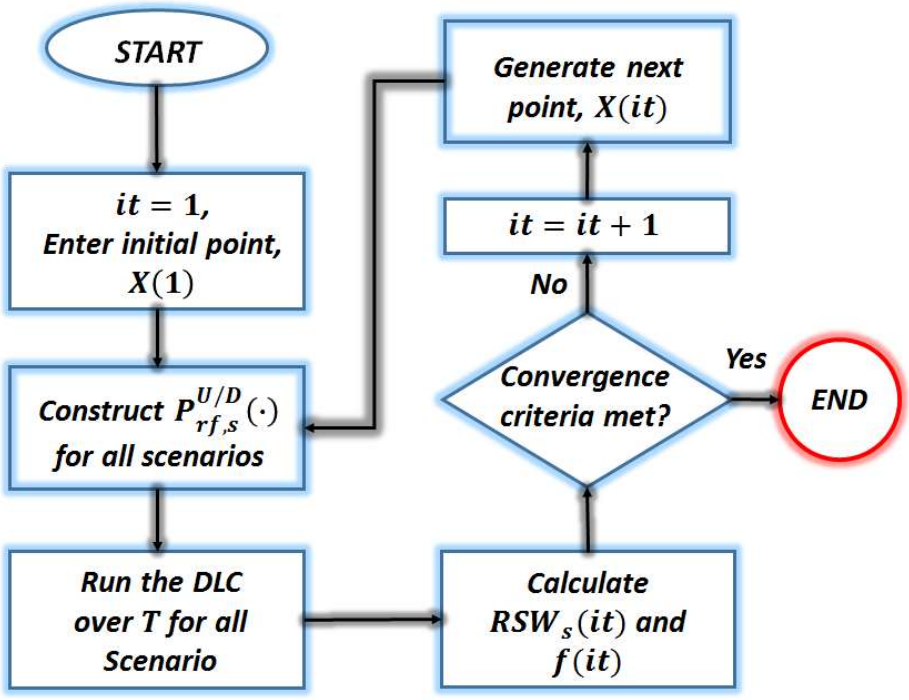

Fig. 4.5. General framework of solving the optimization problem.

To solve the constrained optimization model, the constraint in (4-15) is modeled by adding the constraint to the objective function through a large penalty factor so that the optimal bidding strategy is derived by solving the following unconstrained optimization problem,

$$\min_{\substack{C^U(t),\, C^D(t) \\ 1 \le t \le T}} \left[-f + PF \frac{1}{N_s} \sum_{s=1}^{N_s} g(RSW_s) \right] \tag{4-18}$$

where

$$g(RSW) = \begin{cases} (RSW_s - RSW^*)^2 & if\ (RSW_s \geq RSW^*) \\ 0 & if\ (RSW_s < RSW^*) \end{cases} \tag{4-19}$$

$$f = \frac{1}{N_s} \sum_{s=1}^{N_s} \left[\sum_{t=1}^{T} (RCI_s^U(t) + RCI_s^D(t)) + \sum_{t=1}^{T} \left(RPI_s^U(t) + RPI_s^D(t) \right) \right],$$

According to the form of the objective function and the constraint of (4-15), the optimization problem is nonlinear and non-convex; therefore, global optimization solvers are required to solve the problem. In this chapter, the pattern search solver in MATLAB, [51] is used to solve (4-18) and the penalty factor is considered to be $PF = 10^4$.

4.6. Simulation Results

This section presents and discusses the numerical results derived by applying the proposed optimization model for a LA participating in CAISO real-time PBRM. The LA controls the aggregated power consumption of 1000 heterogeneous HPs using the DLC method presented in [21]-[22]. The DLC method is coded using MATLAB programming language and converted to a MEX file to increase the speed of DLC execution, and hence the solving of the optimization problem. The regulation capacity prices, regulation mileage prices, and the regulation signal data corresponding to the first week of Dec. 2015 are adopted from [52]. Therefore, seven scenarios are considered in the simulations ($N_s = 7$). Also, it is noted that,

without loss of generality, the prices for upward and downward regulation capacity are considered to be the same. Similarly, the prices of regulation up/down mileage are considered to be equal. Two simulation cases are studied in this section which is presented as follows.

4.6.1. Case 1: Single Horizon Scheduling

In the first case, the optimization problem is solved only for a single scheduling horizon to demonstrate the results and mainly investigate the effect of confining the RSW on the income from the PBRM. A scheduling horizon of two hours including eight time intervals is considered ($T = 8$) and therefore, the number of decision variables is sixteen. The profiles of $P_b(\cdot)$ and $\theta_a(\cdot)$ are shown in Fig. 4.2(a) and Fig. 4.2(d). The RSW index is confined to 2.5; i.e. $RSW^* = 2.5$. Figure 6 shows the average price of regulation capacity and mileage where the average price for each time interval is calculated for all scenarios.

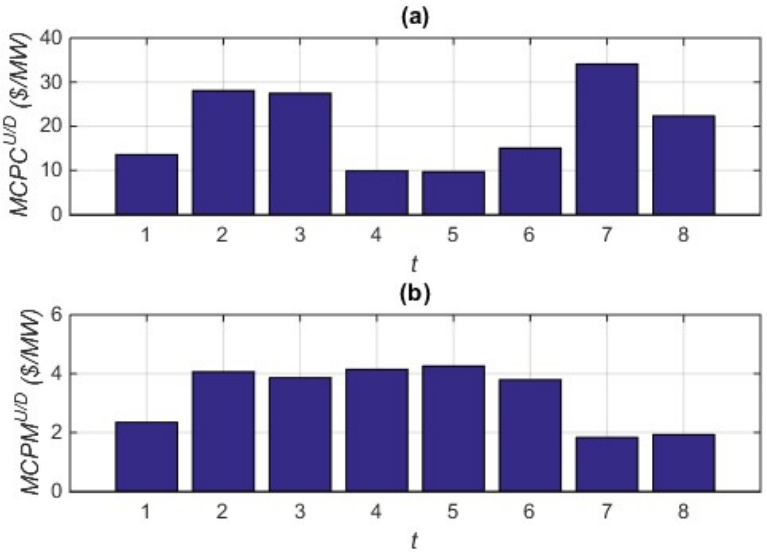

Fig. 4.6. The mean value of (a) regulation up/down capacity prices and (b) mileage up/down prices.

The optimization model of (19) is solved and the income from regulation capacity and regulation performance are derived as $RCI = \$238.3$ and $RPI = \$120.7$, respectively; therefore, the total income from the PBRM is $f = \$359.1$. The total elapsed time to solve (19) using the pattern search solver is approximately six minutes using a PC with i7-4790 CPU @ 3.60 GHz and 16.0 GB of RAM.

Figure 4.7 and Fig. 4.8 represent the optimal decision variables and the mean value of provided mileage up/down at every time interval, respectively. Note that the mean value is calculated over all scenarios, i.e. $\bar{M}^{U/D}(t) = \sum_{s=1}^{7} M_s^{U/D}(t)$.

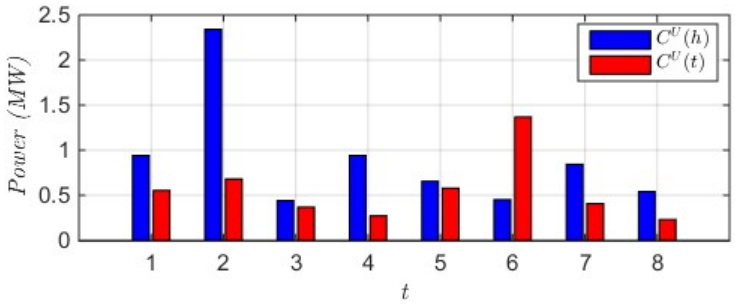

Fig. 4.7. Optimal capacity bids for regulation up and regulation down.

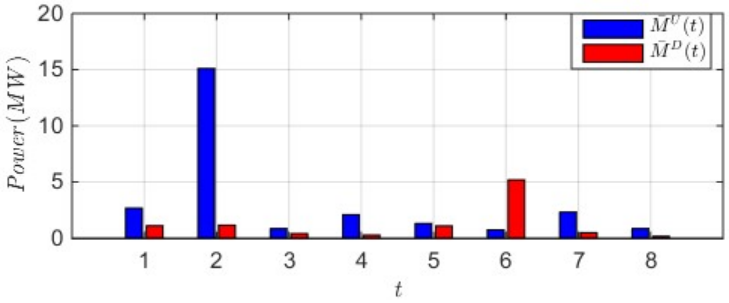

Fig. 4.8. Average regulation mileages.

Figure 4.9 shows the mean value of performance accuracy, $\overline{PA}^{U/D}(t)$. As it is observed form Fig. 4.9, the performance accuracy is relatively high and varies within $[0.83,0.98]$.

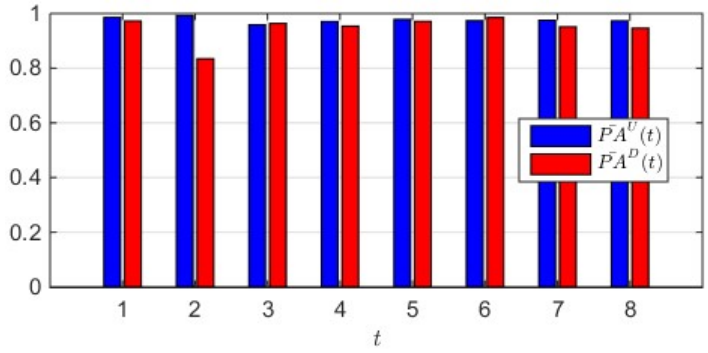

Fig. 4.9. The average performance accuracy.

Figure 4.10 shows the variations of the RCI, RPI, and the total income, f, with respect to RWS^* to better demonstrate the effect of considering this constraint in the optimization model. The RWS^* varies from 1.1 to 9 and the total income changes from \$122.8 to \$1268.2, respectively. As it is expected, the higher value of RWS^* yields higher income. According to the figure, if the RSW is not confined, the optimal capacity bids will result in the excessive switching of HPs ($RSW > 9$) which in turn proves that it is important to model this constraint in optimal bidding problems.

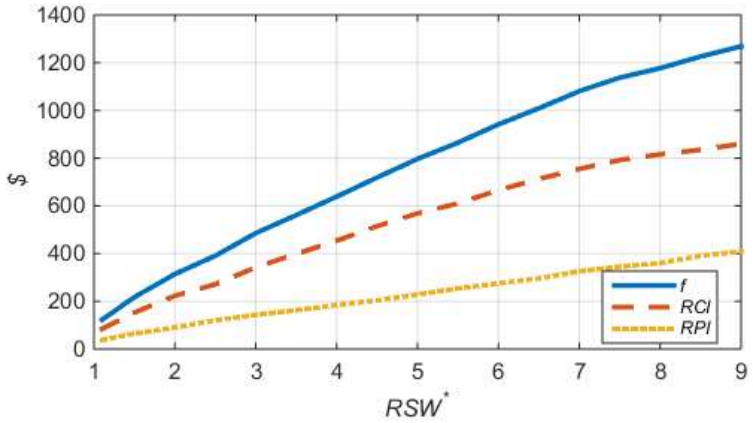

Fig. 4.10. The variations of f, RCI, RPI versus RSW^*.

4.6.2. Case 2: 24-Hour Scheduling

In the second case, the real-time optimal bidding problem is solved repetitively while the scheduling horizon is receding toward the end of a day. The optimization problem is solved once per every 15 minutes, and among all decision variables, only the one corresponding to the first time interval of the scheduling horizon is considered to be the final decision. Therefore, the optimization problem is solved $96 = (24 \times 4)$ times during the day. The RCI and RPI are derived as \$2486.6 and \$1308.7 respectively; therefore, the total income is \$3795.3 for the whole day. Figure 4.11 shows the derived optimal bids together with the average regulation capacity prices where it is observed that within the time intervals with high capacity prices either $C^U(t)$ or $C^D(t)$ have high values. For instance, within $17 \leq t \leq 19$ and $31 \leq t \leq 36$ the capacity bids are relatively large.

Figure 4.12 shows the average value of mileage up/down, the average regulation up/down mileage prices, and performance accuracy index. Figure 4.13 represents the regulation up/down performance accuracy within the day where it is seen that the $\overline{PA}^U$ and $\overline{PA}^D$ varies within [0.84,0.99] and [0.83,0.98].

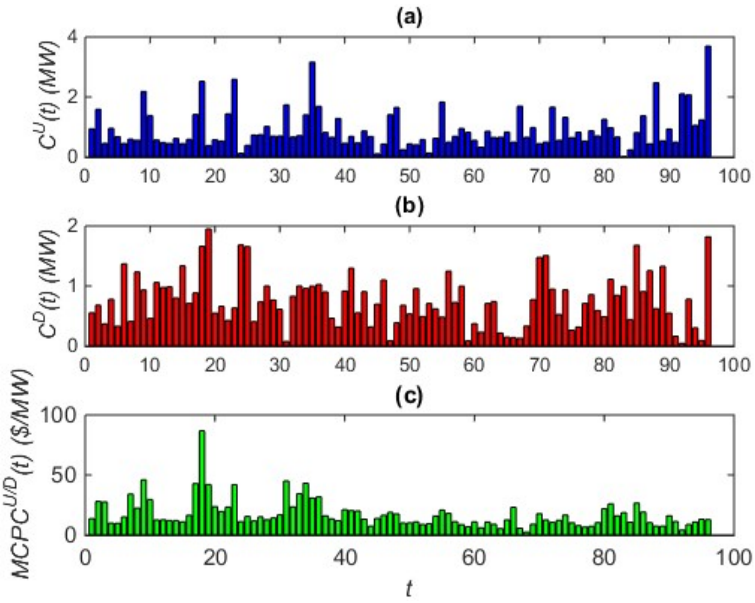

Fig. 4.11. (a) Optimal regulation up capacity bid, (b) Optimal regulation down capacity bid, (c) the average regulation up/down prices.

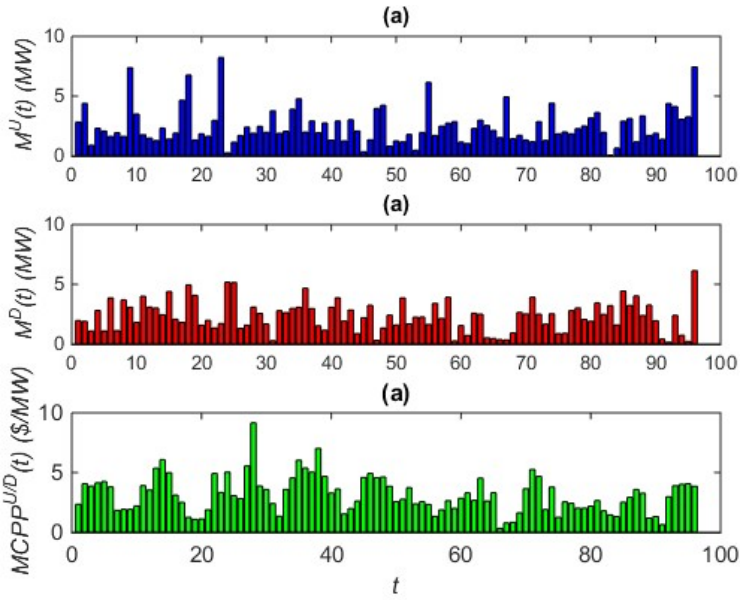

Fig. 4.12. (a) The provided mileage up, (b) provided mileage down, and (c) average mileage prices.

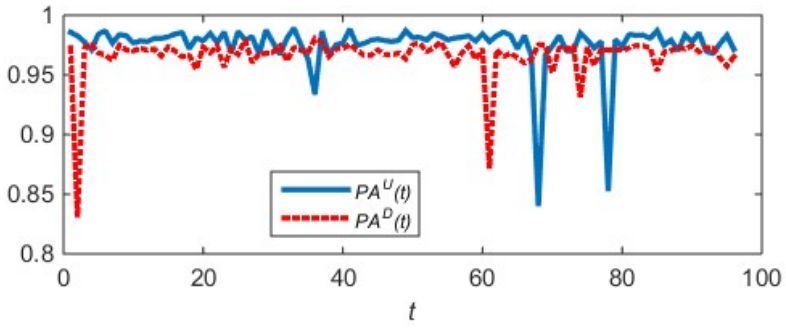

Fig. 4.13. The average performance accuracy.

4.7. Summary

This chapter presents a stochastic optimization model to obtain the optimal bidding strategy for an aggregator of thermostatically controlled loads (TCLs) participating in real-time performance-based regulation market (PRBM) where the quality of regulation service affects the payment to the service provider. Without loss of generality, the conventions of California Independent System Operator (CAISO) for mileage and performance accuracy calculations are used while formulating the problem. The goal of the stochastic optimization model is to maximize the income from the PBRM while respecting the end-users comfort level, minimum on/off time of TCLs, and also confining the amount of extra switching imposed on the loads in effect of regulation service provision. The presented optimization model uses the detached model of individual TCLs in order to model RSW constraint. The numerical evaluation of the objective function and RSW constraint is performed after implementing the direct load control (DLC) over the scheduling time horizon and at every iteration of the optimization algorithm.

The constraint on the switching is modeled by the ratio of switching index (RSW). The simulation results of an optimal bidding problem considering a LA controlling 1000 heterogeneous heat pumps (HPs) show that ignoring the RSW constraint yields excessive switching of the TCLs, while using the proposed algorithm, a realistic operation schedule for each TCL can be achieved to maximize the LA profile while meeting the comfort and wear-and-tear requirement from the TCL owners.

Chapter 5

A Reward Allocation Mechanism for Thermostatically Controlled Loads Participating in Regulation Services

Abstract-When properly controlled, thermostatically controlled loads (TCLs) can shift their electricity consumption by storing heat in the thermal masses. This capability makes them proper resources to provide variety of services in power grids, specifically intra-hour ancillary services, like regulation services. Because TCLs have diverse thermal characteristics, their capabilities of service provision can be different. Therefore, their contribution in service provision and their monetary reward might be different as well. This chapter presents a reward allocation mechanism for a load aggregator (LA) to determine the payment to be made to TCLs according to their contribution in the provided regulation services. A service provision capability index (SPCI) is proposed to quantify the TCLs capability and prioritize them accordingly. Based on the prioritization results, a reward curve is constructed to determine the TCLs payment according to their contribution to the overall provided service. The proposed rewarding system is demonstrated and verified through numerical simulations using a group of 10,000 heterogeneous heat pumps (HPs).

5.1. Nomenclature

Acronyms

DLC	Direct load control
HP	Heat pump
LA	Load aggregator
MSC	Maximum service capacity
TCL	Thermostatically controlled load
SPCI	Service provision capability index

Indices, Parameters, and Variables

N	Total number of TCLs
i	Subscript of a TCL ($1 \leq i \leq N$)
R_i	Equivalent thermal resistance (℃/KW) for i^{th} TCL
C_i	Equivalent thermal capacity (KWh/℃) for i^{th} TCL
Q_i	Heat rate of i^{th} TCL unit (KW)
COP_i	Coefficient of performance for i^{th} TCL
$P_{Rated,i}$	Rated power of i^{th} TCL (KW)
$U_i(\cdot)$	On/off status of i^{th} TCL ($\{0,1\}$)
$U_{c,i}(\cdot)$	On/off control command for i^{th} TCL ($\{0,1\}$)
$\theta_a(\cdot)$	Ambient temperature profile (℃)
$\theta_i(\cdot)$	Indoor temperature profile of i^{th} TCL (℃)
$[\theta_i^-, \theta_i^+]$	Desired indoor temperature range of i^{th} TCL

$\theta_{set,i}/Db_i$	Temperature setpoint/deadband of i^{th} TCL (℃)
$T_{on,i}/T_{off,i}$	On/Off cycling time of i^{th} TCL (Minute)
$T_{on,i}^{ml}/T_{off,i}^{ml}$	Minimum lock time in on/off status for i^{th} TCL (Minute)
T_H	Regulation service provision time horizon (24 hours in this chapter)
T_S	Discretization time period (4-Seconds in this chapter)
N_{TI}	Number of regulation time intervals in the time horizon T_H ($24 \times 60 \times 15 = 21600$ in this chapter)
n	Number of regulation time intervals (4-second intervals) within a market settlement time interval ($225 = 15 \times 15$)
MTI	The total number of regulation market settlement time intervals in a time horizon of T_H ($MTI = 96 = 24 \times 4$ in this chapter)
k	Index of 4-second time intervals ($1 \leq k \leq 21600$)
l	Index of market settlement time interval ($1 \leq l \leq 96$)
$P_a(\cdot)$	Aggregated power profile of TCLs (MW)
$P_{rf}(\cdot)$	Reference power profile (MW)
$P_b(\cdot)$	Baseline power profile of TCLs (MW)
$P_{rg,ins}(\cdot)$	The instructed regulation service power profile (MW)
$P_{rg}(\cdot)$	The regulation service power profile provided by the load aggregation (MW)

$P_{rg}^{n}(\cdot)$	Normalized regulation service power profile (MW) provided by the load aggregation (MW)
λ	Scaling factor of $P_{rg}^{n}(\cdot)$
SQ	Service quality index
P_c	Breakpoint value for power (MW)
$\overline{N}_{cnt}^{sw}/\overline{N}_{cnc}^{sw}$	Average number of switching for a group of TCLs in controlled/uncontrolled mode
$N_{cnt,i}^{sw}/N_{unc,i}^{sw}$	Number of switching for i^{th} TCL in the controlled/uncontrolled mode
RSW	Ratio of switching index
RSW^{*}	Upper limit for ratio of switching index
$P_{rg,a}^{n,U}(\cdot)$	Positive part of a normalized regulation service power profile (MW)
$P_{rg,a}^{n,D}(\cdot)$	Negative part of a normalized regulation service power profile (MW)
$\lambda_1^{max}(k)$	Maximum scaling factor of $P_S^{n-}(k)$
Λ_1^{max}	Maximum scaling factor of P_S^{n-} within T_H
$\lambda_2^{max}(k)$	Maximum scaling factor of $P_S^{n+}(k)$
Λ_2^{max}	Maximum scaling factor of P_S^{n+} within T_H
MP	Maximum aggregated power consumption for a group of TCLs (MW)

MSC	Maximum service capacity for a group of heterogeneous TCLs
Λ	Upper bound for MSC
$\lambda(m)$	Solution guess for MSC at m^{th} iteration of bisection method
$LB(m)/UB(m)$	Lower/Upper bound in a search interval at m^{th} iteration when using the bisection method
ϵ	Convergence criteria of the bisection method
N_h	Number of TCLs in a homogeneous control group
$MSC_i^{N_h}$	Maximum service capacity for a group of homogeneous TCLs including N_h of i^{th} TCL
$SPCI_i$	Service provision capability index of i^{th} TCL
r	Rank of a TCL in the prioritization list ($1 \leq r \leq N$)
n_{pl}	The set of first n_{pl} TCLs in the priority list, from the top to the bottom of the list ($1 \leq n_{pl} \leq N$)
RW_{tot}	The total reward to be shared among all TCLs
$RW(n_{pl})$	The reward to be shared among the first n_{pl} HPs in the priority list.
RW_r	The reward of r^{th} TCL in the priority list

5.2. Introduction

Thermostatically controlled loads (TCLs) are considered as one of the main demand-side management resources. Although the power rating of an individual TCL is only 2-6 kW,

there are millions of TCLs in residential and commercial sectors, making them an important type of distributed energy resources for providing energy and ancillary services. For instance, about 20% of electricity in the U.S. is consumed by the TCLs, [14]. By varying the length of the cycling intervals of a TCL while keeping temperature variation within its upper and lower temperature limits, the power consumption of the TCL can be modified with no impact on customers' convenience or comfort. Therefore, in recent years, a massive amount of research have been conducted on the development of control and scheduling strategies of TCLs aggregation for providing a wide range of grid services. Examples of such services include peak load shaving and load shifting [53]-[54], renewable generation smoothing [16], [40], regulation services, [21]-[26], intra-hour energy market arbitration [41], contingency type reserve [44], etc.

The increasing interest in using TCLs for providing grid services has heightened the need for designing reward systems that motivate the TCLs to perform at their highest level. Although considerable research has been devoted for developing different control and scheduling methods, rather less attentions has been paid to design rewarding mechanisms to compensate individual demand response resources (TCLs). Specifically, this lack of attention is observed for the demand response programs wherein TCLs are recruited to provide regulation services.

Often times, when loads participate in energy/reserve services, they are charged/payed based on the "average power" consumption/reduction. A service price is determined for the entire charge/payment time interval (e.g. 1-hour or 15-minutes). Therefore, as long as the average power consumption of the load remains the same for that interval, the power profile

the load falling within that time interval does not matter, [14], [16]-[19]. However, when loads provides regulation service, their "actual intra-hour power profiles" need to be closely monitored instead of their average power. Therefore, a load service entity (LA) needs to regulate its aggregated power consumption to track a reference power profile based on the service requirement, for example, on a 4-seconds basis. The quality of power tracking capability will directly affect the reward from the market and providing power more or less than the required amount results in a penalty cost to the LA according to payment strategy in performance-based regulation markets [35]-[40], [55].

An LA will need to recruit thousands of TCLs to provide MW-level regulation service. Therefore, it is critical for an LA to decide how to distribute the earned reward from the regulation market among the dispersed resources (TCLs). While using TCLs for provision of regulation services, the underlying fact is that they are not equally contributed to the overall service because TCLs have different thermal characteristics; thermostat settings (setpoint and deadband) and related thermal parameters (thermal mass, insulation, etc.). This diversity makes them different regarding their flexibility to shift their power consumption and hence, their contribution in the whole service. For example, assume that a load aggregator (LA) can provide 1 MW bidirectional regulation service with the same service quality using either 1000 Type-A TCL or 500 Type-B TCL. Thus, the service provision capability of Type-B is obviously more than that of Type-A and the LA should pay Type-B more than Type-A. Otherwise, if all TCLs are paid equally as long as the participation has been verified, those superior TCLs contributing more in service provision will ultimately be discouraged from selecting more flexible settings that allow them providing more services at higher quality. The fundamental principle of a

payment mechanism is its fairness so that resources are paid based on their contribution to the service. Therefore, a proper reward allocation strategy that differentiates the resources by their contribution is essential to recruit TCLs while paying customers fairly and keeping them satisfied.

Unlike the energy/reserve service payment, applying pay-by-average-power strategy is not suitable for rewarding in regulation services. In each control time interval (4-seconds), the "on" and "off" status of the TCLs are optimally determined by the controller to perform the power tracking. Complying with the command is essential to follow the power reference value and avoid the penalty cost. Therefore, rewarding TCLs simply by their "on" and "off" status is not an option either.

In addition, if a TCL complies with the control command, regardless of its "on" or "off" status, the TCL contributes to the overall power tracking service at that given time interval. For instance, assume that power increase is required within a time interval and the controller issues control commands to turn on 100 TCLs and let the rest remain off. In this manner, it is not correct to assume that the "off" TCLs are not contributing to the service because if those TCLs were turned on, the level of power increase would have exceeded the required amount resulting in service quality degradation and penalty cost. Therefore, it is not correct to assume that only the TCLs that are turned on or turned off at a given time interval have contributed to the service and hence, should be paid.

The main contribution of this chapter is to present a reward allocation mechanism for TCLs recruited for providing regulation service. Each TCL is paid according to its contribution in the whole provided service. In the first stage, the TCLs are prioritized based on their service

provision capability. This prioritization is performed using a proposed index, called service provision capability index (SPCI). The index is derived based on the concept of maximum service capacity (MSC) for a group of TCLs that is also introduced for the first time in this dissertation to the best of the authors' knowledge. In the second stage, the service procurement curve and reward curve are constructed using the prioritization results. These curves make it possible to estimate the contribution of and therefore, the allocated reward to each TCL, respectively.

The rest of the chapter is organized as follows. Section 5.3 presents some preliminaries used throughout this study. Section 5.4 introduces the concept of MSC and presents an iterative algorithm based on bisection method for MSC calculation. In Section 5.5, the proposed rewarding mechanism is developed to determine the allocated reward to each TCL. The numerical results are provided and discussed in Section 5.6 and finally, conclusion remarks are presented in Section 5.7.

5.3. Preliminaries

In this section, the modeling methods used throughout the chapter are briefly discussed. The dynamic thermal model of an individual TCL is presented where the considered TCL is assumed to be a heat pump (HP) without loss of generality. Then, the adopted direct load control (DLC) method for providing regulation services and the criteria used to evaluate the demand response performance are briefly presented.

5.3.1. HP Models

Variety of models with different orders have been introduced in the literature to capture

the thermal dynamics of residential HPs, like 1st order, 2nd order, 3rd order, and 4th order hybrid models presented in [31]-[32], [49]. In this study, the thermal dynamics of an HP is modeled by the 1st order two-state hybrid model. Considering the heating mode operation and ignoring the noise term, the discretized equations are summarized as follows.

$$\theta_i(k+1) = U_i(k+1)\,\theta_i^{ON}(k+1) + \big(1 - U_i(k+1)\big)\,\theta_i^{OFF}(k+1) \tag{5-1-a}$$

$$\theta_i^{ON}(k+1) = \theta_a(k) + Q_i R_i - \big(\theta_a(k) + Q_i R_i - \theta_i(k)\big)e^{-T_s/R_i C_i} \tag{5-1-b}$$

$$\theta_i^{OFF}(k+1) = \theta_a(k) - \big(\theta_a(k) - \theta_i(k)\big)e^{-T_s/R_i C_i} \tag{5-1-c}$$

$$U_i(k+1) = \begin{cases} 1 & \theta_i(k+1) < \theta_i^- \ or\ U_{c,i}(k) = 1 \\ U_i(k) & \theta_i^- < \theta_i(k+1) < \theta_i^+ \\ 0 & \theta_i^+ < \theta_i(k+1)\ or\ U_{c,i}(k) = 0 \end{cases} \tag{5-1-d}$$

$$Q_i = COP_i\ P_{Rated,i} \tag{5-1-e}$$

$$\theta_i^+ = \theta_{set,i} + Db/2 \qquad \theta_i^- = \theta_{set,i} - Db/2 \tag{5-1-f}$$

According to (5-1-a)-(5-1-d), if an HP is turned on/off ($U_i(k+1) = 1/0$), the indoor temperature, $\theta_i(k+1)$, is derived from the terms $\theta_i^{ON}(k+1)/\theta_i^{OFF}(k+1)$, respectively. Please refer to Chapter 2 for more detailed derivations.

In order to demonstrate and discuss the numerical results throughout this chapter, control groups including heterogeneous HPs are used. The thermal parameters and setting of the HPs and the procedure to randomizer them are presented in the Appendix.

5.3.2. Control of HPs for Power Tracking

While recruited to provide regulation services, HPs are controlled so that their aggregated power consumption tracks a reference power profile. There are different DLC methods in the literature to implement this objective. In this chapter, the centralized DLC

method introduced in [21]-[22] and Chapter 2 of this dissertation is adopted where a central controller sends control commands to HPs and receive measurements feedback from them through two way communication infrastructure. Note that in this study, it is assumed that the HPs parameters/settings are known in advance because differentiating between TCLs (and estimating their contribution) is not possible without any information about the thermal parameters/settings. Therefore, the DLC method of Chapter 2 is implemented in open-loop manner (without receiving feedbacks). The reference power profile, $P_{rf}(\cdot)$, are derived by superimposing the regulation service signal, $P_{rg}(\cdot)$ (e.g. regulation signal or load following signal), on the baseline power consumption profile of the HP control group, $P_b(\cdot)$, so that $P_{rf}(\cdot) = P_{rg}(\cdot) + P_b(\cdot)$.

This concept has been illustrated in Fig. 5.1(a) through Fig. 5.1(c) for a control group of 1000 HPs. Note that $P_b(\cdot)$ is derived considering the 24-hour ambient temperature profile, as shown in Fig. 5.1(d). $P_b(\cdot)$ is the hourly average of the aggregated power consumption of the HPs when they are controlled only by their thermostat logic instead of the central controller. It is highlighted that $P_b(\cdot)$ accounts "only" for HP loads and does not include the average power consumption of other appliances/loads (like lightings, TV, etc.). Also, the shown $P_{rg}(\cdot)$ is a ± 1 MW bidirectional regulation signal, adopted from [52]. For more details about the DLC method and determination of $P_b(\cdot)$ and $P_{rf}(\cdot)$, please refer to Chapter 2.

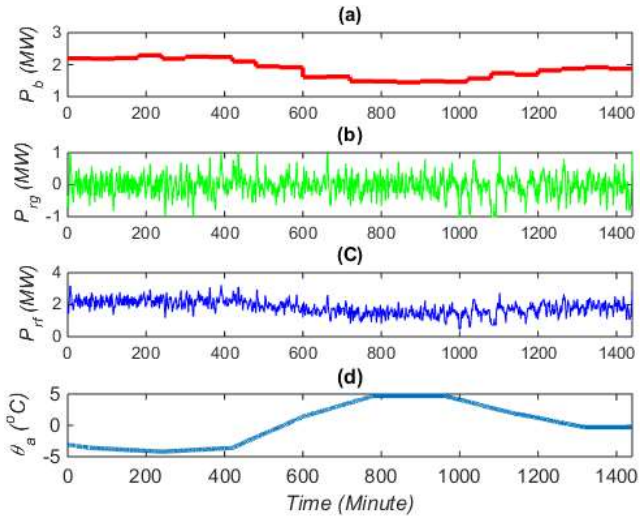

Fig. 5.1. Profile of (a) $P_b(\cdot)$, (b) a typical $P_{rg}(\cdot)$, (c) $P_{rf}(\cdot)$, (d) and $\theta_a(\cdot)$.

5.3.3. Performance Evaluation Criteria

In this sub-section, the performance criteria used for evaluation of regulation service provided by HPs aggregation are briefly presented. The DR performance are evaluated regarding two main aspects: service quality and HPs wear-and-tear, as mentioned earlier in Chapter 2-4.

In Chapter 2-4 a performance accuracy index was presented for service quality evaluation. The index is based on the performance accuracy index practiced by the CAISO. It is calculated for every 15-minutes time intervals using the mean value of the absolute signals. The index is presented as follows,

$$PA^{U/D}(l) = \frac{\overline{P_{rg,in}^{U/D}}(l) - \overline{E_m^{U/D}}(l)}{\overline{P_{rg,in}^{U/D}}(l)} \tag{5-2}$$

where

$$\overline{E_m^{U/D}}(l) = \begin{cases} 0 & \overline{E^{U/D}}(l) \le P_c \\ \left(\overline{E^{U/D}}(l) - P_c\right) & \overline{E^{U/D}}(l) > P_c \end{cases} \quad (5\text{-}3\text{-a})$$

$$\overline{E_m^{U/D}}(l) = \sum_{k \in l} \left| P_{rg,in}^{U/D}(k) - P_{rg,a}^{U/D}(k) \right|. \quad (5\text{-}3\text{-b})$$

In this study, as we will see later in Section 5.4, an acceptable performance over the service provision time horizon (T_h) is defined when the performance accuracy is greater or equal than a predefined value, PA^* at all of the time intervals, $1 \le l \le MTI$. In order to quantify the service quality over the entire service provision time horizon with only one single value, the following

$$SQ = \sum_{l=1}^{MTI} [sq^U(l) + sq^D(l)] \quad (5\text{-}4)$$

where

$$sq^{U/D}(l) = \begin{cases} 0 & PA^* \le PA^{U/D}(l) \le 1 \\ \dfrac{\left(PA^* - PA^{U/D}(l)\right)}{PA^{U/D}(l)} & PA^{U/D}(l) < PA^* \end{cases} \quad (5\text{-}5)$$

The SQ index is derived by summing the value of $sq^{U/D}(\cdot)$ calculated over every regulation market settlement time interval (15-minutes). According to (5-5), if $PA^{U/D}(l)$ is above a predefined value, PA^*, at all of the time intervals, the service quality is considered to be acceptable over the whole time horizon. Otherwise, if the $PA^{U/D}(l)$ is smaller than PA^* in at least one of the market intervals, then $SQ > 0$. It is obvious that SQ is always greater than or equal to zero. Similar to P_c, the numerical value of PA^* is determined by the choice and practical considerations of the LA. In this study, we consider $PA^* = 1$ meaning that an

acceptable service quality over the entire service provision time horizon is when the performance accuracy index is one at all of the 15-minutes time intervals.

In order to quantitatively evaluate the wear-and-tear imposed on HPs in effect of being externally controlled, the ratio of switching index, RSW, presented in Chapter 2 is used and presented as follows,

$$RSW = \frac{\bar{N}_{Cnt}^{sw}}{\bar{N}_{Unc}^{sw}} \tag{5-6}$$

Where

$$\bar{N}_{Cnt}^{sw} = \frac{1}{N}\sum_{i=1}^{N} N_{Cnt,i}^{sw} \tag{5-7-a}$$

$$\bar{N}_{Unc}^{sw} = \frac{1}{N}\sum_{i=1}^{N} N_{Unc,i}^{sw} \tag{5-7-b}$$

The RSW index reflects the wear-and-tear forced on HP by calculating the relative increase of HP switching activities when it is used to provide service.

5.4. Maximum Service Capacity (MSC)

In this section, the concept of MSC is introduced and an iterative algorithm based on bisection method is used for computationally efficient calculation of MSC. The introduction of MSC enables the prioritization of TCLs and subsequently reward allocation among them based on their contribution, as it will be explained in Section 5.5. Therefore, we consider the introduction and quantification of MSC as one of the contributions of the dissertation.

Consider a control group of including HPs (regardless they are homogeneous or heterogeneous) which are recruited to provide regulation service. Given the HPs thermal model, ambient temperature data ($\theta_a(\cdot)$), and a normalized regulation service signal data ($-1MW \leq P_{rg}^n(\cdot) \leq 1MW$), MSC is defined as the maximum scale of $P_{rg}^n(\cdot)$ that the control group can provide while meeting the following performance criteria

1) $SQ = 0$ (i.e. according to (5-4) and (5-5), $PA^{U/D}(l) \geq PA^*$ for all $1 \leq l \leq MTI$) and
2) $RSW \leq RSW^*$.

Therefore, considering the predetermined profile of $P_{rg}^n(\cdot)$, the maximum amount of regulation service that can be provided by the control group is defined as $P_{rg}^{max} = MSC\ P_{rg}^n$ ($MSC \geq 0$). Note that in the rest of this chapter, the notion of RSW^* stands for the upper limit for RSW index. Later in Section 5.5.3, it is discussed in detail how to select the proper value for RSW^* and how to derive the profile of $P_{rg}^n(\cdot)$.

One straightforward method to determine MSC is to run exhaustive search simulations by increasing the $P_{rg,a}^n$ using a scaling parameter, λ, that starts from 0 and is increased by small enough steps (say 0.01) until at least one the performance criteria is violated, i.e. $SQ > 0$ or $RSW > RSW^*$. Thus, the MSC would be the largest λ while both criteria are met. Figure 5.2 shows the variations of performance indices in effect of increasing λ for a control group including 1000 heterogeneous HPs. The time horizon for regulation service provision is considered to be $T_h = 24$ hours with $P_{rg}^n(\cdot)$ and $\theta_a(\cdot)$ shown in Fig.5.1(b) and Fig. 5.1(d), respectively. The scaling parameter is increased from 0 to 2.5 by a step size of 0.01, as shown

in Fig. 5.2.

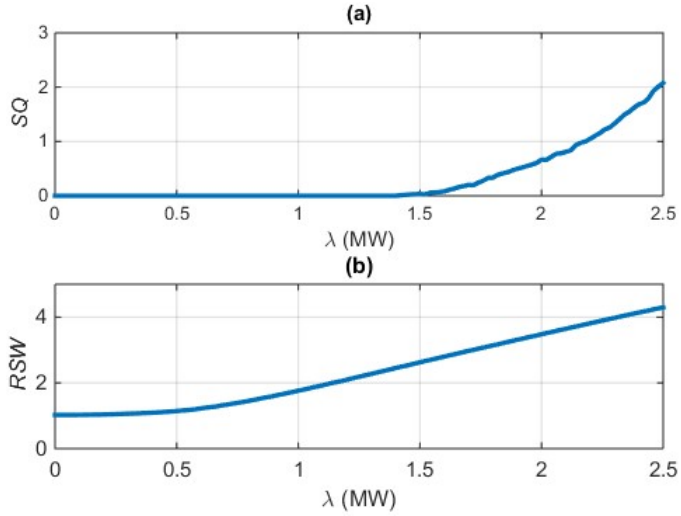

Fig. 5.2. Variations of performance criteria in effect of regulation signal magnitude, (a) SQ and (b) RSW.

From Fig. 5.2(a), it is observed once λ is above 1.41 MW, the SQ become greater than zero and then starts increasing sharply after that. Once λ exceeds a certain threshold (e.g. 1.58 MW in Fig. 5.2(a)), the regulation service signal becomes so large that there are not enough HPs available for power tracking at some time intervals. As a result, the performance accuracy in at least one of the time intervals become less than one that yields $SQ > 0$, according to (5-4) and (5-5). Also, once λ increases above 0.5 MW, the RSW starts increasing considerably. This is because when the magnitude of regulation service signal increases, $P_{rf}(\cdot)$ will differ from the $P_b(\cdot)$ with a higher magnitude as $P_{rf}(\cdot) = P_b(\cdot) + \lambda P_{rg}^n(\cdot)$. Thus, on average, larger number of HPs are required to be toggled (at every time interval) for power tracking and subsequently, higher value of λ brings about the increase of RSW, as also shown and discussed in [21], [34].

It is noted that the value of MSC can be limited by either switching constraint ($RSW \leq RSW^*$), or service quality constraint ($SQ = 0$). For instance, if $RSW^* = 1.5$, then the MSC of the control group is derived as 0.83 MW which is limited by the criterion $RSW \leq RSW^*$. However, if $RSW^* = 3$, then the MSC is derived as 1.41 which is limited by the criterion $SQ = 0$. Exhaustive search simulation method is straightforward but it is time consuming when the HP population is large or when MSC is to be calculated for a large number of control groups.

Our further analysis shows that the MSC of a control group is within a range and therefore, because of the increasing characteristics of SQ and RSW, it is possible to calculate MSC by an iterative process using bisection method. It is evident that the minimum power consumption of the group is zero and it occurs when all HPs are "off". Also, the maximum power consumption of the group, represented by MP, occurs when all HPs are "on" and is derived as $MP = \sum_{i=1}^{N} P_{Rated,i}$. Therefore, the necessary condition to have $P_{rf}(\cdot)$ trackable by the control group is $0 \leq P_{rf}(\cdot) \leq MP$. This necessary condition can be used to set an upper bound for MSC value derived as follows.

According to the definition of $P_{rf}(\cdot)$,

$$P_{rf}(k) = P_{rg}(k) + P_b(k) = \lambda\, P_{rg}^{n}(k) + P_b(k), \qquad 1 \leq k \leq N_{TI} \tag{5-8}$$

The maximum power reduction is achieved by turning off all the HPs so that $P_{rf}(\cdot) = 0$. From (5-8), when $P_{rf}(\cdot) = 0$, the maximum scale of the $P_{rg}^{n}(\cdot)$ at each time interval is derived as

$$\lambda_1^{max}(k) = -\frac{P_b(k)}{P_{rg}^{n,D}(k)} \tag{5-9}$$

where

$$P_{rg,a}^{n,D}(k) = \begin{cases} 0 & P_{rg}^{n}(k) > 0 \\ P_{rg}^{n}(k) & P_{rg}^{n}(k) < 0 \end{cases}. \tag{5-10}$$

Therefore, the maximum scale that guarantees $P_{rf}(\cdot) \geq 0$ for all k is derived as follows.

$$\Lambda_1^{max} = \min_{1 \leq k \leq N_{TI}} \lambda_1^{max}(k) \tag{5-11}$$

On the other hand, the maximum power that a control group can consume is MP. Therefore, by substituting $P_{rf}(\cdot)$ with MP in (5-8), the maximum scale of P_{rg}^{n} at each time interval is derived as

$$\lambda_2^{max}(k) = \frac{MP - P_b(k)}{P_{rg,a}^{n,U}(k)} \tag{5-12}$$

where

$$P_{rg,a}^{n,U}(k) = \begin{cases} P_{rg}^{n}(k) & P_{rg}^{n}(k) > 0 \\ 0 & P_{rg}^{n}(k) < 0 \end{cases}. \tag{5-13}$$

Therefore, the maximum scale guaranteeing $P_{rf}(\cdot) \leq MP$ for all k is derived as follows.

$$\Lambda_2^{max} = \min_{1 \leq k \leq N_{TI}} \lambda_2^{max}(k) \tag{5-14}$$

According to (5-11) and (5-14), in order to guarantee $0 \leq P_{rf}(\cdot) \leq MP$, the MSC cannot be larger than an upper bound, derived as follows.

$$0 \leq MSC \leq \Lambda = min\{\Lambda_1^{max}, \Lambda_2^{max}\} \tag{5-15}$$

Applying the above analysis on the considered control group results in $MP = 5.66\ MW$, $\Lambda_1^{max} = 1.57$, $\Lambda_2^{max} = 3.34$, and $\Lambda = 1.57$ implying that the MSC should be within $[0,1.57]$.

Once we know the upper bound for MSC, a bisection method can be used to determine the MSC rather efficiently. The steps of the algorithm are outlined in Table 5.1 where $LB(m)$ and $UB(m)$ represents the lower and upper bounds of the search interval, $[LB(m), UB(m)]$, at the m^{th} iteration, respectively. Also, $\lambda(m)$ stands for the solution guess at the m^{th} iteration, which is always within the search interval, and ϵ represents the convergence criteria for the iterative algorithm.

Table 5.1. The Steps of MSC Calculation using Bisection Method.

1	Set m =1, $LB(m) = 0$, $UB(m) = \Lambda$, and $\lambda(m) = UB(m)$.
2	Run DLC while instructing the control group with $P_{rg,in}(\cdot) = \lambda(m)P_{rg}^{n}(\cdot)$ during T_h and calculate the performance indices.
3	If both performance criteria are met ($SQ = 0$ and $RSW \leq RSW^{*}$), then $MSC = \lambda(m)$. If at least one of the criteria is not met, update the guessed solution for the next iteration using $\lambda(m+1) = (UB(m) + LB(m))/2$ and go to the next step.
4	Set $m = m + 1$, run the DLC for provision of $P_{rg,in}(\cdot) = \lambda(m)P_{rg}^{n}$ during T_h, and calculate the performance indices.

5	If both performance criteria are met, update the lower bound by setting $LB(m+1) = \lambda(m)$. If either of the criteria is not met, update the upper bound by setting $UB(m+1) = \lambda(m)$.
6	Update the solution guess for the next iteration using $\lambda(m+1) = (UB(m) + LB(m))/2$.
7	If the convergence criteria is satisfied, i.e. $\lvert(\lambda(m+1) - \lambda(m))/\lambda(m+1)\rvert \leq \epsilon$, then $MSC = \lambda(m+1)$. If not, go back to step 4.

The flowchart of the algorithm is also shown in Fig.5.3.

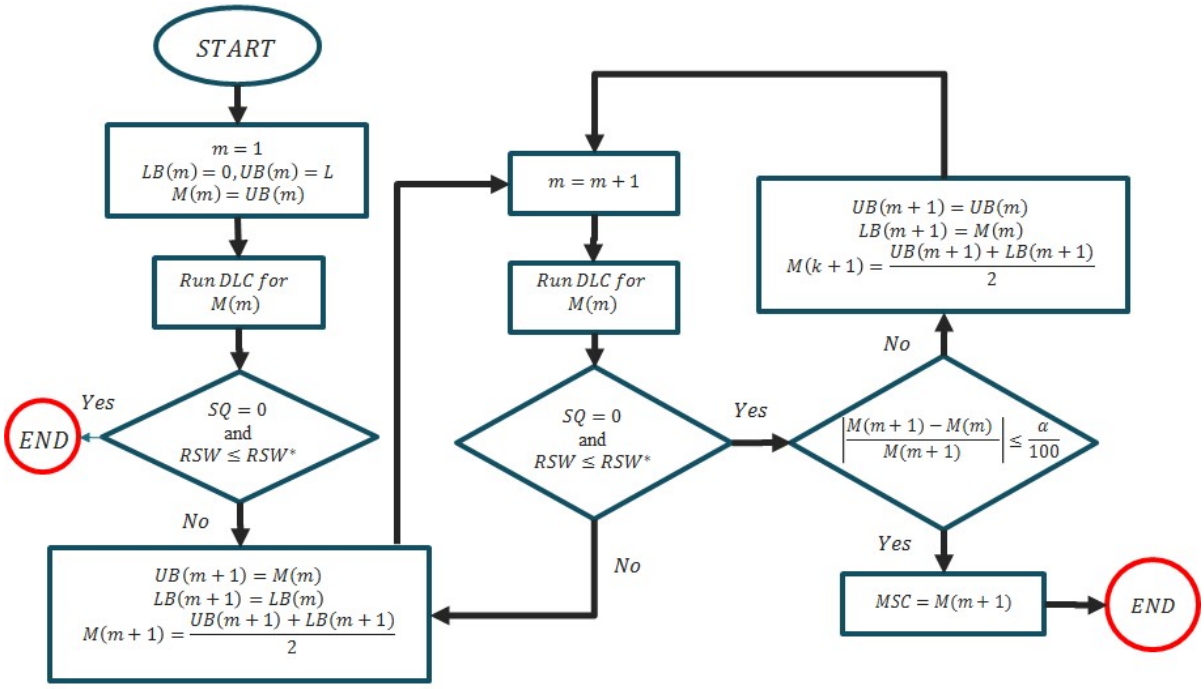

Fig. 5.3. The flowchart of the bisection method algorithm for MSC calculation.

Figure 5.4 shows the quantitative evolution of UB, LB, and λ in each iteration during the MSC calculation when $RSW^* = 1.5$ and the convergence criteria of $\epsilon = 10^{-4}$ is considered. As it is observed from the figure, the initial value for $[UB, \lambda, LB,]$ is $[1.57, 1.57, 0]$ and they are updated at each iteration till the convergence criteria is met where $\lambda = 0.83\ MW$ which is compatible with the result of extensive search simulation method.

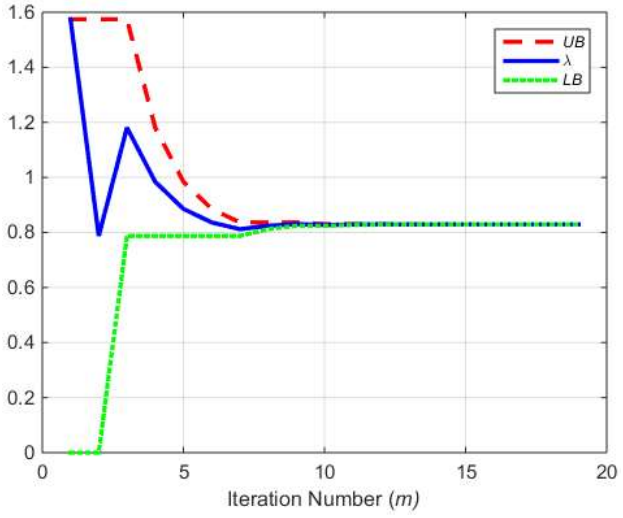

Fig. 5.4. Evolution of UB, LB, and λ at each iteration in the process of MSC calculation using the bisection method.

As a comparison among the presented methods to calculate MSC value, it is noteworthy that the elapsed time for MSC calculation is 102.7 seconds and 18.3 seconds for the extensive simulation method and the bisection method, respectively.

Note that the definition of MSC and the MSC calculation method presented in this section are applicable to other TCLs as well (e.g. water heaters). For instance, if an LA chooses to use water heaters, the water heater model will be used instead of the HP model when simulating the DLC (steps 2 and 4 in Table 5.1).

5.5. The Proposed Reward Allocation Mechanism

In this section, a two-stage reward allocation mechanism is presented so that an LA be able to pay HPs fairly and according to their contribution in regulation services provision. In the first stage, HPs are prioritized according to their service provision capability. In order to do so, an index called $SPCI$ is proposed to quantify the service provision capability of each HP. As a result, HPs are prioritized according to their $SPCI$ value. In the second stage, a reward curve is constructed based on the prioritization results derived from the first stage. While the reward curve is constructed, the LA can estimate the reward of each HP using incremental reward calculation. The two-stage reward allocation mechanism is developed using the MSC concept and calculation method presented in Section 5.4. Also, it is noted that the proposed payment mechanism is performed after the service is delivered and therefore, the profile of θ_a, P_{rg}, and P_{rg}^n over the horizon of regulation service provision are assumed to be known to the LA.

5.5.1. Prioritization of HPs

The first stage of the proposed payment mechanism is to prioritize HPs according to their service provision capability. Therefore, the service provision capability of each participating HP needs to be quantified. In order to better illustrate the prioritization method, we start with a simple example wherein it is desired to make comparison between HP_i and HP_j regarding their service provision capability. Thus, the following procedure is proposed.

First, construct two "homogeneous" groups corresponding to each HP. One group includes N_h of HP_i and the other group includes N_h of HP_j. Knowing the profiles of P_{rg}^n, θ_a, and the predetermined value of RSW^*, calculate the MSC of each "homogeneous" group and

represent them by $MSC_i^{N_h}$ and $MSC_j^{N_h}$. Assume the result is $MSC_i^{N_h} > MSC_j^{N_h}$. Because $MSC_i^{N_h}$ and $MSC_j^{N_h}$ are derived under the same condition (P_{rg}^n, θ_a, N_h, and RSW^*), it is evident that the homogeneous group comprising N_h of HP_i has higher capability in service provision than the homogeneous group comprising N_h of HP_j. Therefore, one can conclude that the capability of HP_{i} is higher than that of HP_j. As a result, by calculating $MSC_i^{N_h}$ $(1 \leq i \leq N)$ for each HP in the control group and under the same conditions, an LA can easily prioritize the HPs regarding their service provision capability simply by comparing their MSC^{N_h}.

It is evident that MSC^{N_h} is proportional to N_h, i.e. if the population of a homogeneous control group gets twice, then the MSC^{N_h} gets twice as well. This fact is illustrated in Fig. 5.5 where MSC^{N_h} is plotted versus N_h for five different HPs with different parameters and settings. While calculating MSC^{N_h}, the RSW^* is assumed to be 1.5 and the profiles of P_{rg}^n and θ_a are considered to be those shown in Fig. 5.1(b) and Fig. 5.1(d), respectively. The data points show the variation of MSC^{N_h} with respect to N_h and the dotted lines show the best fitted lines to the corresponding data points. As it is observed, the linear curves fit the data points very well and therefore, the slope of this line is defined as the service provision capability index ($SPCI$) of an HP and is calculated as

$$SPCI_i = \frac{MSC_i^{N_h}}{N_h} \qquad 1 \leq i \leq N \tag{5-16}$$

Note that if the same N_h is used to calculate MSC^{N_h} for all HPs in a control group, then an LA can directly use the values of MSC^{N_h} for the sake of prioritization. But the $SPCI$ in (5-16) is more general in the sense that if MSC^{N_h} is calculated using different values of N_h for

different HPs, they should still be comparable for the sake of prioritization because of the linear characteristics of MSC^{N_h} with respect to N_h. The $SPCI$ of an HP can be calculated for an arbitrary value of N_h according to the discussed linear characteristics. However, using high values of N_h increases the computational time and using very low values of N_h (say 10) may result in lack of resources (HPs) for power adjustment. Therefore, we recommend that a number between 300 and 1000 is selected for N_h. The required steps for prioritizing HPs are summarized in Table 5.2.

Table 5.2. The Steps for Prioritizing HPs.

1	Correspond to each HP, construct a homogeneous group including $\boldsymbol{N_h}$ of that HP.
2	Calculate the MSC^{N_h} for the homogeneous group.
3	Calculate the $SPCI$ of the HP using (5-16).
4	Complete steps 1-3 for all HPs in the control group.
5	Then, prioritize HPs according to their $SPCI$s and construct the priority list.

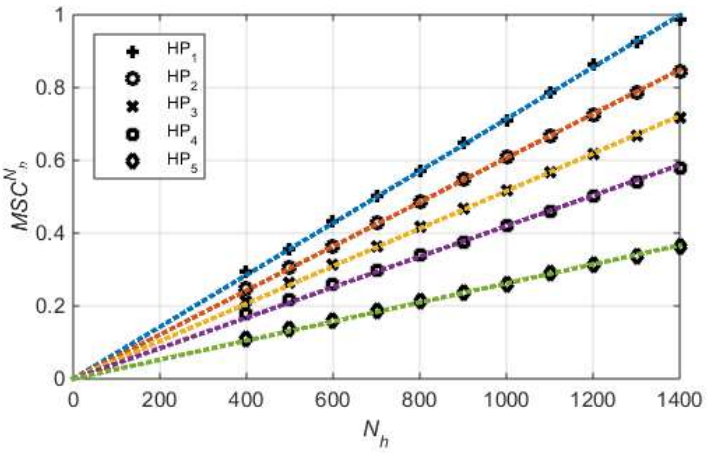

Fig. 5.5. Variation of MSC^{N_h} versus N_h for five different HPs.

The value of $SPCI$ for an HP depends on its thermal parameters ($p = [R, C, Q, P_{Rated}, T_{on}^{ml}, T_{off}^{ml}]$) and thermal settings ($s = [\theta_{set}, Db]$). To study the sensitivity of $SPCI$ with respect to the parameter/settings, we let only one parameter/setting change at a time for some different HPs (see Fig. 5.6). Note that the minimum lock time for both the on and off periods are assumed to be equal ($T_{on}^{ml} = T_{off}^{ml}$) in order to reduce the number of combinations required for conducting the simulations. Therefore, both parameters are simply shown by MLT standing for the minimum lock time for an HP to stay in a state.

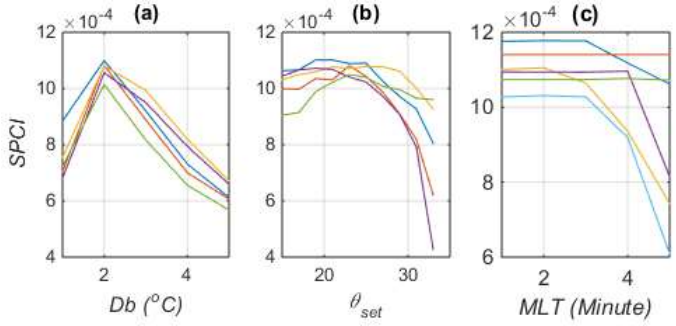

Fig. 5.6. Sensitivity of $SPCI$ with respect to (a) Db, (b) θ_{set}, (c) MLT.

Figure 5.6(a) shows the variations of $SPCI$ with respect to the operating Db where it is observed that the $SPCI$ is optimal for a certain value of Db and if the Db becomes smaller or larger than that optimal value, the $SPCI$ decreases. This behavior is justified as follows. Small values of Db results in shorter cycling periods (i.e. shorter T_{on} and T_{off}) and hence, more frequent switching. Because after each switching, an HP is locked to satisfy the operational constraint of MLT, a higher number of switching makes the HP unavailable for more often. This limits the HP's flexibility to vary its cycling periods and results in inferior capability of regulation service provision. On the other hand, large values of Db decrease the number of

switching cycles in the uncontrolled mode. Therefore, for a specific value of RSW index (1.5 in this simulations), the amount of allowed switching in the controlled mode is decreased, according to (5-2), $N_{cnt}^{sw} = RSW\ N_{unc}^{sw}$, which in turn degrades the flexibility of the HP.

Figure 5.6(b) shows the variation of $SPCI$ with respect to θ_{set} where nonlinear behavior is observed similar to that in Fig. 5.6(a). It is observed that there is an optimal value of θ_{set} that maximizes the $SPCI$ value for an HP. When the θ_{set} is too high, T_{off} becomes much shorter than T_{on} and the HP is mostly "on" to keep the room temperature within the range. Therefore, the availability of the HP in "off" status gets limited, causing its capability to provide regulation-up service to be decreased. Similarly, when the θ_{set} of an HP is too low, T_{on} becomes much shorter than T_{off} and the HP is "off" most of the times to keep the room temperature within the deadband. Therefore, the availability of the HP in "on" status becomes limited, causing a degradation in its capability to provide regulation-down service.

The variation of $SPCI$ with respect to MLT is shown in Fig. 5.6(c). As it is seen from the figure, a larger MLT generally yields a smaller $SPCI$. A larger MLT forces the HP to be locked in an on/off state for a longer time period. Therefore, the HP will be unavailable (to respond to control signals) over a longer time during the control time horizon which in turn makes it less flexible to change its on/off status and hence, power consumption.

Because the thermal parameters/settings are determined by the occupants (not the LA), the choice of an occupant has a significant impact on the service provision capability of an HP. Therefore, if an LA pays more to the HPs with higher service provision capability, the occupants are incentivized to select more optimal settings to increases their HPs' service capability.

5.5.2. Reward Curve Construction

By prioritizing the HPs based on their $SPCI$ value, an LA can construct a priority list to rank them with respect to their service provision capability. However, the ranking information itself is not sufficient for award allocation. For example, even if we know that HP_i ranks higher than HP_j, we still need to know how much more we shall pay HP_i compared with HP_j.

To address this issue, a reward curve is constructed using the following procedure to determine the payment to be made to each HP. First, a curve called "service procurement curve" is constructed to represent the functionality of MSC versus the number of HPs in the priority list. From the curve, one can determine the MSC if only the first n_{pl} HPs from the priority list were used for service provision. Then, "reward curve" is derived by linearly scaling up the Y-axis of service procurement curve. The scaling factor we propose to use is $RW_{Tot}/MSC(N)$ where RW_{Tot} represents the total amount of reward that the LA wants to share with the HPs and $MSC(N)$ represents the MSC of the whole control group. The reason is that the total reward RW_{Tot} has been earned while the whole control group are providing regulation service. Thus, the data point $(N, MSC(N))$ on the service procurement curve corresponds to $(N, RW(N))$ on the reward curve, in which $RW(\cdot)$ stands for the reward curve and $RW(N) = RW_{Tot}$ is the total amount of money/reward to be shared among all participating HPs. This curve shows the LA that what the total reward would be if only the first n_{pl} HPs in the priority list were recruited for service provision under the same condition (the same normalized profile of regulation service signal, $P_{rg,a}^{n}(\cdot)$, the same outdoor temperature profile,

$\theta_a(\cdot)$, and the same imposed tear-and-wear on HPs, RSW^*),. The steps to construct the reward curve are summarized in Table 5.3.

Table 5.3. Steps for Constructing the Reward Curve.

1	Calculate the $MSC(n_{pl}^0)$ for the first top n_{pl}^0 HPs on the priority list. In our case, we set $n_{pl}^0 = 200$.
2	Increase the number of HPs by ΔN so that $n_{pl}^m = n_{pl}^{m-1} + \Delta N$. Calculate the $MSC(n_{pl}^m)$ for the top n_{pl}^m HPs on the priority list. In our case, we set $\Delta N = 200$ as well.
3	Repeat step 2 until $n_{pl}^m = N$.
4	Construct the service procurement curve by fitting a polynomial to the derived data points obtained in steps 1-3, $\left[\left(n_{pl}^0, MSC(n_{pl}^0)\right), \dots, \left(n_{pl}^m, MSC(n_{pl}^m)\right), \dots, (N, MSC(N))\right]$.
5	Construct the reward curve by linearly scaling up the Y-axis of service procurement curve. The scaling factor is $RW_{Tot}/MSC(N)$.

After constructing the reward curve, the reward of each individual HP can be calculated as follows,

$$RW_r = RW\left(n_{pl} = r\right) - RW(n_{pl} = (r-1)) \tag{5-17}$$

This process suggests that the reward to the r^{th} HP in the priority list is calculated by the additional income it brings to the LA, i.e. if the r^{th} HP is added, what is the amount of the additional/incremental revenue by providing the additional service.

5.5.3. Remarks

Note that while calculating $SPCI$ to prioritize HPs, MSC calculation is performed for groups of "*homogeneous HPs*". However, when constructing service procurement curve and reward curve, the MSC calculated is performed for groups of "*heterogeneous HPs*".

Within the process of MSC calculation, the SQ index is to be calculated at every iteration Therefore, it is important to explain how to define the instructed and actual regulation signals as the SQ is calculated based on them according to (5-3) to (5-5). While calculating MSC, we are interested to derive the scale of a normalized regulation signal that has already been provided by the original control group. Therefore, at m^{th} iteration of the bisection method, the instructed regulation signal is considered as $P_{rg,in}(\cdot) = \lambda(m)P_{rg}^{n}(\cdot)$. Then, after running DLC and considering $\lambda(m)P_{rg}^{n}(\cdot)$ as the instructed regulation signal, the actual response of control group is derived, and the SQ is calculated using (5-4)-(5-5).

Recall that for calculation of $SPCI$ and MSC while prioritizing HPs and constructing the reward curve, the upper limit RSW^{*} is considered to be known in advance. Note that the RSW^{*} is considered to be the RSW^{a} representing the actual value of the RSW index for the original control group. This value is selected for the RSW^{*} to account for the realistic amount of wear-and-tear imposed on the HPs as a result of service provision. It should be noted that the numerical value of RSW^{a} needs to be known either through measurements or some estimation methods. It is noteworthy that the DLC method presented in Chapter 2 provides the opportunity for the LA to fairly well estimate the numerical value of RSW^{a} using the forecasts of on/off status for all HPs. While performing the control, the central controller can save the

forecasts of HPs on/off status so that they are used to estimate the value of RSW^a after delivering the service.

It should be noted that $MSC(N) = \max_{1 \le k \le N_{TI}} \left| P_{rg}(k) \right|$. In other words, considering all HPs in the service, $SQ = 0$, and $RSW \le RSW^* = RSW^a$, the MSC is the maximum absolute value of the provided regulation signal, $P_{rg}(\cdot)$. The $MSC(N)$ cannot be smaller because $P_{rg}(\cdot)$ has already been provided by the control group while satisfying the operational constraints, i.e. $SQ = 0$ and $RSW \le RSW^*$. On the other hand, it cannot be larger than that because it results in $RSW > RSW^*$. Recall that in Fig. 5.2(b) that the RSW index increases when λ is enlarged.

5.5.4. Summary of the Proposed Reward Allocation Mechanism

The presented rewarding mechanism is summarized as follows,

1) Construct the normalized regulation signal profile ($P_{rg}^n(\cdot)$) from the recorded regulation signal that has already been provided by the original control group, $P_{rg}(\cdot)$. Note that the normalization is performed over the entire service provision time horizon (24-Hours in this study).
2) Estimate (or read the measurements to calculate) the RSW^a.
3) Using the recorded, $\theta_a(\cdot)$, constructed $P_{rg}^n(\cdot)$, and estimated RSW^a, calculate the $SPCI_i$ for all TCLs in the original control group ($1 \le i \le N$) using the steps presented in Table 5.2.
4) Construct the priority list according to the calculated $SPCI_i$ ($1 \le i \le N$).
5) Construct the reward curve using the steps of table 5.3.
6) Calculate the allocated reward to each individual TCL by applying the incremental

method (equation (5-17)) on the constructed reward curve.

5.6. Simulation Results

In this section the proposed reward allocation mechanism is illustrated through numerical simulations where 10,000 heterogeneous residential HPs are participated in regulation service. The thermal parameters and settings of the HPs are derived based on Table A.1, Table A.2 and (A-1)-(A-3) presented in the appendix. It is assumed that the control group has already provided regulation service for a time horizon of 24 hours ($T_h = 24$ Hours). The provided regulation signal, $P_{rg}(\cdot)$ has the granularity if 4-second and has the maximum magnitude of 7.1 MW as shown in Fig. 5.7. The ambient temperature profile during is also assumed to be the profile shown in Fig 5.1(d).

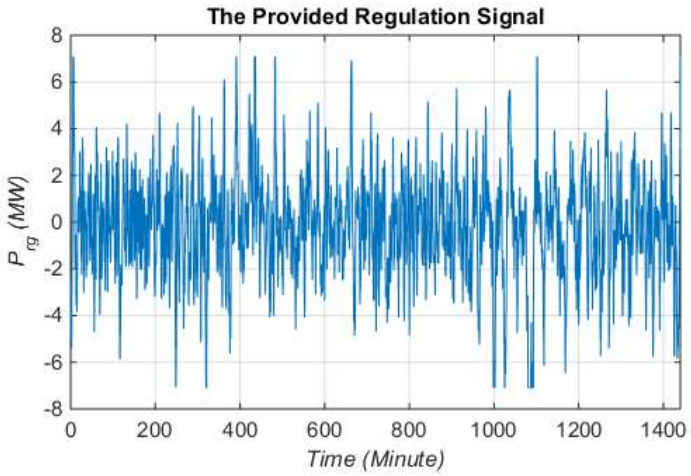

Fig. 5.7. Profile of the provided regulation signal, $P_{rg,a}$.

After performing the power tracking control, the ratio of switching index is derived as $RSW^a = 1.5$. Therefore, the upper limit for the ratio of switching index for the proposed

reward allocation strategy is considered to be $RSW^* = 1.5$. The $SPCI$ for all 10,000 HPs are determined using the introduced method in Section 5.1 and by choosing $N_h = 500$ and $\varepsilon = 10^{-4}$. Then, the HPs are prioritized based on their $SPCI$ values as shown in Fig. 5.8(a) where it is observed that the maximum and minimum value of $SPCI$ is 1.175×10^{-3} and 0.056×10^{-3}, respectively. Figure 5.8(b) also shows the distribution of the $SPCI$s where it is observed that majority of HPs have $SPCI$ value between 0.389×10^{-3} and 0.717×10^{-3}. After prioritization of HPs, the service procurement curve data points are derived based on the procedure presented in Section 5.2. It is observed that a 10th order polynomial is sufficient to fit the data points with the maximum percentage error of 1%, as shown in Fig. 5.9.

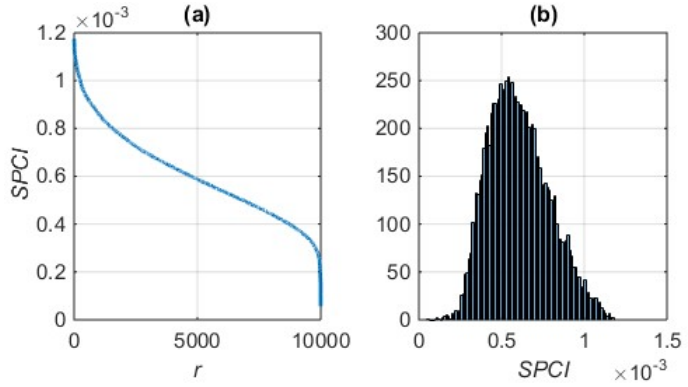

Fig. 5.8. (a) Prioritized $SPCI$ value and (b) the distribution of $SPCI$.

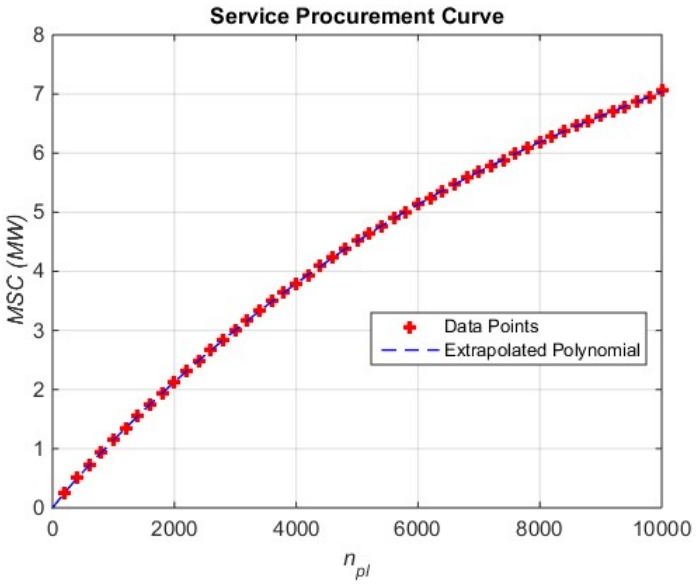

Fig. 5.9. The derived service procurement curve.

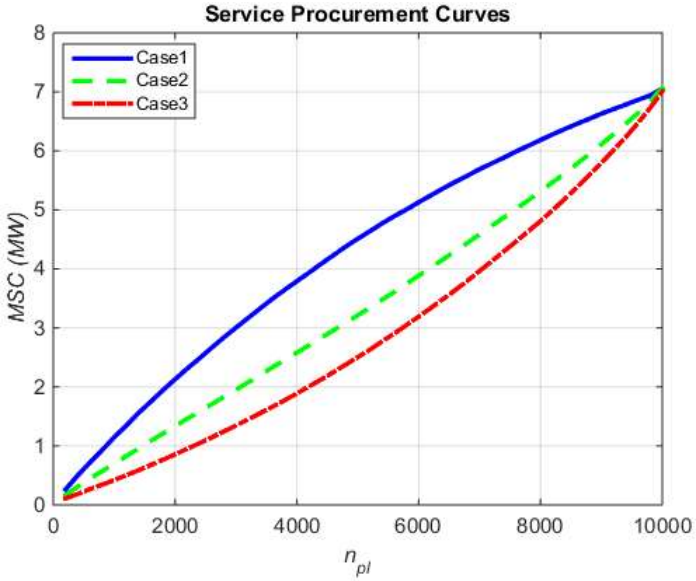

Fig. 5.10. Service procurement curves for three cases.

To better demonstrate the effectiveness of the proposed prioritization method in Section 5.1, three possible service procurement curves are shown in Fig. 5.10. In Case1, the curve is

obtained using the presented prioritization method where HPs are prioritized according to their $SPCI$ value in a descending order. In Case2, the curve is derived without any resource prioritization and for constructing the curve using the steps in Table 5.3, HPs are selected randomly and without any specific order. Finally in Case3, the curve is obtained by prioritizing HPs according to their $SPCI$ value in an ascending order, as opposed to Case1.

The service procurement curves shown in Fig. 5.10 clearly verifies the effectiveness of the proposed prioritization method. For any number of HPs, n_{pl}, the value of MSC is the highest for curve of Case1 derived using the proposed prioritization method. For instance, when using 5000 HPs, the MSC in Case1, Case2, and Case3 are 4.51 MW, 3.21 MW, and 2.5 MW respectively. Therefore, the first n_{pl} HPs picked using the proposed prioritization method are more effective (regarding service provision capability) in comparison to the Case2 where no prioritization is performed. As expected, the curve in Case 3 has the lowest MSC in comparison to the other two cases because the HPs are ranked using $SPCI$ in "ascending" order and therefore, the first n_{pl} HPs selected from the priority list are the least effective units.

After constructing the service procurement curve, the reward curve is derived by properly scaling up the Y-axis of service procurement curve. For instance, assuming that the average hourly price of bidirectional regulation signal is $PR_h = 34$ \$/MW $(1 \leq h \leq 24)$, then the total revenue of the provided regulation service of Fig. 5.7 is derived as $RW_{tot} = \sum_{h=1}^{24}\left[PR_h \times \max\left|P_{S,h}\right|\right] = 4333.3$ \$. Without loss of generality it is assumed that the whole revenue is shared among the participating HPs. Therefore, the reward curve is derived as shown in Fig. 5.11.

Assume that the HPs are clustered to N/N_g groups such that each group consists of N_g HPs and the m^{th} group includes HPs with $(m-1)N_g + 1 \leq n_{pl} \leq mN_g$ in the priority list. If $N_g = 200$, then it is observed from Fig. 5.9 and Fig. 5.10 that $MSC(n_{pl} = 200) = 0.26$ MW and $RW(n_{pl} = 200) = 158.5$ \$. In other words, the LA was able to provide 0.26 MW regulation signal (i.e. 0.26 P_S^n) if it would hire "*only*" the best 200 HPs (the top 200 HPs in the priority list) and "*without*" using the rest of the HPs. Therefore, the corresponding reward for provision of the first 0.26 MW would belong to the first 200 HPs in the priority list. Hiring the second group together with the first group increase the MSC and reward to 0.50 MW and 304.2 \$, respectively. Therefore, the contribution of the second group in the regulation service provision is 0.24 MW (=0.50-0.26) and their contribution in the whole reward would be $RW(n_{pl} = 400) - RW(n_{pl} = 200) = 145.7$ \$. As expected, the contribution of the second group in regulation service provision (0.24 MW) is less than that of the first group (0.26 MW) because the second group consists of HPs with lower ranking and hence, less capable HPs regarding service provision. Similarly, the contribution of each group in the provided service and in the total reward can be calculated. Therefore, by decreasing N_g to 1, an LA can estimate the monetary share of each individual HP in the service provision using in (5-17), as shown in Fig. 5.12. As expected, the payment to the HPs decreases from the top to the bottom of priority list. The first HP in the priority list is paid at 0.84 \$ and the HP in the bottom of the list is paid at 0.25 \$ for participating in the provided regulation service.

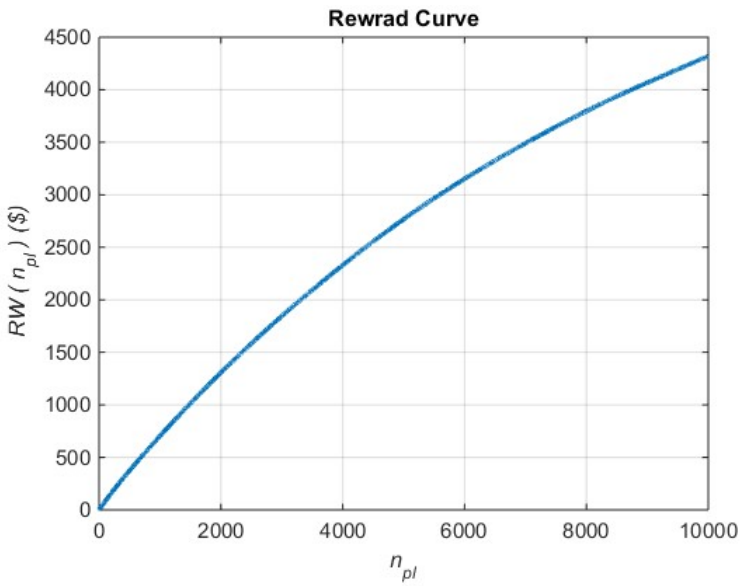

Fig. 5.11. Reward curve (reward w.r.t. the number of HPs selected from priority list from top to the bottom).

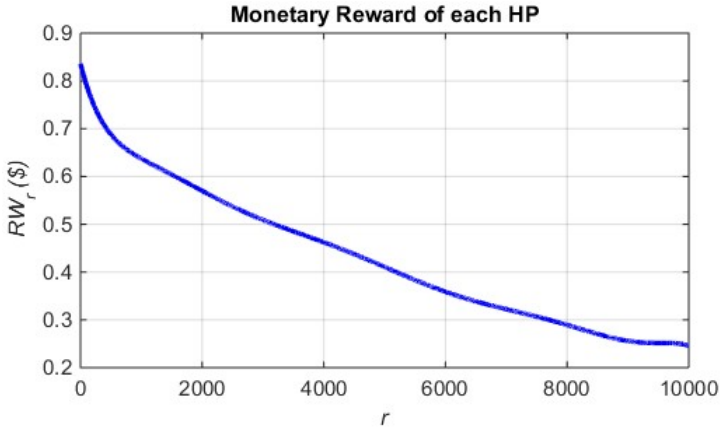

Fig. 5.12. Payment curve derived by the incremental reward method.

5.7. Summary

This chapter presents a reward allocation mechanism for an LA to pay its resources (TCLs) based on their capability and contributions when participating in regulation services. The

concept of maximum service capacity (MSC) is introduced and an iterative algorithm based on the bisection method is presented to numerically calculate MSC for a group of TCLs. Then, the reward allocation mechanism is presented where the concept of MSC is used for calculating service provision capability indices (SPCIs) to rank the TCLs and then construct the reward curve. The proposed reward allocation mechanism includes the following two stages:

1) The TCLs are prioritized according to their SPCI values that quantify their service provision capability.

2) The reward curve is constructed based on the prioritization results. Then, an LA can estimate the payment made to each TCL using the incremental reward method.

The effectiveness of the proposed prioritization method has been verified through simulation results. We have shown that the amount of service provided by TCLs with better ranking in the priority list is larger so the rewards to those TCLs are higher. Because the setting of a TCL is determined by its owners based on comfort preference and consumption patterns, associating rewards with service provision capability will provide proper economic incentives for encouraging the TCL owners to make decisions in favor of providing more grid services.

Chapter 6

Conclusions

6.1. Dissertation Overview

The increasing penetration of intermittent renewable energy resources in power grids accompany with higher demand for load balancing services. The advancement in required technologies envisioned in smart grids, like communication, control, sensor network, large data management techniques, etc., have been facilitating to realize the considerable benefits DR programs can potentially provide to the grids. TCLs are seen as one of the promising load resources to accommodate part of the increasing balancing services. In this dissertation we specifically focused on DR programs using TCLs for provision of balancing services. This dissertation is summarized as follows.

In order to achieve the desired response from the aggregation of TCLs, a proper control method is required. In Chapter 2, a centralized DLC method based on temperature priority list were presented. The task of the controller is to perform a power tracking control so that the aggregated power of TCLs tracks a reference power profile. The performance criteria to evaluate the DR provided by the TCLs aggregation were presented and the performance of the DLC under different scenario investigated. The numerical results demonstrate the proper performance of the DLC method. This DLC method considered to be the control method all over the dissertation.

Chapter 3 presents performance improvement for the presented DLC method in

Chapter 2. It is proposed that in addition to TCLs states (temperature and on/off status) two more pieces of information is communicated to the central controller. The performance improvement shown through the numerical results. Although the amount of communicated data is increased, it is seen the sampling period can be prolonged while having better performance in comparison to the original DLC method. This in turn alleviates (to some extent) upgrading the communication infrastructure required for the original DLC method.

Policy makers are facilitating the participation of LAs in different power markets so that they are treated similar to other conventional resources, like generators. In chapter 4, a stochastic optimization model is presented for a LA to obtain optimal bidding strategies while participating in real-time PBRMs. The features of the PBRM including the performance accuracy and mileage calculation were modeled in the objective function while considering the CAISO convention. One of key features of the proposed formulation is confining the amount-of-tear and were imposed on the TCLs. It is shown through the numerical results that this constraint has considerable effect on the optimal decision and the amount of income from PBRMs. The optimization model is considered to be stochastic specifically because of the uncertainty in the profile of regulation signal profile as it affects the numerical value of the RSW index.

After a LA delivers balancing services and earn money from ancillary service markets (or utilities), it has to make decision about "*how to distribute the total reward among the participating TCLs according to their contribution in the whole provided service*". In order to address this problem, Chapter 5 proposes a two-step reward allocation mechanism. In the first step, TCLs are prioritized according to their service provision capability. An index called $SPCI$

is proposed to quantify the TCLs capability and therefore, prioritize them. Then, as the second stage, a reward curve is constructed. The curve represents the total possible reward in terms of the number of the TCLs in the priority list, from the top to the bottom. Both stages are based a newly defined concept, called MSC. The proposed prioritization method are verified through the numerical results where it is observed that top TCLs in the priority list results in more reward in comparison to those with lower ranking in the priority list.

6.2. Future Work Recommendations

The recommendations for future work are presented as follows

1) One of the main limitations of the presented optimization model in Chapter 4 is high computational burden in comparison to the optimization models for the other counterparts like generators, battery bank, etc. This limitation is even more highlighted when a LA wants to make the optimal decision while participating in multiple power markets. This limitation is because of the fact that the optimization model is simulation based. This means that for numerical evaluation of the objective function and the constraints at every iteration of the solver algorithm, a DLC should be simulated over a time horizon of some hours. In the simulations, thousands of TCLs are modeled separately. As mentioned earlier, this detached modelling is because of modeling the RSW constraint.

One of the possible solution to this issue is using an aggregate model for heterogeneous TCLs while it can provide information about the RSW index, as it is required to be confined and hence, modelled in the optimization model.

2) One interesting area for future research can be finding analytical methods (versus the

presented simulation based method) to prioritize TCLs according to their parameters and settings. This method can save computational time and burden facilitating the application of the TCLs prioritization for other operational purposes.

3) Another interesting area for future research is the application of the presented prioritization method in the operation or decision making stage while assuming that a LA is not necessarily a non-profit organization. In this case, the LA can selectively determine the participating TCLs so that it maximizes the profit for the entire community of loads.

Appendix

In this section, we developed a process to randomize the cycling characteristics of the HPs based on target probability density functions (PDF) and therefore, to get a diversified combination of HPs in a load control group. The process includes three steps as presented below.

Step 1: Generate the $T_{on,i}$, $T_{off,i}$, COP_i, and $P_{Rated,i}$ for all HPs ($1 \leq i \leq N$) using any desired PDF. In this study, we assume that all those parameters are independent random numbers generated by continuous uniform PDFs within a and b, as shown in Table A.1.

Table A.1. Parameters of Continuous Uniform PDF, $X \sim U(a, b)$.

X	a	b
$T_{on,i}$ (Minute)	5	15
$T_{off,i}$ (Minute)	10	30
$P_{Rated,i}$ (KW)	4	7
COP_i	2	3

Step 2: Using the derived parameters in step 1 and assuming that $\theta_a = 0$℃, $\theta_{set} = 19$℃, and $Db = 1$℃, calculate the parameters $[R_i, C_i, Q_i]$ by solving (A-1)-(A-3), respectively.

$$R_i C_i = -T_{off,i} / ln\left(\frac{\theta^- - \theta_a}{\theta^+ - \theta_a}\right) \tag{A-1}$$

$$Q_i R_i = \frac{\theta^+ - \theta^- \, e^{-(T_{on,i}/R_i C_i)}}{1 - e^{-(T_{on,i}/R_i C_i)}} - \theta_a \tag{A-2}$$

$$Q_i = COP_i \, P_{Rated,i} \tag{A-3}$$

The derivations of (A-2) and (A-3) are presented in the following.

The 1st order thermal dynamic model of the i^{th} HP in the continuous time domain is as follows, [11] and [23],

$$\frac{d\theta_i(t)}{dt} = \frac{-1}{R_i C_i}\theta_i(t) + \frac{1}{R_i C_i}\,\theta_a(t) + \frac{1}{C_i}\,U_i(t)Q_i \tag{A-4-1}$$

$$U_i(t) = \begin{cases} 1 & \theta_i(t) < \theta_i^- \;\; or \; U_{c,i}(t) = 1 \\ U_i(t^-) & \theta_i^- < \theta_i(t) < \theta_i^+ \\ 0 & \theta_i^+ < \theta_i(t) \; or \; U_{c,i}(t) = 0 \end{cases} \tag{A-4-2}$$

where t^- represents the time step right before the time instant t. It should be noted that the discretized model of (4-1) is derived based on (A-4).

Let $T_{off,i}$ be the "off" time of the i^{th} HP. During the "off" period, (A-4-1) can be simplified as

$$\frac{d\theta_i(t)}{dt} = \frac{-1}{R_i C_i}\theta_i(t) + \frac{1}{R_i C_i}\,\theta_a(t). \tag{A-5}$$

Assuming that the ambient temperature, $\theta_a(t)$, remains unchanged within the off period, $\theta_i(t)$ is calculated as

$$\theta_i(t) = \theta_a - \big(\theta_a - \theta_i(0)\big)e^{-t/R_i C_i} \tag{A-6}$$

If the initial and final temperature are θ_i^+ and θ_i^-, respectively, we have

$$\theta_i^- = \theta_a - (\theta_a - \theta_i^+)e^{-\left(T_{off,i}/R_i C_i\right)}. \tag{A-7}$$

Solving (A-7) for the time constant, $R_i C_i$, results in

$$R_i C_i = -T_{off,i} / ln\left(\frac{\theta^- - \theta_a}{\theta^+ - \theta_a}\right) \quad \text{(A-8)}$$

which is equation (A-1).

Let $T_{on,i}$ be the "on" time of the i^{th} HP. During the "on" period, (A1-1) can be simplified as

$$\frac{d\theta_i(t)}{dt} = \frac{-1}{R_i C_i}\theta_i(t) + \frac{1}{R_i C_i}\,\theta_a(t) + \frac{1}{C_i}\,Q_i. \quad \text{(A-9)}$$

Similarly, when assuming $\theta_a(t)$ is constant within the "on" period, we have

$$\theta_i(t) = \theta_a + Q_i R_i - \left(\theta_a + Q_i R_i - \theta_i(0)\right)e^{-t/R_i C_i}. \quad \text{(A-10)}$$

By substituting the initial and final temperatures, θ_i^- and θ_i^+, in (A-10), the following equation is derived.

$$\theta_i^+ = \theta_a + Q_i R_i - (\theta_a + Q_i R_i - \theta_i^-)e^{-(T_{on,i}/R_i C_i)} \quad \text{(A-11)}$$

Reordering (A-11) to solve for $Q_i R_i$, yields

$$Q_i R_i = \frac{\theta^+ - \theta^-\, e^{-(T_{on,i}/R_i C_i)}}{1 - e^{-(T_{on,i}/R_i C_i)}} - \theta_a \quad \text{(A-12)}$$

Which is actually equation (A-2).

After implementing the above steps in step 2, the PDFs of the derived R, C, and Q, for 10,000 HPs are derived as shown in Fig. A.1.

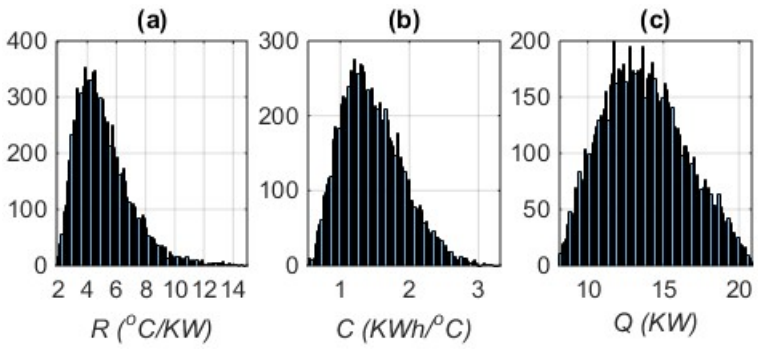

Fig. A.1. PDF of R, C, and Q for 10,000 HPs.

Step 3: Generate θ_{set}, Db, T_{off}^{ml}, and T_{on}^{ml} of HPs using the desired PDFs. In this study it is assumed that they are independent random numbers generated by discrete uniform PDFs with parameters shown in Table A.2.

Table A.2. Parameters of Discrete Uniform Distribution PDF, $X \sim U(a, b, n)$.

X	Interval Bounds, $[a, b]$	Number of Intervals, n
$\theta_{set,i}$ (℃)	[19,23]	4
Db_i (℃)	[2,5]	3
$T_{on,i}^{ml}/T_{off,i}^{ml}$ (Minute)	[1,4]	3

It should be noted that HP refers to the actual heating device together with the space it heats up. The thermal parameters of an HP are $p = [R_i, C_i, Q_i, P_{Rated,i}, T_{on,i}^{ml}, T_{off,i}^{ml}]$ that depends on the building design and the HP ratings. On the other hand, the thermal settings of an HP, $s = [\theta_{set,i}, Db_i]$, are values set by the occupants based on his/her comfort preferences.

REFERENCES

[1] Benefits of demand response in electricity markets and recommendations for achieving them," tech. rep., U.S. Department of Energy, Feb. 2006.

[2] A. H. Mohsenian-Rad and A. Leon-Garcia, "Optimal residential load control with price prediction in real-time electricity pricing environments," *IEEE Trans. Smart Grids*., vol. 1, no. 2, pp. 120-133, Sep. 2010.

[3] M. A. A. Pedrasa, T. D. Spooner, and I. F. Macgill, "Scheduling of demand side resources using binary particle swarm optimization," *IEEE Trans. Power Syst*., vol. 24, no. 3, pp. 1173–1181, Aug. 2009.

[4] A. J. Conejo, J. M. Morales, L. Baringo, "Real-time demand response model," *IEEE Trans. Smart Grids*., vol. 1, no. 3, pp. 236-242, Dec. 2010.

[5] P. Du and N. Lu, "Appliance commitment for household load scheduling," *IEEE Trans. Smart Grid*, vol. 2, no. 2, pp. 411–419, Jun. 2011.

[6] M. Beaudin, H. Zareipour, A. K. Kiani Bejestani, and A. Schellenberg, "Residential energy management using a two-horizon algorithm," *IEEE Trans. Smart Grid*, vol. 5, no. 4, pp. 1712–1723, Jul. 2014.

[7] A. Anvari-Moghaddam. H. Monsef, A. Rahimi-Kian, "Optimal smart home energy management considering energy saving and a comfortable lifestyle," *IEEE Trans. Smart Grid*, vol. 6, no. 1, pp. 324–332, Jan. 2015.

[8] N. Gudi, L. Wang, V. Devabhaktuni, and S. S. S. R. Depuru, "Demand response simulation implementing heuristic optimization for home energy management," in Proc. N. Amer. Power Symp., Arlington, TX, USA, Sep. 2010, pp. 1–6.

[9] A. Basit, G. A. S. Sidhu, A. Mahmood, and F. Gao, “Efficient and Autonomous Energy Management Techniques for the Future Smart Homes,” *IEEE Trans. Smart Grid*, vol. 8, no. 2, pp. 917–926, Mar. 2017.

[10] B. Shen, G. Ghatikar, C. C. Ni, and J. Dudley, “Addressing energy demand through demand response: international experiences and practices," tech. rep., Environmental Energy Technologies Division Lawrence Berkeley National Laboratory, June 2012.

[11] B. Kirby and M. Ally, “Spinning reserve from supervisory thermostat control," tech. rep., Transmission Reliability Research Review, US Department of Energy, Dec. 2002.

[12] D. J. Hammerstrom, et al., “Pacific northwest gridwise testbed demonstration projects: part 1. Olympic peninsula project," tech. rep., Pacific Northwest National Laboratory, Oct. 2007.

[13] V. Trovato, I. M. Sanz, B. Chaudhuri, G. Strbac, “Advanced Control of Thermostatic Loads for Rapid Frequency Response in Great Britain,” *IEEE Trans. Power Syst.*, vol. 32, no. 3, pp. 2106–2117, May. 2017.

[14] U.S. Energy Information Administration, annual energy review, 2010 [Online]. Available: http://www.eia.gov/totalenergy/data/annual/#consumption.

[15] C. Perfumo, E. Kofman, J. H. Braslavsky, J. K. Ward, “Load management: Model-based control of aggregate power for populations of aggregate power for populations of thermostatically controlled loads,” *Energy Convers. Manage.*, vol. 55, no. 5, pp. 36–48, March 2012.

[16] D. S. Callaway, “Tapping the energy storage potential in electric loads to deliver load following and regulation with application to wind energy,” *Energy Convers. Manage.*, vol. 50,

no. 5, pp. 1389–1400, May 2009.

[17] W. Zhang, J. Lian, C-Y. Chang, K. Kalsi, “Aggregated modelling and control of air conditioning loads for demand response,” *IEEE Trans. Power Syst.*, vol. 28, no. 4, pp. 4655-4664, Nov. 2013.

[18] J. L. Mathieu, S. Koch, D. S. Callaway, “State estimation and control of electric loads to manage real-time energy imbalance,” *IEEE Trans. Power Syst.*, vol. 28, no. 1, pp. 430-439, Feb. 2013.

[19] S. Banash and H. Fathy, “Modeling and control insights into demand-side energy management through setpoint control of thermostatic loads,” in *Proc. Amer. Control Conf.*, Jun. 2011.

[20] S. Kundu, N. Sinitsyn, S. Backhaus, and I. Hiskens, “Modeling and control of thermostatically controlled loads,” in Proc. *17th Power Syst. Computation Conf.*, Stokholm, Sweden, 2011.

[21] N. Lu, “An of the HVAC load potential for providing load balancing service,” *IEEE Trans. Smart Grid*, vol. 3, no. 3, pp. 1263-1270, Sept. 2012.

[22] N. Lu and Y. Zhang, “Design considerations of a centralized load controller using thermostatically controlled appliances for continuous regulation reserves,” *IEEE Trans. Smart Grid*, vol. 4, no. 2, pp. 914-921, Jun. 2013.

[23] M. Liu, Y. Shi, "Model predictive control of aggregated heterogeneous second-order thermostatically controlled loads for ancillary services", *IEEE Trans. Power Syst.*, vol. 31, no. 3, pp. 1963-1971, May 2016.

[24] J. Short, D. Infield, and L. Freris, “Stabilization of grid frequency through dynamic

demand control," *IEEE Trans., Power Syst*., vol. 22, no. 3, pp. 1284–1293, Aug. 2007.

[25] A. Molina-Garcia, F. Bouffard, and D. S. Kirschen, "Decentralized demand-side contribution to primary frequency control," *IEEE Trans. Power Syst.*, vol. 26, no. 1, pp. 411–419, Feb. 2011.

[26] K. Samarakoon, J. Ekanayake, and N. Jenkins, "Investigation of domestic load control to provide primary frequency response using smart meters," *IEEE Trans. Smart Grid*, vol. 3, no. 1, pp. 282–292, Mar. 2012.

[27] S. Tindemans, V. Trovato, and G. Strbac, "Decentralized control of thermostatic loads for flexible demand response," *IEEE Trans. Control Syst. Technol*., vol. 23, no. 5, pp. 1685–1700, Sep. 2015.

[28] J. Hu, J. Cao, T. Yong, J. M. Guerrero, M. Z.Q. Chen, Y. Li, "Demand response load following of source and load systems," *IEEE Trans. Control Syst. Technol.,* to be published.

[29] M. Liu, Y. Shi, X. Liu, "Distributed MPC of aggregated heterogeneous thermostatically controlled loads in smart grid", *IEEE Trans. Ind. Electron.*, vol. 63, no. 2, pp. 1120-1129, Feb. 2016.

[30] H. Madsen and J. Holst, "Estimation of continuous-time models for the heat dynamics of a building," *Energy and Buildings*, vol. 22, no. 1, pp. 67–79, Mar. 1995.

[31] P. Bacher and H. Madsen, "Identifying suitable models for heat dynamics of a building," *Energy and Buildings*, vol. 43, no. 7, pp. 1511–1522, Jul. 2011.

[32] California ISO. [Online]. Available: https://www.caiso.com/Documents/Business-RequirementsSpecification-Pay-Performance.pdf.

[33] PJM Manual 12: Balancing Operations, [online] Available: http://www.pjm.com/media/-

documents/manuals/m12.ashx.

[34] M. Vanouni and N. Lu, "Performance indices for evaluating demand response services provided by thermostatically controlled appliances," in *Proc. IEEE/PES Transm. Distrib. Conf. Expo*., Apr. 2014, pp. 1-6.

[35] U.S. Federal Energy Regulatory Commission, Washington, DC, FERC 755, Dockets RM11-7-000 AD10-11-000, Oct. 2011. Available: http://www.amdahl.com/doc/products/bsg-/intra/infra/html.

[36] Y. Chen, R. Leonard, M. Keyser, and J. Gardner, "Development of performance-based two-part regulation reserve compensation on MISO energy and ancillary services," *IEEE Trans. Power Syst.*, vol. 30, no. 1, pp. 142–155, Jan. 2015.

[37] G. He, Q. Chen, C. Kang, P. Pinson, and Q. Xia, "Optimal bidding strategy of battery storage in power markets considering performance-based regulation and battery cycle life," *IEEE Trans. Smart Grid*, vol. 7, no. 5, pp. 2359–2367, Sep. 2016.

[38] T. Zhang, S. X. Chen, H. B. Gooi, and J. M. Maciejowski, "A hierarchical EMS for aggregated BESSs in energy and performance-based regulation Markets," *IEEE Trans. Power Syst.*, vol. 32, no. 3, pp. 1751–1760, May. 2017.

[39] A. Sadeghi-Mobarakeh and H. Mohsenian-Rad, "Optimal bidding in performance-based regulation markets: an MPEC analysis with system dynamics," *IEEE Trans. Power Syst.*, vol. 32, no. 2, pp. 1282–1292, Mar. 2017.

[40] O. Mali and P. Havel, "Active demand-side management system to facilitate integration of RES in low voltage distribution networks," *IEEE Trans. Sustain. Energy*, vol. 5, no. 2, pp. 673-681, Apr. 2014.

[41] J. L. Mathieu, M. Kamgarpour, J. Lygeros, G. Anderson, and D. S. Callaway, "Arbitraging intraday wholesales energy market prices with aggregations of thermostatic loads," *IEEE Trans. Power Syst.*, vol. 30, no. 2, pp. 763-772, Mar. 2015.

[42] E. Vrettos, C. Ziras, J. Lygeros, G. Andersson, "Fast and reliable primary frequency reserves from refrigerators with decentralized stochastic control," *IEEE Trans. Power Syst.*, to be published.

[43] M. Vanouni and N. Lu, "Improving the centralized control of thermostatically controlled appliances by obtaining the right information," *IEEE Trans. Smart Grid*, vol. 6, no. 2, pp. 946-948, Mar. 2015.

[44] A. Abiri-Jahromi and F. Bouffard, "Contingency-type reserve leveraged through aggregated thermostatically-controlled loads-Part I: characterization and control," *IEEE Trans. Power Syst.*, vol. pp, 2015.

[45] A. Alahäivälä, J. Corbishley, J. Ekström, J. Jokisalo, M. Lehtonen, "A control framework for the utilization of heating load flexibility in a day-ahead market," *Electr. Power Syst. Research.*, vol. 145, no. , pp. 44–54, Apr. 2017.

[46] Y. Zhou, C. Wang, J. Wu, J. Wang, M. Cheng, and G. Li, "Optimal scheduling of aggregated thermostatically controlled loads with renewable generation in the intraday electricity market," *Appl. Energy*, vol. 188, pp. 456–465, Feb. 2017.

[47] V. Trovato, S. Tindemans, and G. Strbac, "Leaky storage model for optimal multi-service allocation of thermostatic loads," *IET Gener., Transm., Distrib.*, vol. 10, no. 3, pp. 585–593, 2016.

[48] H. Hao,B. M. Sanandaji, K. Poolla, L. Vincent, "Aggregate Flexibility of Thermostatically

Controlled Loads", *IEEE Trans. Power Syst.*, vol. 30, no. 1, pp. 189-198, Jan. 2015.

[49] Katipamula and N. Lu, "Evaluation of residential HVAC control strategies for demand response programs," *ASHRAE Trans*., vol. 1, no. 12, pp. 1–12, 2006.

[50] K. S. Ko, S. Han, and K. Sung, "Performance-based settlement of frequency regulation for electric vehicle aggregators," *IEEE Trans. Smart Grid*, to be published.

[51] R. Hooke and T. A. Jeeves, "Direct Search solution of numerical and statistical problems," *Journal of the ACM (JACM)*, vol. 8, no. 2, pp. 212–229, 1961.

[52] PJM Regulation Data [Online]. Available: http://www.pjm.com/-markets-and-operations/ancillary-services.aspx.

Chapter 5

[53] J. H. Yoon, R. Baldick, and A. Novoselac, "Dynamic demand response controller based on real-time retail price for residential buildings," *IEEE Trans. Smart Grid*, vol. 5, no. 1, pp. 121-129, Jan. 2014.

[54] C. Perfumo, J. H. Braslavsky, and J. K. Ward, "Model-based estimation of energy savings in load control events for thermostatically controlled loads," *IEEE Trans. Smart Grid*, vol. 5, no. 3, pp. 1410-1420, May. 2014.

[55] A. D. Papalexopoulos and P. E. Andrianesis, "Performance-based pricing of frequency regulation in electricity markets," *IEEE Trans. Power Syst.*, vol. 29, no. 1, pp. 441-449, Jan. 2014.